

AUG 14 1976

AEDC-TR-76-44

AFATL-TR-76-32

cy.2



**FLOW-FIELD CHARACTERISTICS NEAR THE MIDWING  
WEAPONS PYLON OF THE F-16 AIRCRAFT AT  
MACH NUMBERS FROM 0.4 TO 0.95**

**PROPULSION WIND TUNNEL FACILITY  
ARNOLD ENGINEERING DEVELOPMENT CENTER  
AIR FORCE SYSTEMS COMMAND  
ARNOLD AIR FORCE STATION, TENNESSEE 37389**

**August 1976**

**Final Report for Period November 12 – 18, 1975**

Approved for public release; distribution unlimited.

F10000-76-0-0001

**Prepared for**

**AIR FORCE ARMAMENT LABORATORY (DLJC)  
EGLIN AFB, FLORIDA 32542**

## NOTICES

When U. S. Government drawings specifications, or other data are used for any purpose other than a definitely related Government procurement operation, the Government thereby incurs no responsibility nor any obligation whatsoever, and the fact that the Government may have formulated, furnished, or in any way supplied the said drawings, specifications, or other data, is not to be regarded by implication or otherwise, or in any manner licensing the holder or any other person or corporation, or conveying any rights or permission to manufacture, use, or sell any patented invention that may in any way be related thereto.

Qualified users may obtain copies of this report from the Defense Documentation Center.

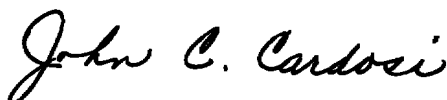
References to named commercial products in this report are not to be considered in any sense as an endorsement of the product by the United States Air Force or the Government.

This report has been reviewed by the Information Office (OI) and is releasable to the National Technical Information Service (NTIS). At NTIS, it will be available to the general public, including foreign nations.

## APPROVAL STATEMENT

This technical report has been reviewed and is approved for publication.

FOR THE COMMANDER



JOHN C. CARDOSI  
Lt Colonel, USAF  
Chief Air Force Test Director, PWT  
Directorate of Test



WILLIAM K. OFFICER  
Colonel, USAF  
Director of Test, Acting

# UNCLASSIFIED

REPORT DOCUMENTATION PAGE		READ INSTRUCTIONS BEFORE COMPLETING FORM
1 REPORT NUMBER <b>AEDC-TR-76-44 AFATL-TR-76-32</b>	2 GOVT ACCESSION NO.	3 RECIPIENT'S CATALOG NUMBER
4 TITLE (and Subtitle) <b>FLOW-FIELD CHARACTERISTICS NEAR THE MID- WING WEAPONS PYLON OF THE F-16 AIRCRAFT AT MACH NUMBERS FROM 0.4 TO 0.95</b>		5. TYPE OF REPORT & PERIOD COVERED <b>Final Report - November 12-18, 1975</b>
		6. PERFORMING ORG. REPORT NUMBER
7 AUTHOR(s) <b>E. G. Allee, Jr., ARO, Inc.</b>		8 CONTRACT OR GRANT NUMBER(s)
9 PERFORMING ORGANIZATION NAME AND ADDRESS <b>Arnold Engineering Development Center (XO) Air Force Systems Command Arnold Air Force Station, Tennessee 37389</b>		10 PROGRAM ELEMENT, PROJECT, TASK AREA & WORK UNIT NUMBERS <b>Program Element 62602F Project 2567 Task 01</b>
11 CONTROLLING OFFICE NAME AND ADDRESS <b>Air Force Armament Laboratory (DLJC) Eglin AFB, Florida 32542</b>		12 REPORT DATE <b>August 1976</b>
		13 NUMBER OF PAGES <b>87</b>
14 MONITORING AGENCY NAME & ADDRESS (if different from Controlling Office)		15 SECURITY CLASS. (of this report)  <b>UNCLASSIFIED</b>
		15a DECLASSIFICATION/DOWNGRADING SCHEDULE <b>N/A</b>
16 DISTRIBUTION STATEMENT (of this Report)  <b>Approved for public release; distribution unlimited.</b>		
17 DISTRIBUTION STATEMENT (of the abstract entered in Block 20, if different from Report)		
18 SUPPLEMENTARY NOTES  <b>Available in DDC</b>		
19 KEY WORDS (Continue on reverse side if necessary and identify by block number) <b>flow field                      scale models                      angles characteristics                F-16 aircraft                    simulation (altitude) weapons                        Mach numbers struts (midwing)              flaps</b>		
20 ABSTRACT (Continue on reverse side if necessary and identify by block number)  <b>Wind tunnel tests using 0.0667-scale models were conducted to determine the characteristics of the flow field near the midwing weapons pylon (wing stations 3 and 7) of the F-16 aircraft. The investigation was conducted by positioning an MK-84 LDGP store at various locations beneath the pylon, by use of a pressure probe to measure the flow-field velocities and angles relative to the freestream, and by separation trajectories using the MK-84</b>		

# UNCLASSIFIED

# UNCLASSIFIED

## 20. ABSTRACT (Continued)

LDGP launched from the pylon. Test conditions ranged from Mach number 0.4 to 0.95 for aircraft angles of attack from 0 to 16 deg. Wing leading-edge flaps of the F-16 model were set at angles of 0, 4, and 15 deg. All trajectories were obtained at a simulated altitude of 5,000 ft.

UNCLASSIFIED

## PREFACE

The work reported herein was conducted by the Arnold Engineering Development Center (AEDC), Air Force Systems Command (AFSC), at the request of the Air Force Armament Laboratory (AFATL/DLJC), under Program Element 62602F, Project 2567. The AFATL project monitor was Mr. Al Marrin. The test results were obtained by ARO, Inc. (a subsidiary of Sverdrup & Parcel and Associates, Inc.), contract operator of the AEDC, AFSC, Arnold Air Force Station, Tennessee, under ARO Project No. P41C-A4A. The author of this report was E. G. Allee, Jr., ARO, Inc. The data reduction was completed on December 12, 1975, and the manuscript (ARO Control No. ARO-PWT-TR-76-8) was submitted for publication on January 27, 1976.

## CONTENTS

	<u>Page</u>
1.0 INTRODUCTION . . . . .	5
2.0 APPARATUS	
2.1 Test Facility . . . . .	5
2.2 Test Articles . . . . .	6
2.3 Instrumentation . . . . .	6
3.0 TEST DESCRIPTION	
3.1 Test Conditions . . . . .	7
3.2 Data Acquisition . . . . .	7
3.3 Corrections . . . . .	9
3.4 Precision of Data . . . . .	9
4.0 RESULTS AND DISCUSSION	
4.1 Aerodynamic Loads Data . . . . .	9
4.2 Flow-Field Data . . . . .	10
4.3 Trajectory Data . . . . .	11

## ILLUSTRATIONS

### Figure

1. Isometric Drawing of a Typical Store Separation Installation and a Block Diagram of the Computer Control Loop . . . . .	13
2. Schematics of Test Installations . . . . .	14
3. Dimensional Sketch of the F-16 Parent Model . . . . .	16
4. Dimensional Sketches of the Store Models . . . . .	17
5. F-16 Model Pylons . . . . .	22
6. Details of the 40-deg Conical Pressure Probe . . . . .	25
7. Installation Photographs . . . . .	27
8. Aircraft Configurations . . . . .	29
9. Axis System Defining Direction and Velocity Vectors for Flow-Field Measurements . . . . .	30
10. MK-84 LDGP Free-Stream Aerodynamic Coefficients . . . . .	31
11. Aerodynamic Coefficients Obtained in the F-16 Parent Flow Field . . . . .	35
12. Effects of the Removal of the 370-gal Fuel Tank on the Aerodynamic Coefficients at $M_\infty = 0.6$ . . . . .	41

<u>Figure</u>	<u>Page</u>
13. Effects of the Removal of the 370-gal Fuel Tank on the Aerodynamic Coefficients at $M_\infty = 0.8$ . . . . .	47
14. Flow-Field Measurements about the Midwing Weapons Pylon with the MK-84 LDGP Installed, Configuration 3, $M_\infty = 0.6$ , $\delta_{LE} = 0$ . . . . .	51
15. Flow-Field Measurements about the Midwing Weapons Pylon with the MK-84 LDGP Installed, Configuration 3, $M_\infty = 0.6$ , $\delta_{LE} = 15$ . . . . .	57
16. Flow-Field Measurements about the Midwing Weapons Pylon with the MK-84 LDGP Installed, Configuration 3, $M_\infty = 0.8$ , $\delta_{LE} = 0$ . . . . .	63
17. Flow-Field Measurements about the Midwing Weapons Pylon without the MK-84 LDGP installed, Configuration 4, $M_\infty = 0.6$ , $\delta_{LE} = 0$ . . . . .	69
18. Flow-Field Measurements about the Midwing Weapons Pylon without the MK-84 LDGP Installed, Configuration 4, $M_\infty = 0.8$ , $\delta_{LE} = 0$ . . . . .	72
19. Effects of Wing Leading-Edge Flap Deflections on Trajectories of the MK-84 LDGP, Configuration 1 . . . . .	75
20. Comparison of Trajectories of the MK-84 LDGP with and without the 370-gal Inboard Fuel Tank, $\delta_{LE} = 0$ , Configurations 1 and 2 . . . . .	77

## TABLES

1. Run Compendium . . . . .	81
2. Survey Points . . . . .	82
3. Uncertainties . . . . .	83
NOMENCLATURE . . . . .	84

## 1.0 INTRODUCTION

To investigate the flow-field characteristics near the midwing weapons pylon (wing stations 3 and 7) of the F-16 aircraft, flow-field survey, store aerodynamic loads, and captive trajectory testing was conducted in the Aerodynamic Wind Tunnel (4T) of the Propulsion Wind Tunnel Facility (PWT). One-fifteenth (0.0667) scale models were used in all three phases of the investigation. Flow-field data were obtained by positioning a 40-deg conical pressure probe at various points in the vicinity of the midwing weapons pylon with an MK-84 LDGP store model mounted on the pylon. The aerodynamic loads data were acquired on the MK-84 LDGP at various vertical distances directly below the pylon. All trajectories were initiated from the midwing weapons pylon and were at a simulated altitude of 5,000 ft. The effects of a 370-gal fuel tank mounted on the adjacent inboard wing pylon, and various aircraft wing leading-edge flap deflections, were ascertained in all three phases of the test. Test parameters included a Mach number range from 0.4 to 0.95 at aircraft angles of attack from 0 to 16 deg.

## 2.0 APPARATUS

### 2.1 TEST FACILITY

The Aerodynamic Wind Tunnel (4T) is a closed-loop, continuous flow, variable density tunnel in which the Mach number can be varied from 0.1 to 1.3 and can be set at 1.6 and 2.0 by placing nozzle inserts over the permanent sonic nozzle. At all Mach numbers, the stagnation pressure can be varied from 300 to 3,700 psfa. The test section is 4 ft square and 12.5 ft long with perforated, variable porosity (0.5- to 10-percent open) walls. It is completely enclosed in a plenum chamber from which the air can be evacuated, allowing part of the tunnel airflow to be removed through the perforated walls of the test section.

Two separate and independent support systems were used to support the models. The parent-aircraft model was inverted in the test section and supported by an offset sting attached to the main pitch sector. The store model (or flow-field survey probe) was supported by the captive trajectory support (CTS) which extends down from the tunnel top wall and provides store (or probe) movement (six degrees of freedom) independent of the parent-aircraft model. An isometric drawing of a typical installation is shown in Fig. 1.

Also shown in Fig. 1 is a block diagram of the computer control loop used during testing. The analog system and the digital computer work as an integrated unit and, utilizing required input information, control the store (or probe) movement. Positioning is



accomplished by use of six individual d-c electric motors. Maximum translational travel of the CTS is  $\pm 15$  in. from the tunnel centerline in the lateral and vertical directions and 36 in. in the axial direction. Maximum angular displacements are  $\pm 45$  deg in pitch and yaw and  $\pm 360$  deg in roll. A schematic showing the test section details and the location of the models in the tunnel is shown in Fig. 2.

## 2.2 TEST ARTICLES

Models used during this test were 0.0667-scale replicas of the F-16 aircraft and associated pylons, the MK-84 LDGP bomb, the AIM-9J missile, the 370-gal fuel tank, and the ALQ-119-12 ECM pod. Details of these models and associated pylons are presented in Figs. 3, 4, and 5. The leading-edge flaps of the F-16 model could be set at angles of 0, 4, and 15 deg. During the flow-field portion of the test, the horizontal stabilizers of the F-16 model were removed to avoid interference with the flow-field probe. The stabilizers were in place during the acquisition of aerodynamic loads and trajectory information.

Store parameters used in the calculation of the aerodynamic loads and trajectories are included in the nomenclature.

The probe used to obtain flow-field measurements was attached directly to the CTS and consisted of a single cone-cylinder with a 40-deg included tip angle (Fig. 6). There were four equally spaced static pressure orifices on the cone surface and a total-pressure orifice at the cone apex. Typical tunnel installation photographs showing parent aircraft, probe, store, and CTS are presented in Fig. 7. The various configurations tested are presented in Fig. 8.

## 2.3 INSTRUMENTATION

Static and total pressures on the cone probe were measured with 5-psid transducers. A six-component internal strain-gage balance was used to obtain store aerodynamic force and moment data. Translational and angular positions of the store were obtained from CTS analog inputs during separation trajectories and from digital computer commands during aerodynamic and flow-field testing.

A touch-wire system was used to accurately position the store and pressure probe with respect to the parent aircraft. The system was also electrically equipped to automatically stop the CTS motion and give visual indication should the store, probe, or sting support make contact with any surface other than the touch wire.

### 3.0 TEST DESCRIPTION

#### 3.1 TEST CONDITIONS

A complete test summary and the wind tunnel test conditions are given in Table 1. Aerodynamic loads data were obtained at Mach numbers from 0.4 to 0.95. Flow-field and separation trajectory data were obtained at Mach numbers 0.6 and 0.8. Tunnel conditions were held constant at the desired Mach number while the data were obtained. The trajectories were terminated when the store or sting contacted the parent-aircraft model or when a CTS limit was reached.

#### 3.2 DATA ACQUISITION

##### 3.2.1 Aerodynamic Loads Data

Store aerodynamic data in the free stream and in the parent-aircraft flow field were obtained in the following manner. After tunnel conditions were established and the aircraft model angle of attack was set (when applicable), the store was set at  $\alpha_s = 0$  (free-stream data) or at the carriage position ( $X_P = Y_P = Z_P = 0$ , flow-field data). Operational control of the CTS was then switched to the digital computer, which controlled the store movement through commands to the CTS (see block diagram, Fig. 1). The preselected orientations of the store programmed into the computer are given in Table 2. At each position set, the wind tunnel operating conditions and the store model forces and moments were measured and recorded. The model aerodynamic loads were then reduced to coefficient form and tabulated point by point by the digital computer.

##### 3.2.2 Flow-Field Survey Data

All flow-field measurements were obtained in the pylon-axis system. Definitions of the positive directions of the flow-field velocity vectors, flow angles, and probe displacements are given in Fig. 9. During testing, tunnel conditions were established and the probe tip was positioned at a known coordinate point relative to the parent aircraft. At this position, initial-point data were obtained which oriented the computer program controlling CTS movement (see block diagram, Fig. 1). After the initial data were recorded, the computer automatically positioned the probe at preselected locations (see Table 2) where tunnel conditions and probe tip pressures were recorded. Using predetermined probe calibration data, the probe pressure measurements were reduced to flow-angularity data,

and these were tabulated point by point with the same digital computer which controlled the CTS movement.

### 3.2.3 Trajectory Data

To obtain a trajectory, test conditions were established in the tunnel and the parent model was positioned at the desired angle of attack. Operational control of the CTS was then switched to the digital computer which automatically oriented the store model at a position corresponding to the carriage location and then controlled the store movement during the trajectory through commands to the CTS analog system (see block diagram, Fig. 1). Data from the wind tunnel, consisting of measured model forces and moments, wind tunnel operating conditions, and CTS rig positions, were input to the digital computer for use in the full-scale trajectory calculations.

The digital computer was programmed to solve the six-degree-of-freedom equations to calculate the angular and linear displacements of the store relative to the parent-aircraft pylon. In general, the program involves using the last two successive measured values of each static aerodynamic coefficient to predict the magnitude of the coefficients over the next time interval of the trajectory. These predicted values are used to calculate the new position and attitude of the store at the end of the time interval. The CTS is then commanded to move the store model to this new position and the aerodynamic loads are measured. If these new measurements agree with the predicted values, the process is continued over another time interval of the same magnitude. If the measured and predicted values do not agree within the desired precision, the calculation is repeated over a time interval one-half the previous value. This process is repeated until a complete trajectory has been obtained.

In applying the wind tunnel data to the calculations of the full-scale store trajectories, the measured forces and moments are reduced to coefficient form and then applied with proper full-scale store dimensions and flight dynamic pressure. Dynamic pressure was calculated using a flight velocity equal to the free-stream velocity component plus the components of store velocity relative to the aircraft, and a density corresponding to the simulated altitude.

The initial portion of each launch trajectory incorporated simulated ejector forces in addition to the measured aerodynamic forces acting on the store. The ejector force was considered to act perpendicular to the pylon-mounting surface. The ejector forces and locations along with other full-scale store parameters used in the trajectory calculations are included in the nomenclature.

### 3.3 CORRECTIONS

Probe free-stream calibration data were used to obtain corrections to account for any minor misalignment in the probe pitch or yaw orientation. However, no attempt was made to correct the measured flow angles for deflections due to aerodynamic loading on the probe.

Balance, sting, and support deflections caused by the aerodynamic loads on the store models were accounted for in the data reduction program to calculate the true store-model angles. Corrections were also made for model weight tares to calculate the net aerodynamic forces on the store model.

### 3.4 PRECISION OF DATA

Accuracy of the data presented was affected by such quantities as uncertainties in setting tunnel conditions, sensitivity of the balance, uncertainties in the flow-field-probe pressure transducers, and the ability of the CTS rig to set a given position. Uncertainties in the full-scale position data resulting from balance precision limitations were determined by assuming that balance measurement errors accumulate as a bias uncertainty in the trajectory calculations. Coefficient uncertainties were calculated for a 95-percent confidence level. Uncertainties for each phase of the test are presented in Table 3.

## 4.0 RESULTS AND DISCUSSION

Selected data are presented from all three phases of the test program. Aerodynamic free-stream data obtained on the MK-84 LDGP store model are presented in Fig. 10. Aerodynamic coefficients obtained with this store in the aircraft flow field are shown in Figs. 11 through 13. The F-16 aircraft flow-field velocities are given in Figs. 14 through 18. Separation trajectories acquired with the MK-84 LDGP are presented in Figs. 19 and 20. With the exception of the free-stream aerodynamic coefficients, the data from the three phases of the test were acquired at the midwing weapons pylons of the F-16 (wing stations 3 and 7; see Fig. 8). Because of the volume of information obtained, only a selected portion of the data is presented. A complete listing of test conditions and model parameters used during the test is given in Table 1. The aircraft configurations are shown in Fig. 8.

### 4.1 AERODYNAMIC LOADS DATA

Aerodynamic loads obtained at  $M_\infty = 0.6$  with the MK-84 LDGP store at various vertical distances from the number 7 weapons pylon are presented in Figs. 10 through 12 for various aircraft angles of attack and wing leading-edge flap deflections. Data acquired at zero leading-edge flap deflection at  $M_\infty = 0.8$  are presented in Fig. 13. The effect of the various leading-edge flap deflections was most noticeable in the pitching-moment,

yawing-moment, and axial-force coefficients. The magnitude of these effects decreased with vertical separation from the carriage position. At distances of 14 ft and greater, the aerodynamic coefficients were essentially the same for all three leading-edge flap deflection angles.

Changes in the aerodynamic coefficients induced by removal of the 370-gal fuel tank and inboard pylon (configurations 1 and 2, Fig. 8) are shown in Fig. 12 for a wing leading-edge flap deflection of zero. The major change in coefficients was noted in the side-force and yawing-moment coefficients at vertical separation distances of less than 10 ft. However, there were some variations in the other coefficients. Differences in the pitching-moment coefficients were evident at vertical distances greater than 14 ft. (Note: As the aircraft angle of attack was increased, the CTS travel limits decreased the maximum vertical separation attainable.)

Differences in the aerodynamic coefficients between configurations 1 and 2, at leading-edge flap deflections of other than zero, were of the same order of magnitude as for the zero flap deflections.

A comparison of the MK-84 LDGP aerodynamic coefficients with and without the adjacent fuel tank at  $M_\infty = 0.8$  is presented in Fig. 13. At this Mach number, data were acquired only with a zero leading-edge flap setting. Again, there were changes in all coefficients with the largest differences being noted in the side-force and yawing-moment coefficients. The differences in coefficients between the two configurations decayed with increasing vertical separation. However, the pitching-moment coefficients indicated that there was still some flow-field influence from the aircraft at distances up to 18 ft.

## 4.2 FLOW-FIELD DATA

Flow-field data, consisting of transverse velocity vector maps, are presented in Figs. 14 through 18. These data are presented as the projection of the velocity vector ( $V_{YZ,P}$ ) in the pylon axis  $Y_P$ - $Z_P$  plane, with the tails of the vectors originating at the position of the measurement for each  $X_P$  location. The magnitudes of the velocities are given by the vector length, and the flow angle is indicated by the angle of the vector as shown.  $X_P$ ,  $Y_P$ , and  $Z_P$  positions are referenced to the forward 30-in. suspension point of the pylon surface at wing stations 3 or 7. During the flow-field phase of the test, it was possible to use the weapons pylons on both wings for data acquisition. Therefore, in configuration 3, the right wing had the 370-gal fuel tank installed on the inboard pylon (identical to configuration 1) while the left wing had the fuel tank and pylon removed (a mirror image of configuration 2, see Fig. 8). This procedure was not possible during the aerodynamic loads and trajectory portions of the test because of instrumentation limitations of the aircraft model.

Flow patterns obtained at angles of attack of 4 and 12 deg with zero leading-edge flap deflection are shown in Fig. 14 for configuration 3. In general, removal of the fuel tank increased the outwash slightly near the wing surface. This effect was most noticeable at the higher angles of attack.

Flow characteristics associated with a leading-edge flap deflection of 15 deg are shown in Fig. 15 for angles of attack of 4 and 12 deg. The effect of the flap deflection was small ahead of the wing leading edge and increased with aft movement along the chord.

Flow-field data acquired on configuration 3 at  $M_\infty = 0.8$  are presented in Fig. 16 for angles of attack of 0 and 4 deg. No data were acquired with leading-edge flap deflections of other than zero.

Flow patterns obtained with the MK-84 LDGP removed are presented in Figs. 17 and 18 for  $M_\infty = 0.6$  and 0.8. The data shown were selected to indicate the maximum change caused by the removal of the stores.

### 4.3 TRAJECTORY DATA

Separation trajectories obtained with the MK-84 LDGP are presented in Figs. 19 and 20 in flight-axis coordinates as a function of full-scale time. A comparison of the effects of leading-edge flap deflection is given in Fig. 19. The major change was in the pitching and yawing motions of the store.

Differences in the trajectories caused by removal of the inboard 370-gal fuel tank and pylon are shown in Fig. 20. Again, the major effect was noted in the pitching and yawing motions of the store, with a slight increase in outboard displacement noted with the tank removed.

The trajectory characteristics were similar for all leading-edge flap deflections at which data were acquired. No store-to-aircraft contact occurred at any of the release conditions.

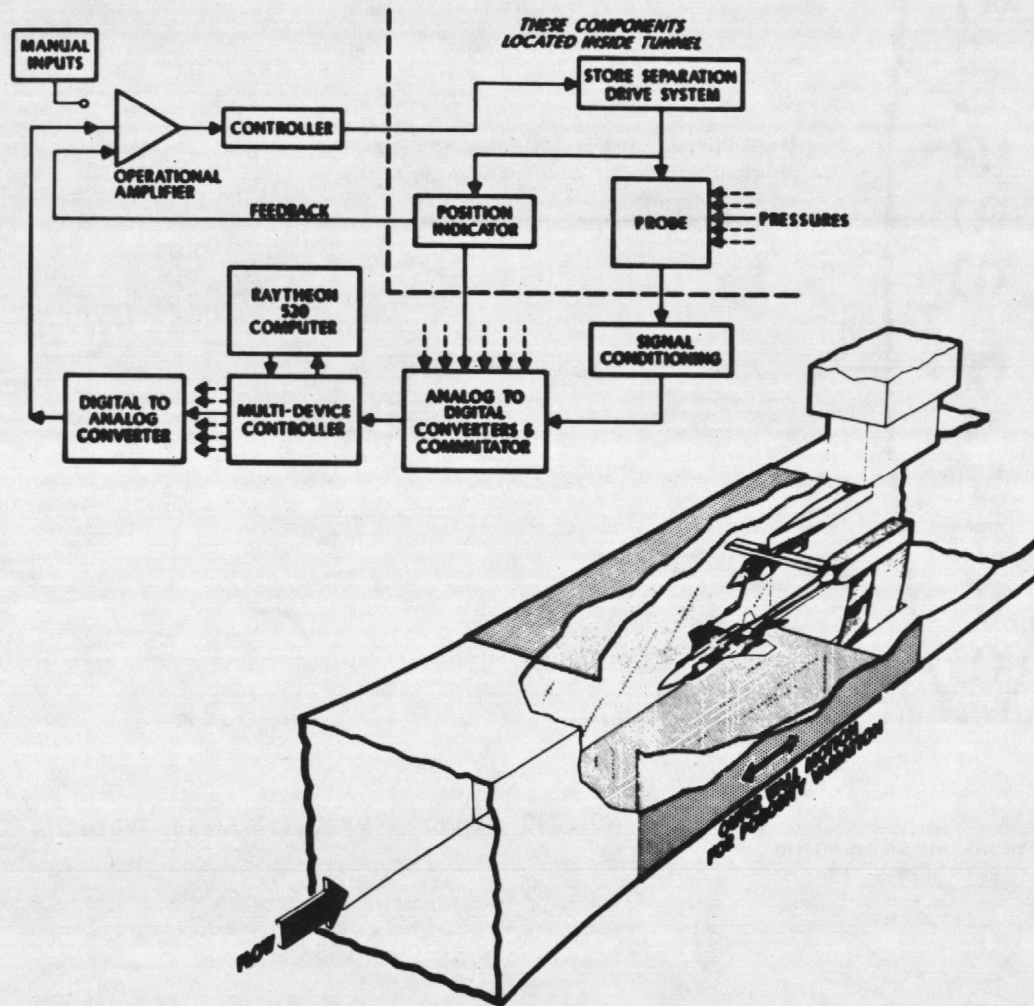
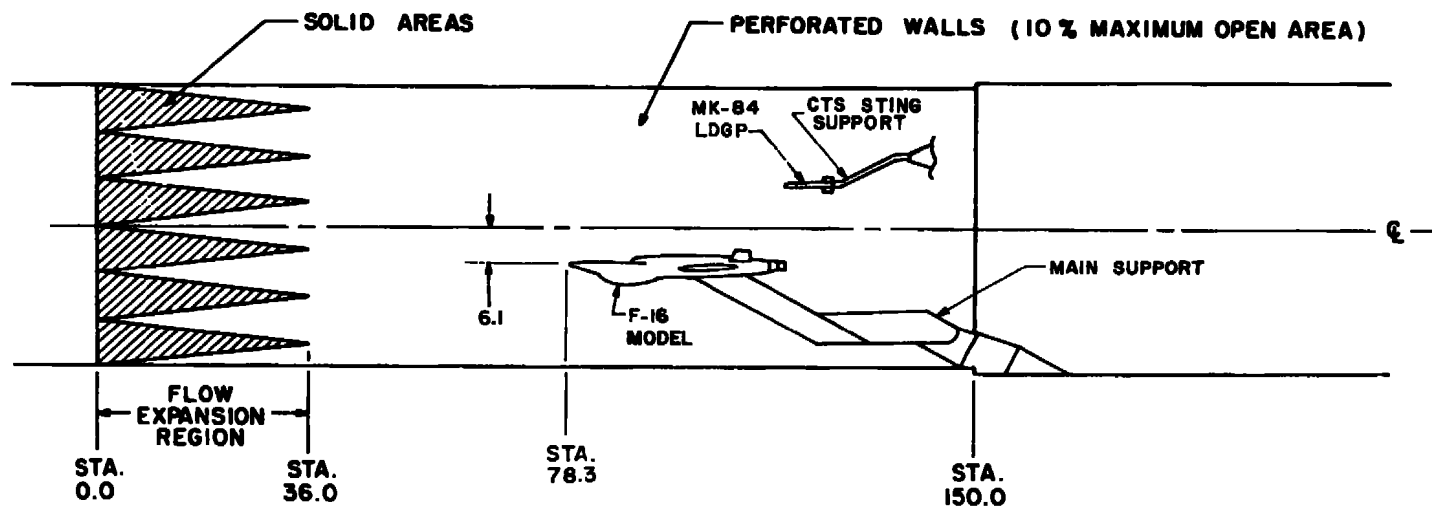
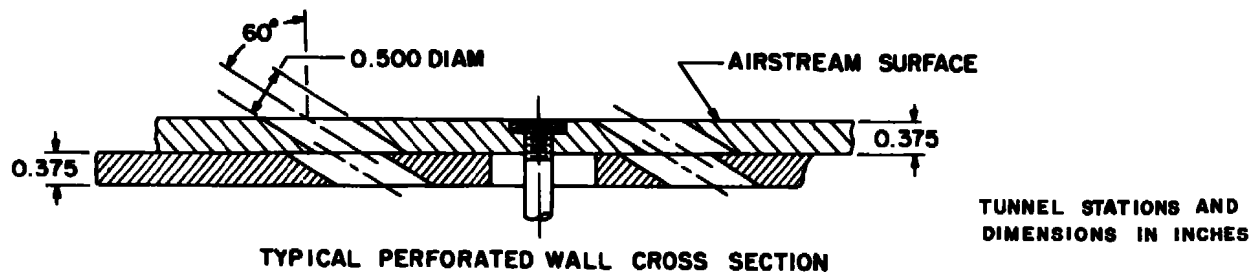
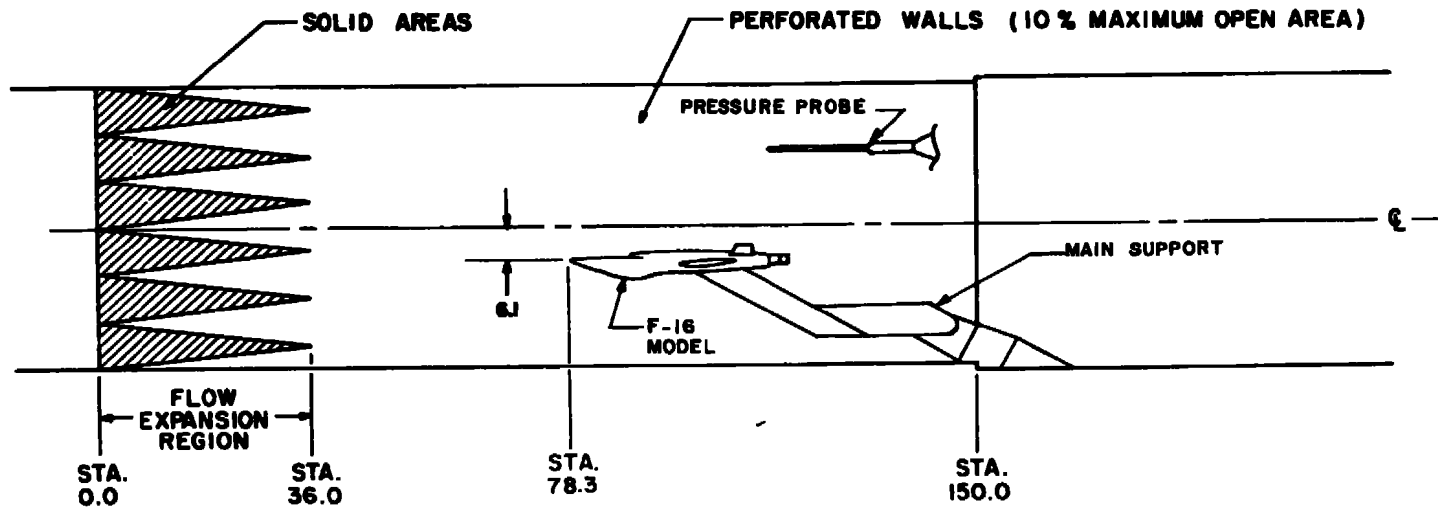
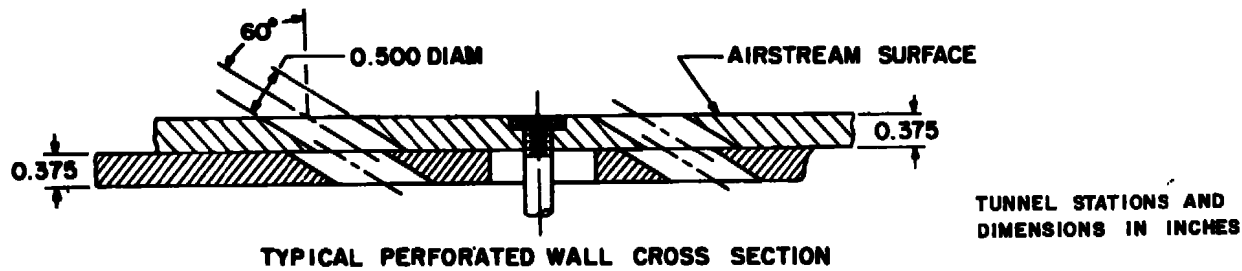


Figure 1. Isometric drawing of a typical store separation installation and a block diagram of the computer control loop.



a. Aerodynamic loads and trajectory installation  
Figure 2. Schematics of test installations.





b. Flow-field installation  
Figure 2. Concluded.

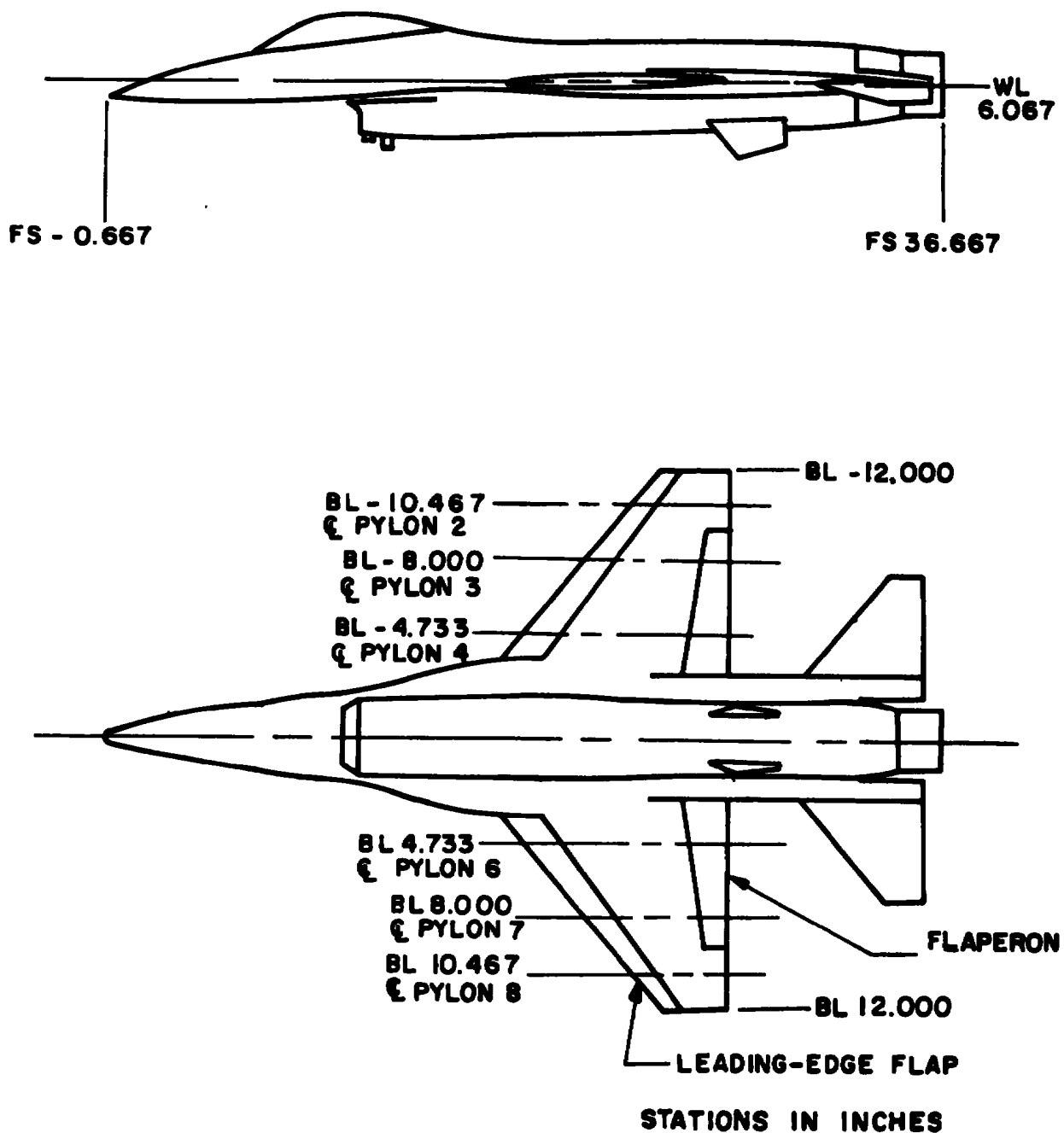
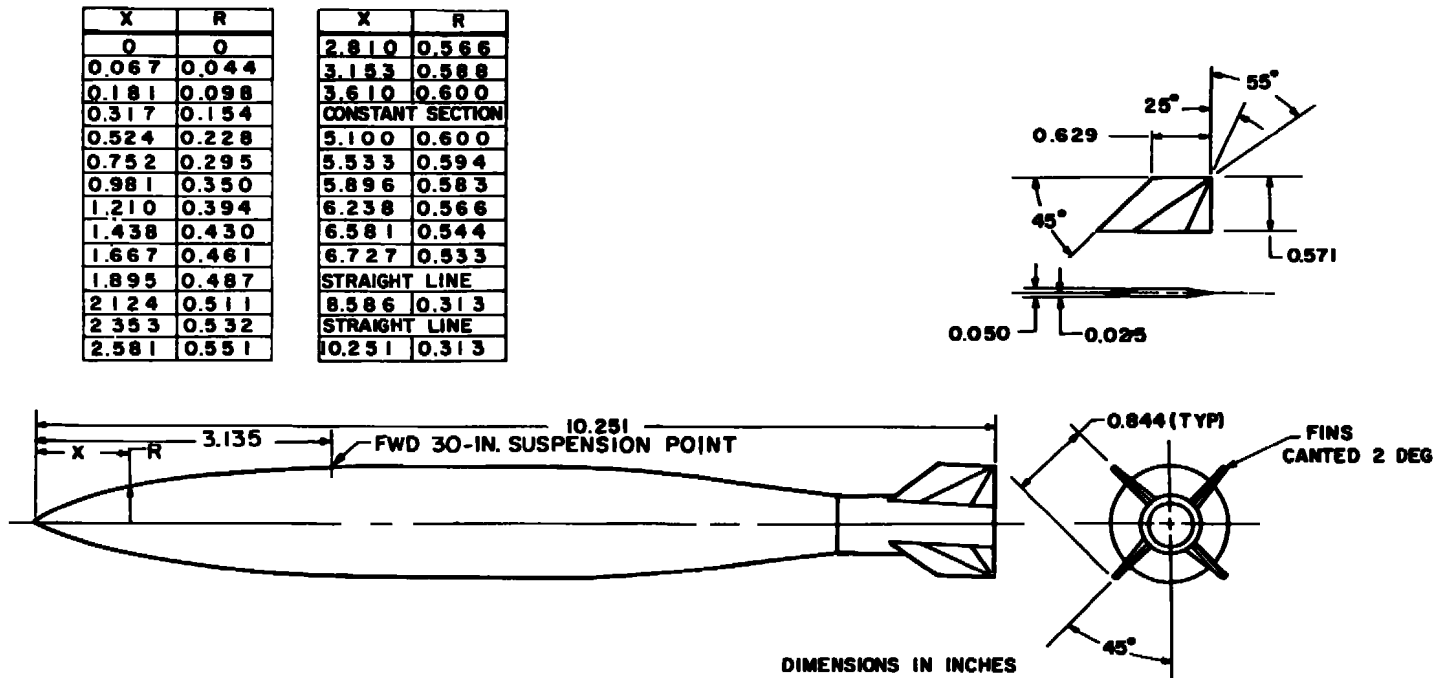
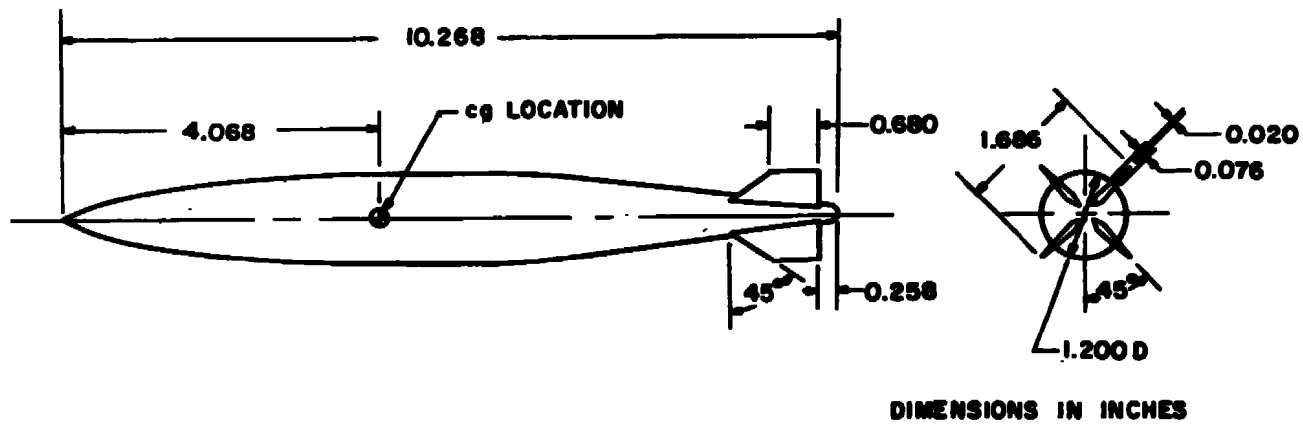


Figure 3. Dimensional sketch of the F-16 parent model.

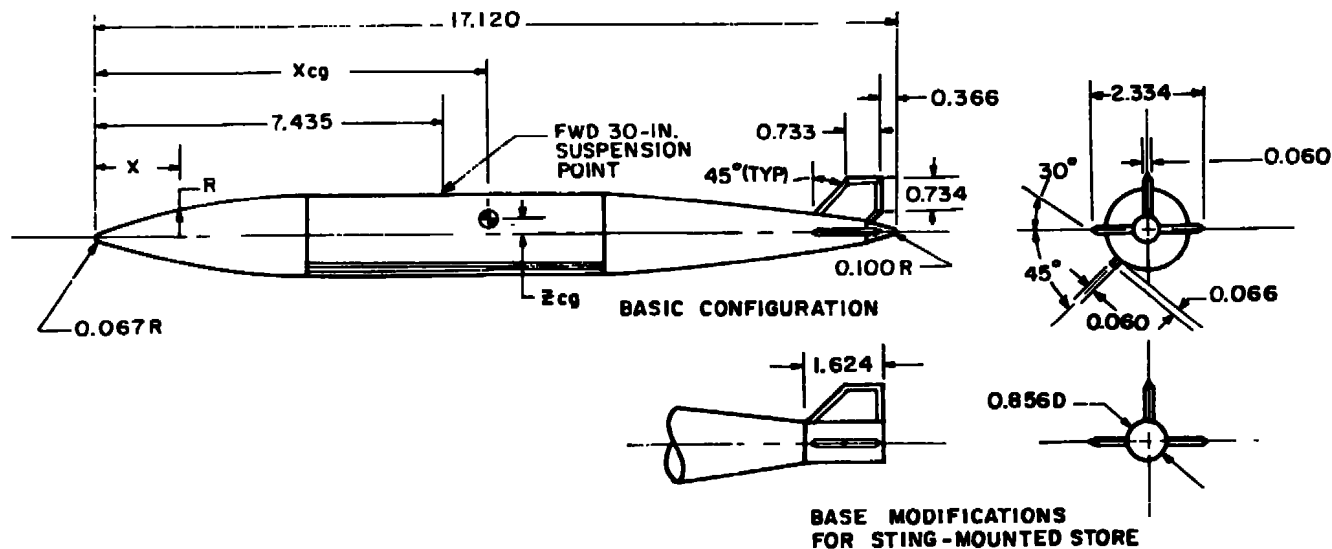


a. MK-84 LDGP metric model  
 Figure 4. Dimensional sketches of the store models.

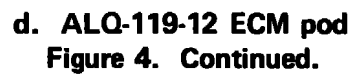


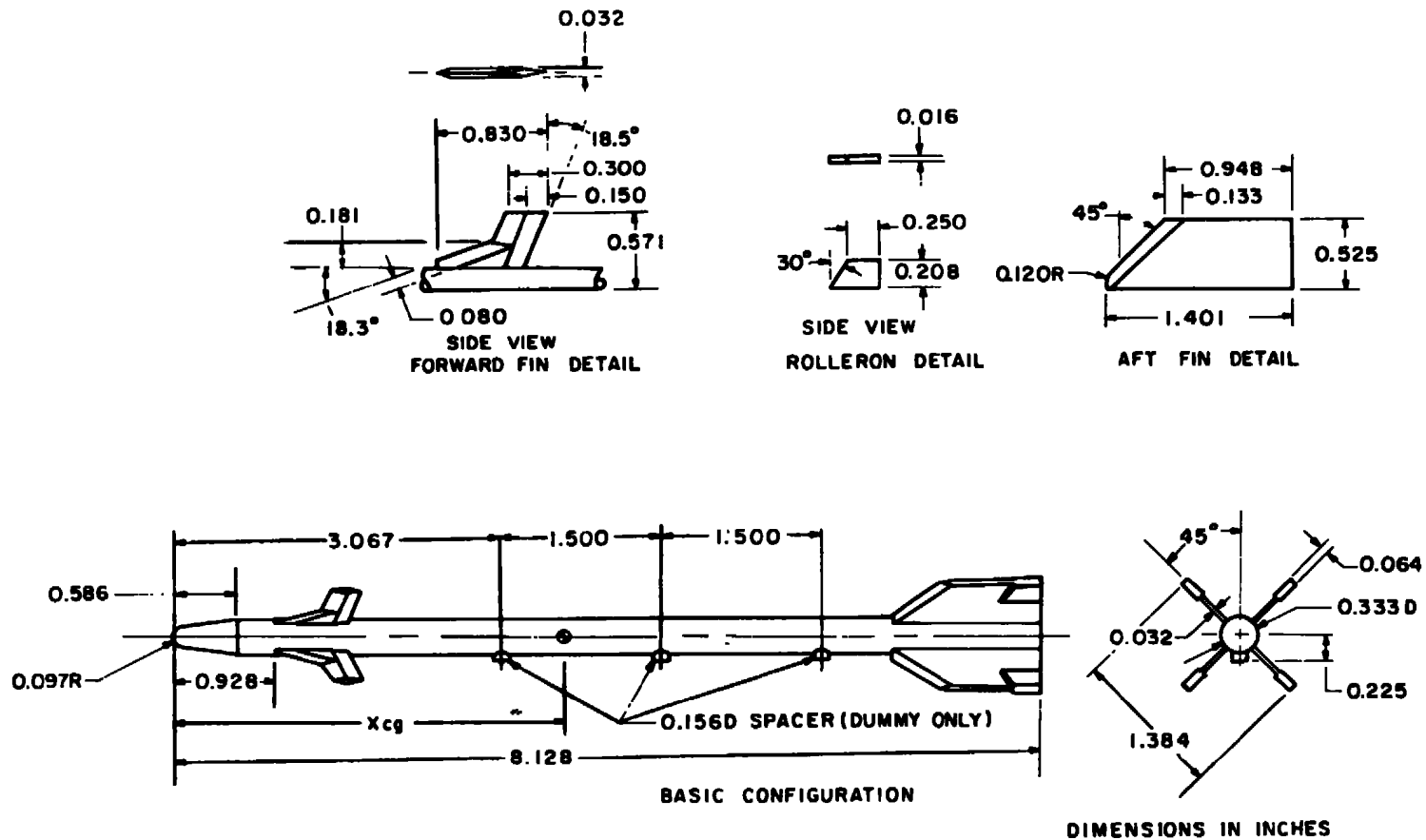
b. Dummy MK-84 LDGP model  
Figure 4. Continued.

X, in.	R, in.	X, in.	R, in.	X, in.	R, in.	X, in.	R, in.
0	0	1.120	0.451	4.520	0.883	14.003	0.577
0.053	0.068	1.253	0.484		CONST DIAM	14.136	0.561
0.120	0.100	1.587	0.554	10.836	0.833		CONST SLOPE
0.186	0.131	1.920	0.611		CONST SLOPE	16.520	0.242
0.320	0.188	2.253	0.660	12.270	0.757	16.587	0.231
0.453	0.242	2.586	0.701	12.336	0.752	16.653	0.220
0.587	0.291	2.920	0.737	12.670	0.721	16.787	0.192
0.720	0.336	3.253	0.770	13.004	0.688	16.920	0.156
0.854	0.377	3.587	0.799	13.337	0.653	17.054	0.097
0.951	0.416		CONST SLOPE	13.670	0.616	17.120	0

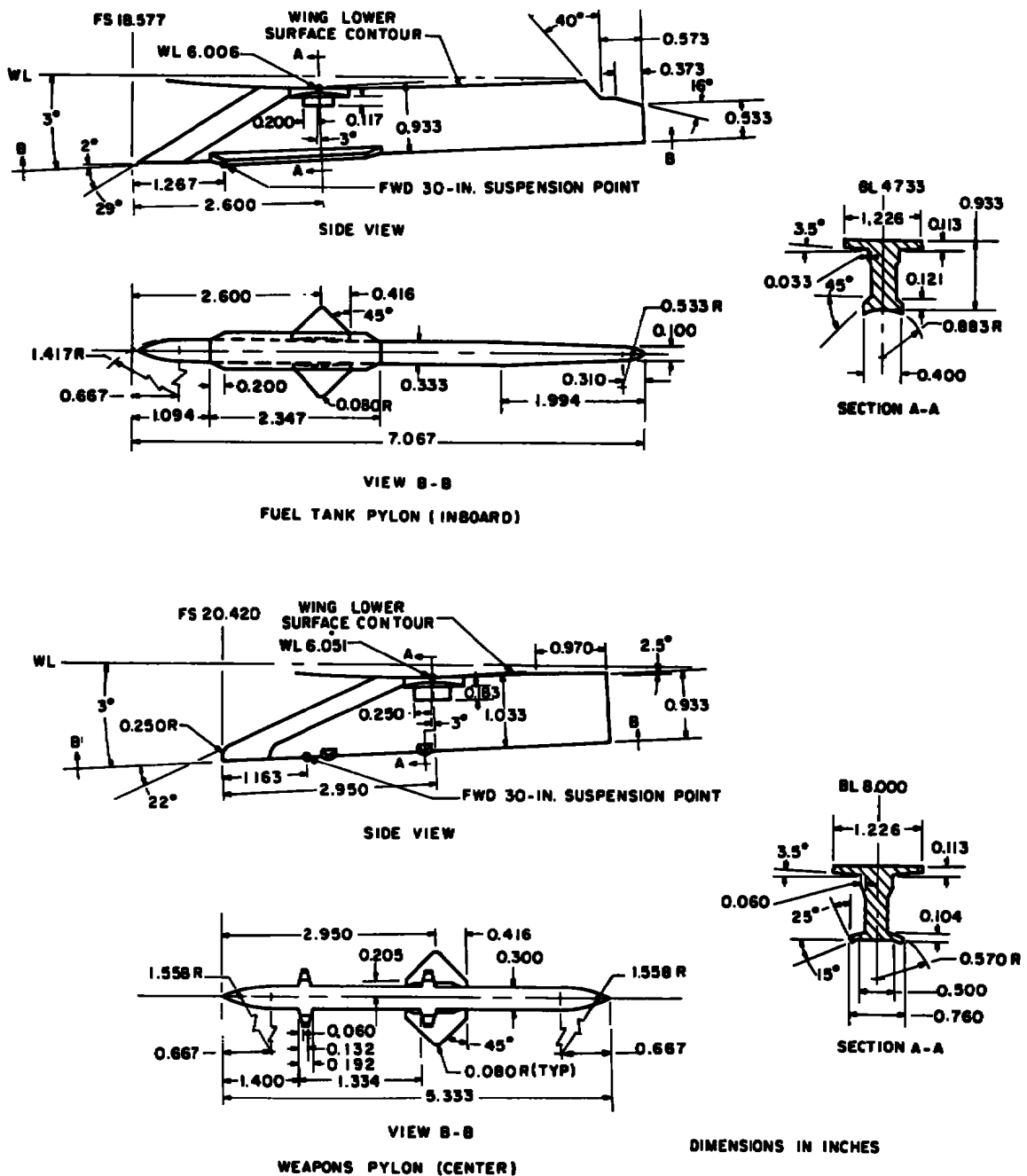


c. 370-gal fuel tank  
Figure 4. Continued.



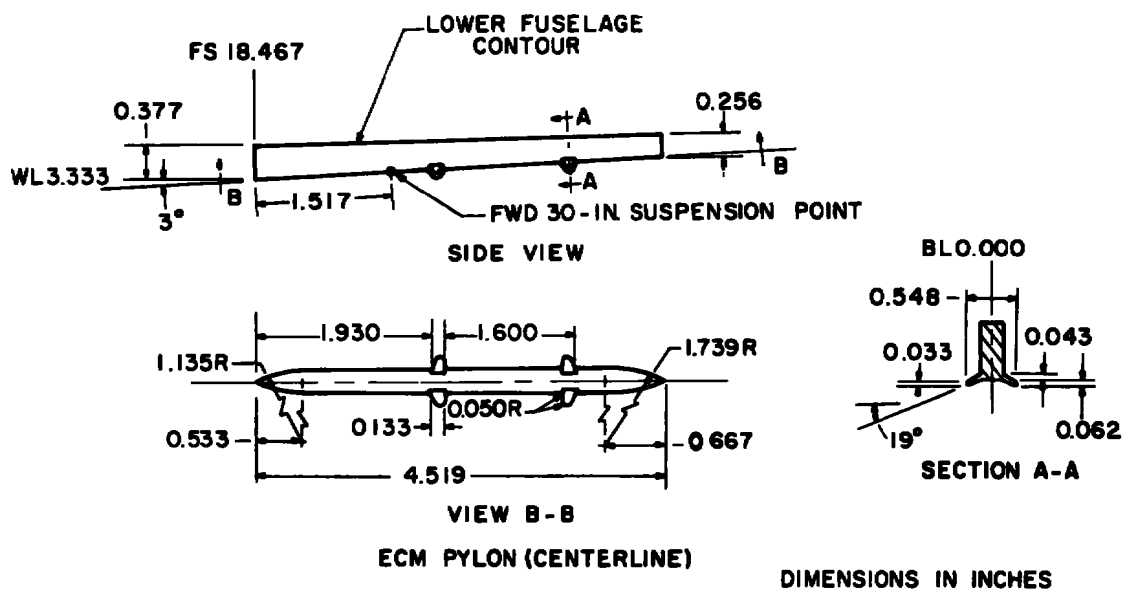


e. AIM-9J missile  
Figure 4. Concluded.

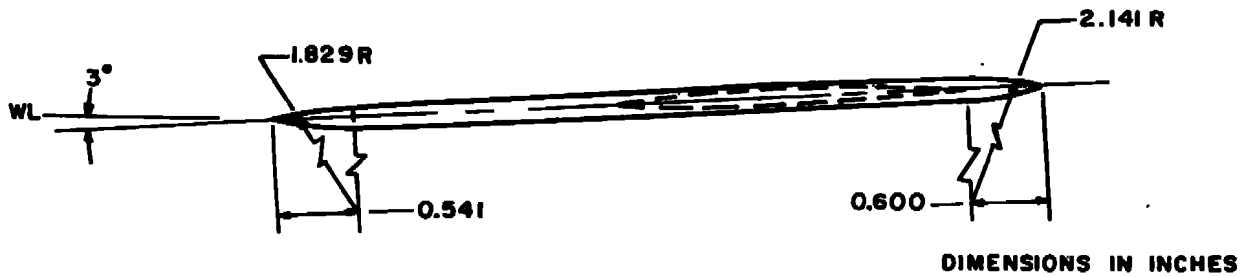
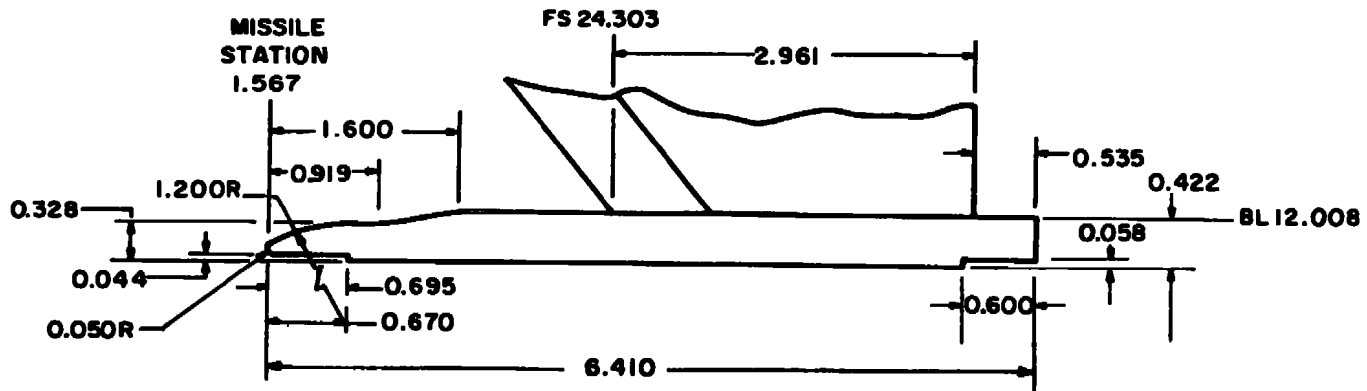


a. Weapons and fuel tank pylons  
Figure 5. F-16 model pylons.

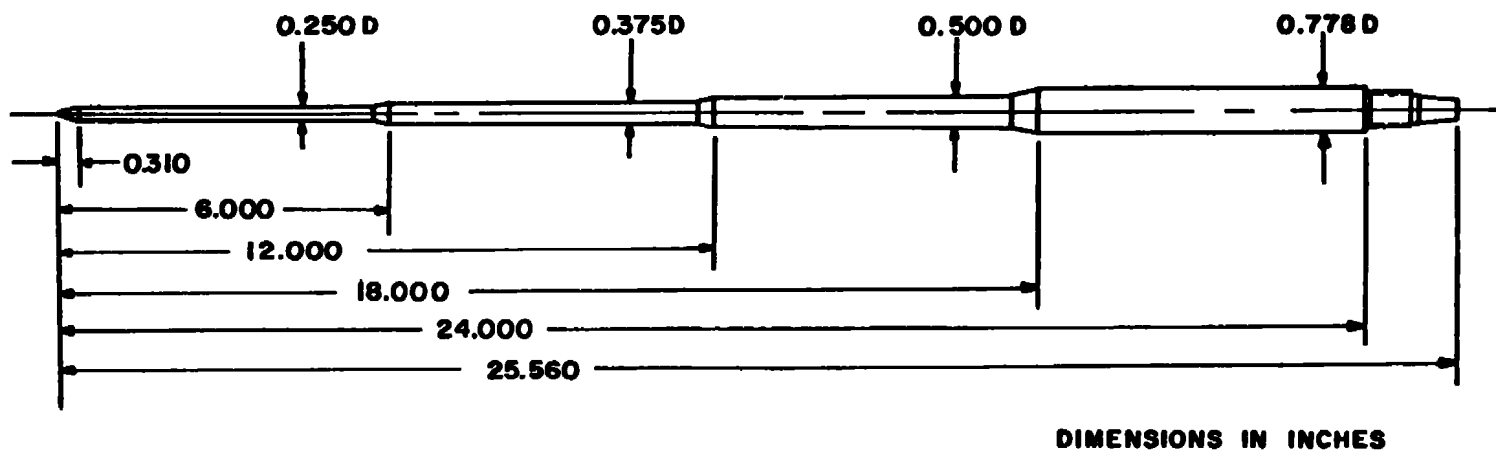




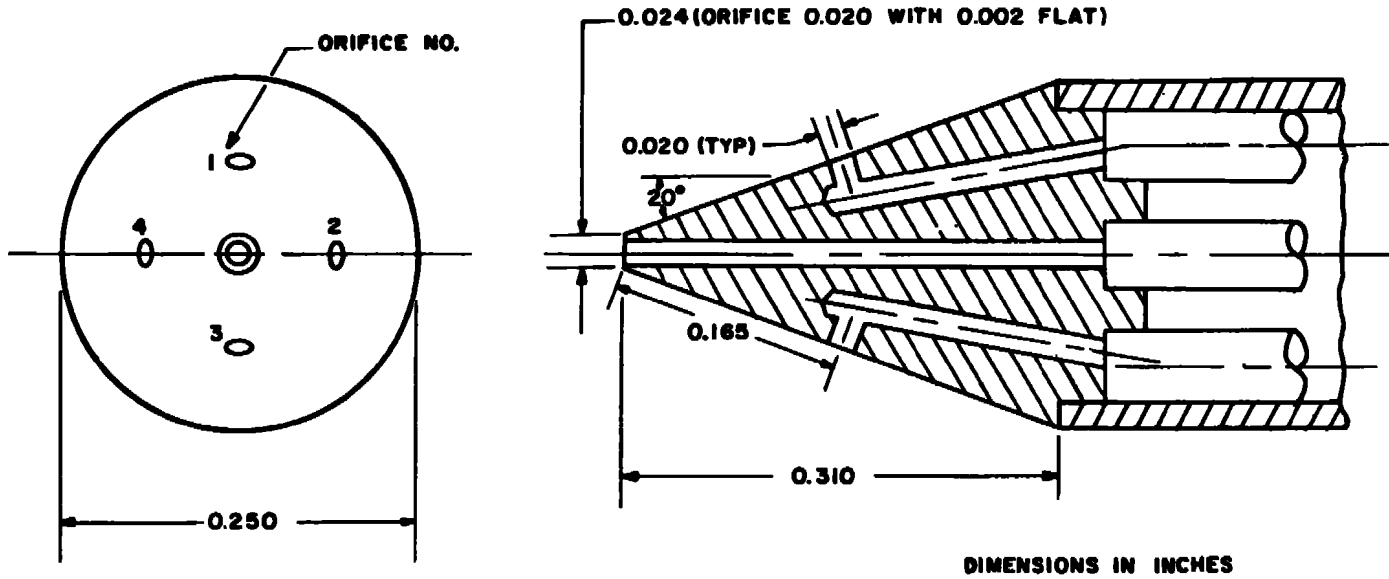
b. ECM pylon  
Figure 5. Continued.



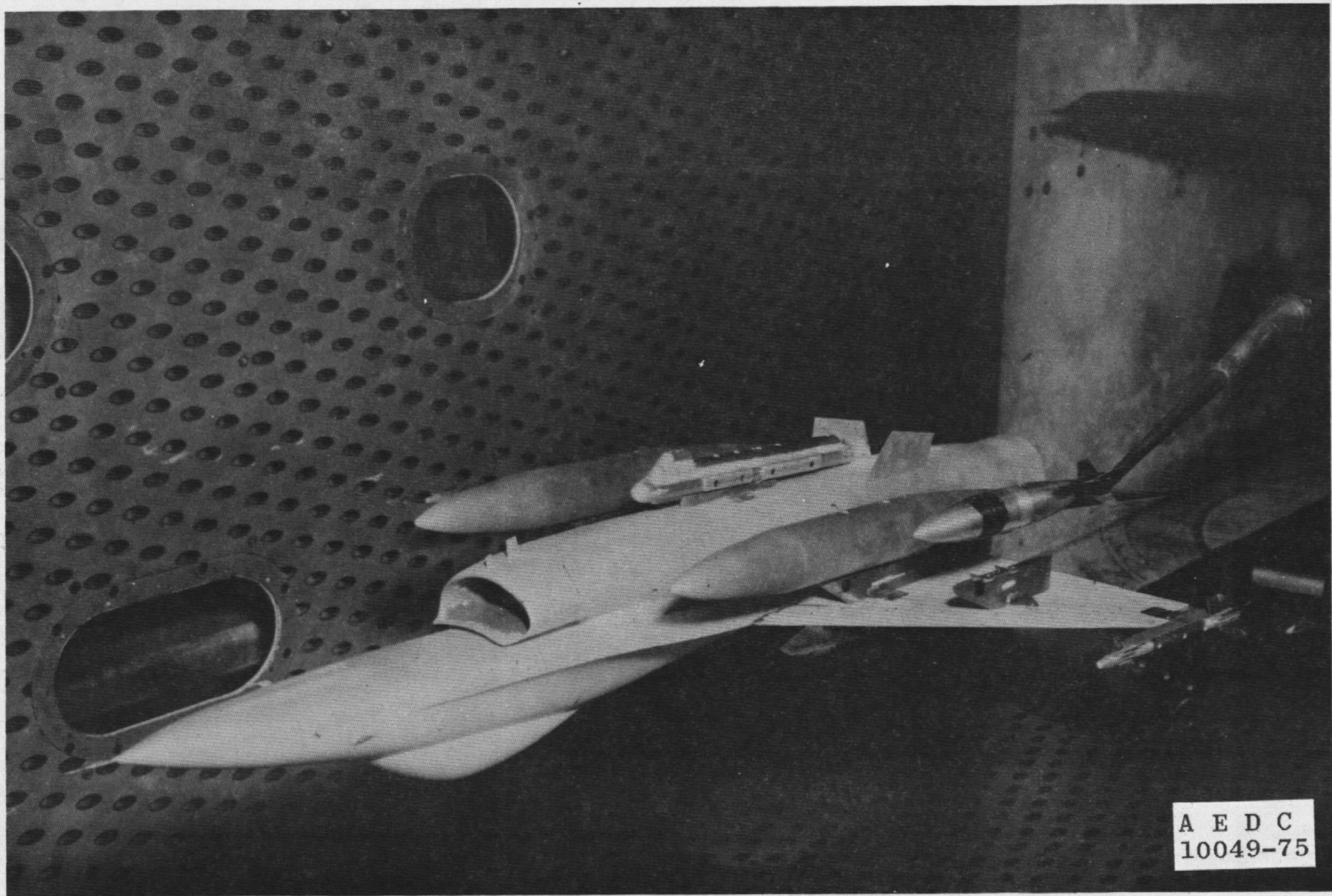
c. AIM-9J wingtip launcher  
Figure 5. Concluded.



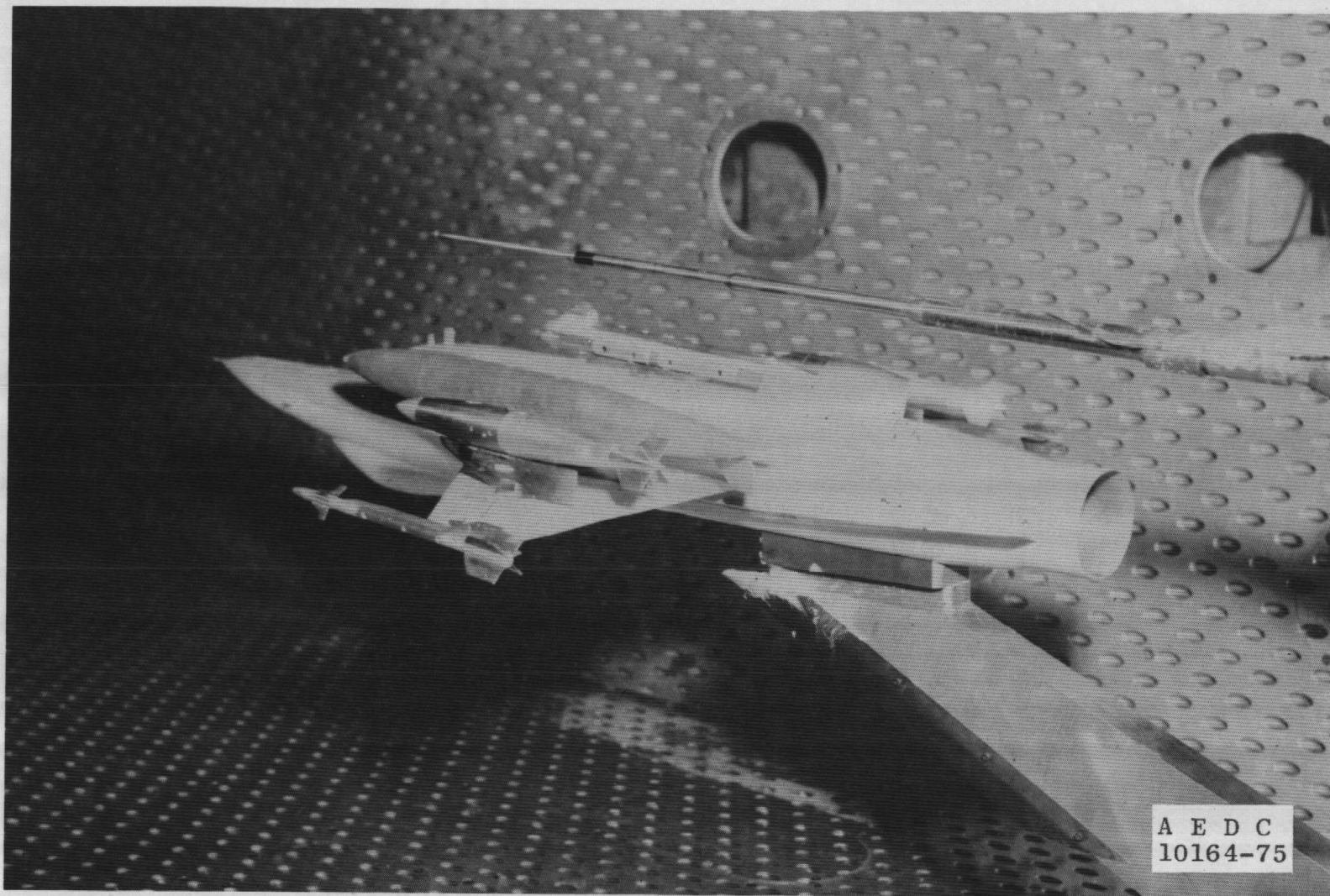
a. Flow-field probe  
Figure 6. Details of the 40-deg conical pressure probe.



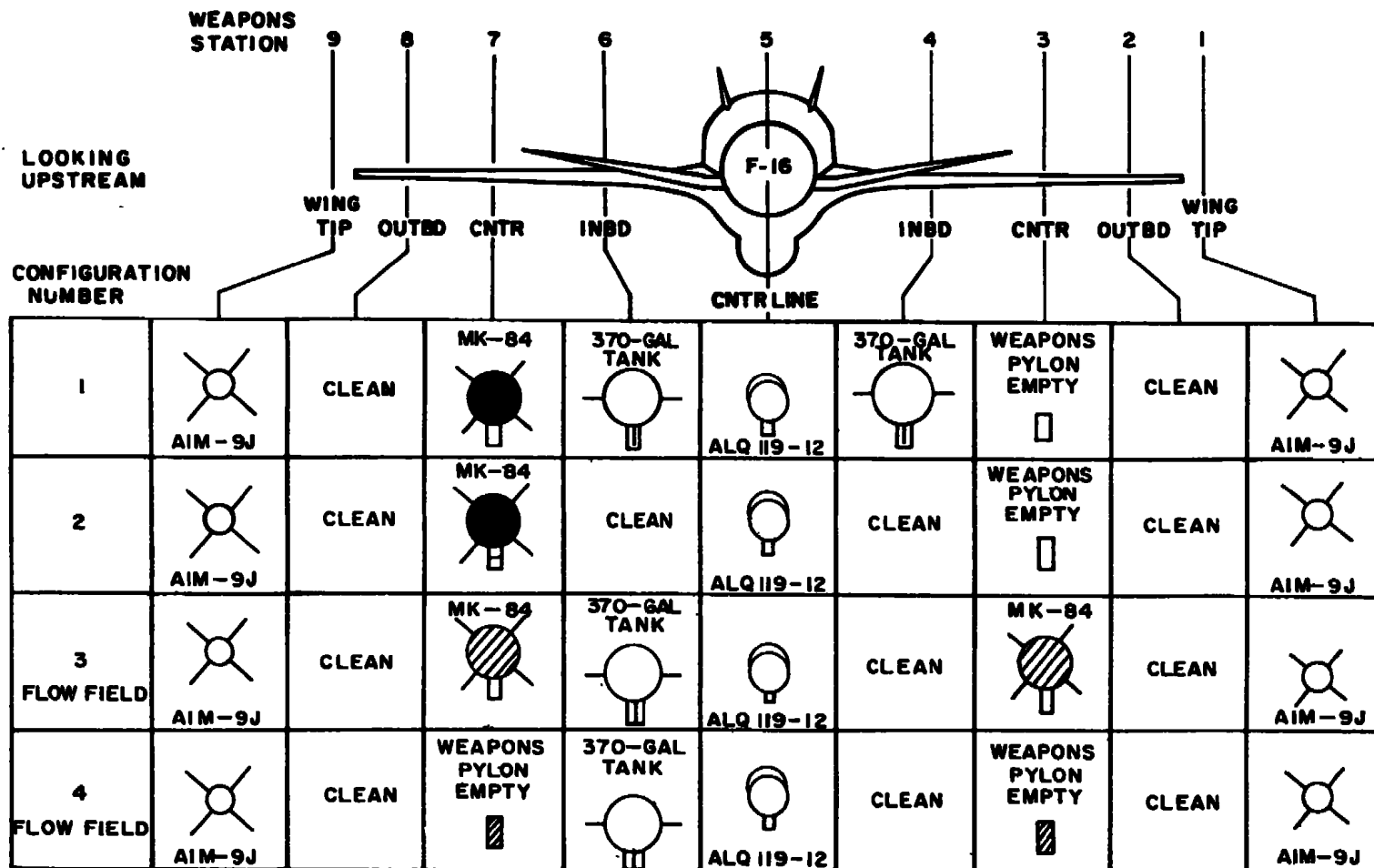
b. Probe tip  
Figure 6. Concluded.



a. Aerodynamic loads and trajectory installation  
Figure 7. Installation photographs.



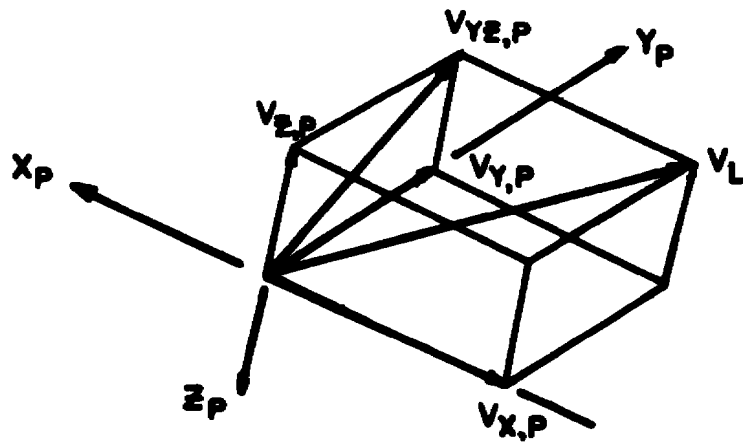
b. Flow-field installation  
Figure 7. Concluded.



● - DENOTES METRIC STORE  
○ - DENOTES DUMMY STORE

CLEAN DENOTES PYLON REMOVED  
EMPTY DENOTES NO STORE ON PYLON  
CROSS HATCH DENOTES SURVEY STATION

Figure 8. Aircraft configurations.

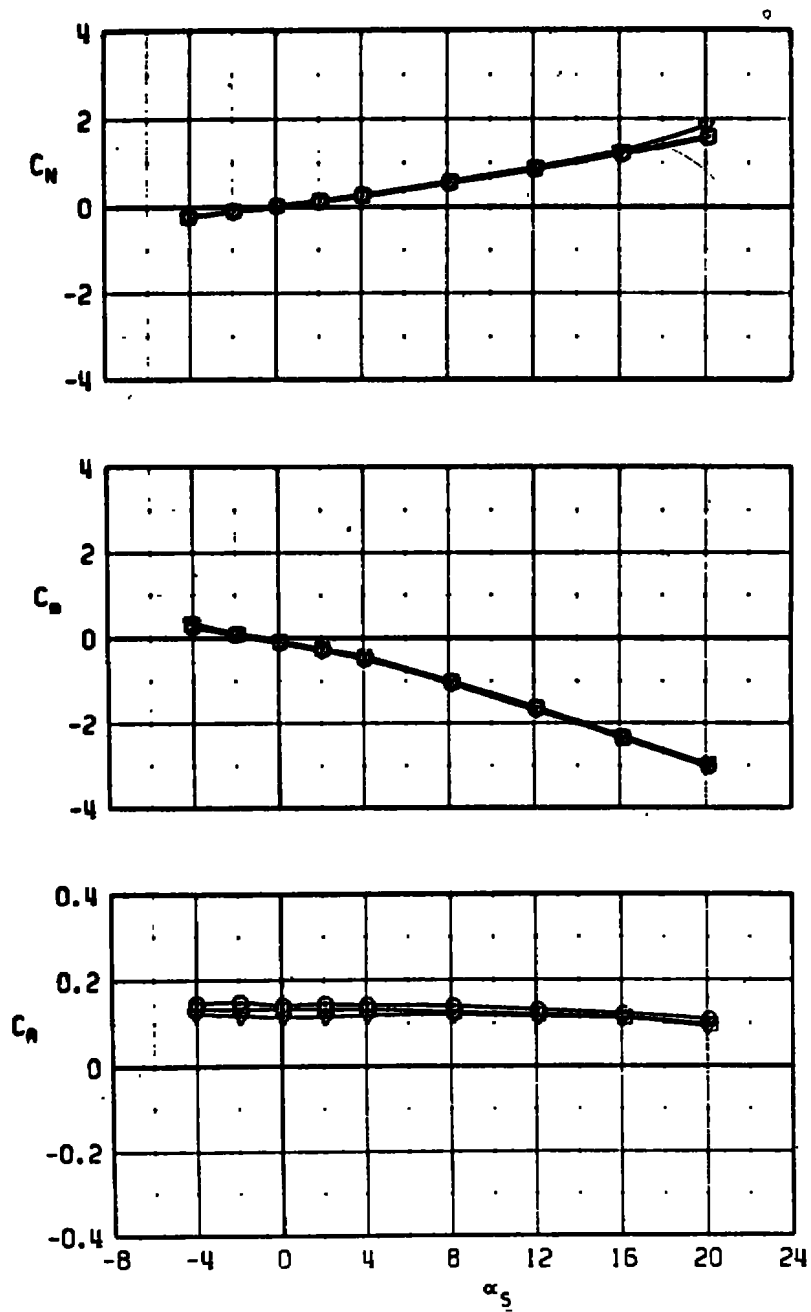


Note: Pylon axis system origin  
 $(X_p = Y_p = Z_p = 0)$  at forward 30-in.  
 suspension point of each pylon (see Fig. 5).

Figure 9. Axis system defining direction and velocity vectors  
 for flow-field measurements.



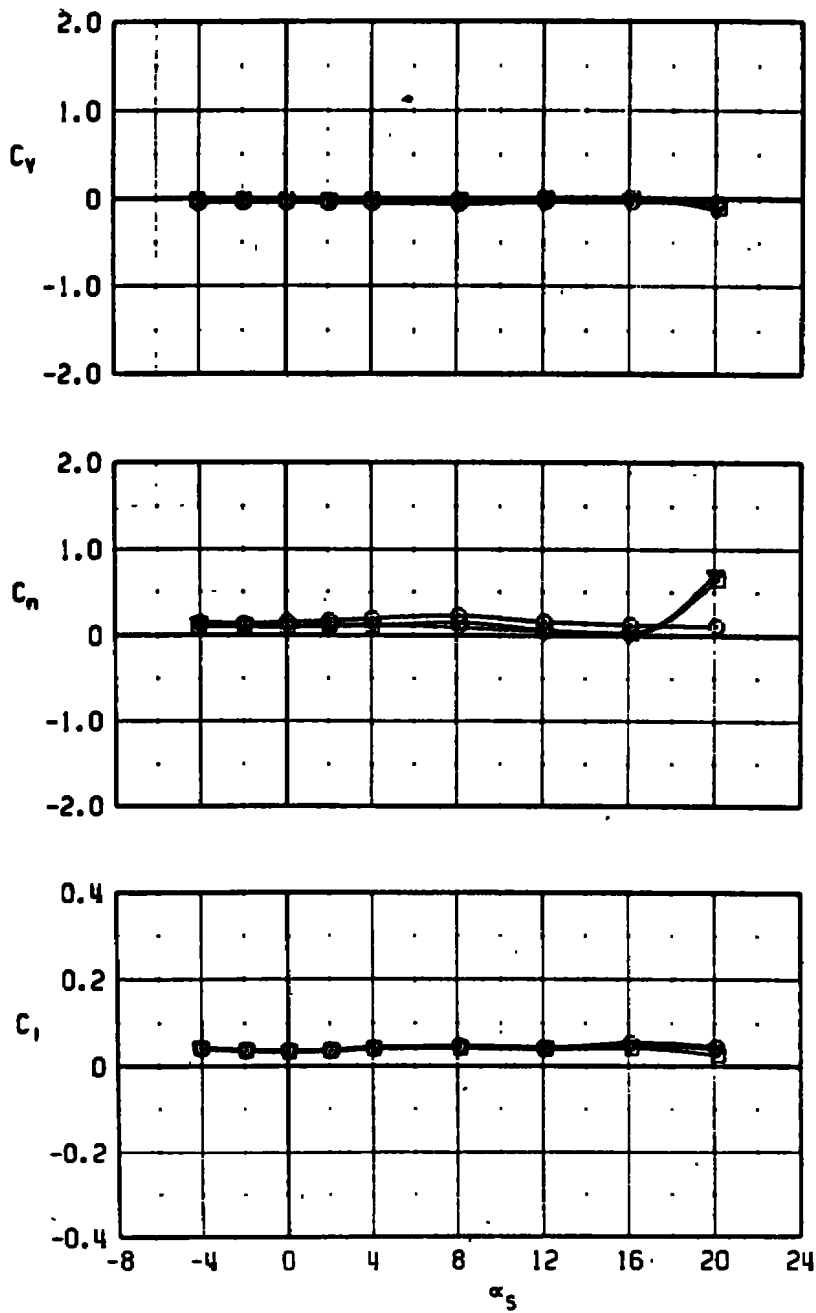
SYM	$M_\infty$	$\alpha_p$	CONFIG	$\delta_{LE}$
○	0.40	NA	0	NA
□	0.60	NA	0	NA
▽	0.80	NA	0	NA



a.  $M_\infty = 0.4, 0.6, \text{ and } 0.8$

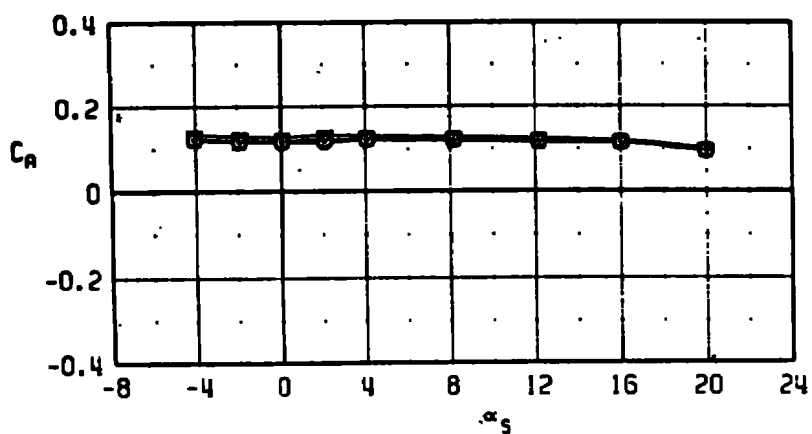
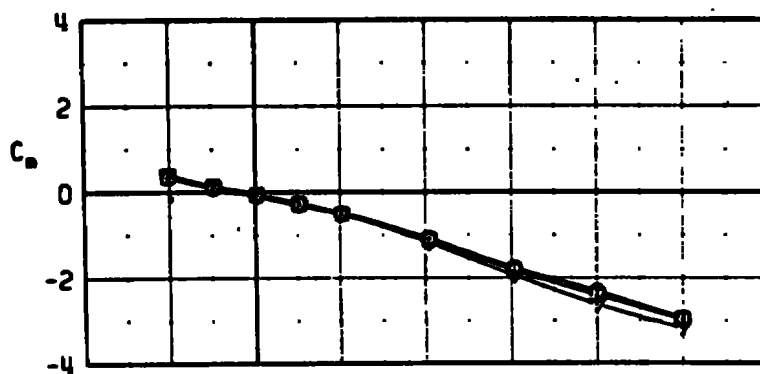
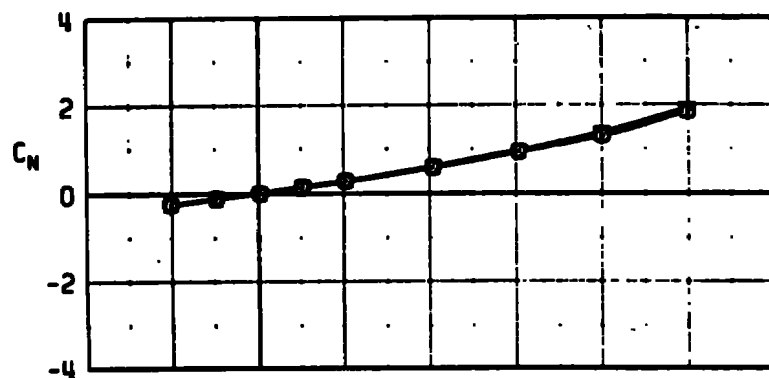
Figure 10. MK-84 LDGP free-stream aerodynamic coefficients.

SYM	$M_\infty$	$\alpha_p$	CONFIG	$\delta_{LE}$
○	0.40	NA	0	NA
□	0.60	NA	0	NA
▽	0.80	NA	0	NA



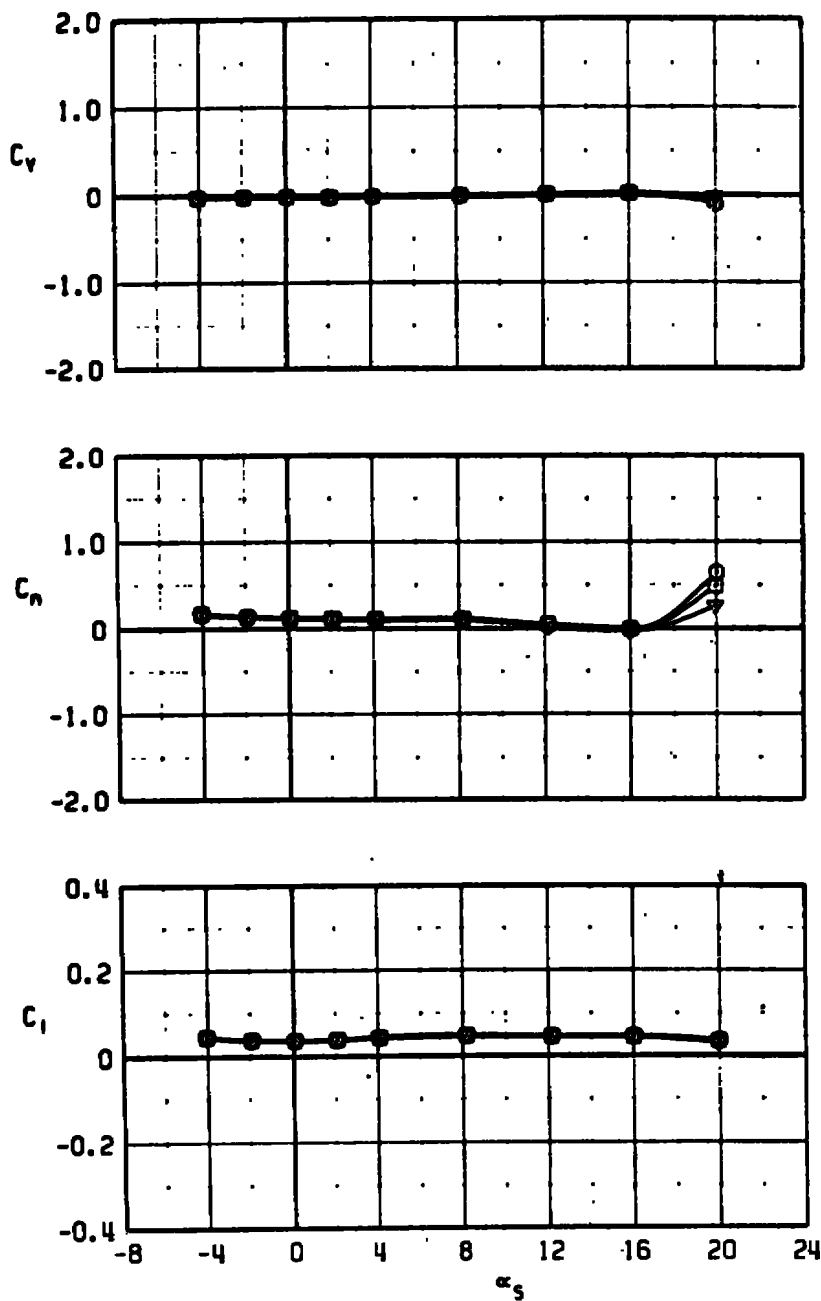
a. Concluded  
Figure 10. Continued.

SYM	$M_\infty$	$\alpha_p$	CONFIG	$\delta_{LE}$
○	0.85	NA	0	NA
□	0.90	NA	0	NA
▽	0.95	NA	0	NA



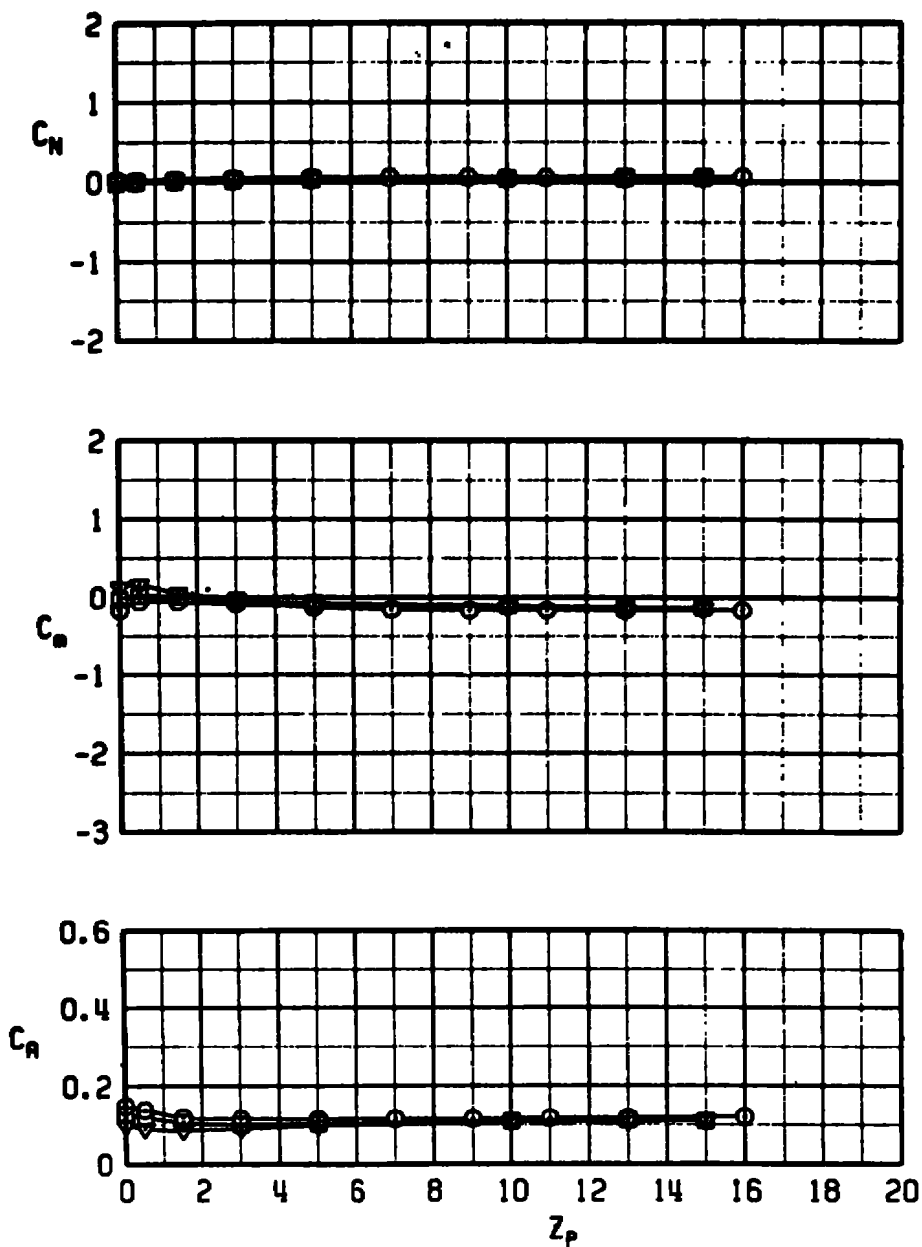
b.  $M_\infty = 0.85, 0.90, \text{ and } 0.95$   
Figure 10. Continued.

SYM	$M_\infty$	$\alpha_p$	CONFIG	$\delta_{LE}$
○	0.85	NA	0	NA
□	0.90	NA	0	NA
▽	0.95	NA	0	NA



b. Concluded  
Figure 10. Concluded.

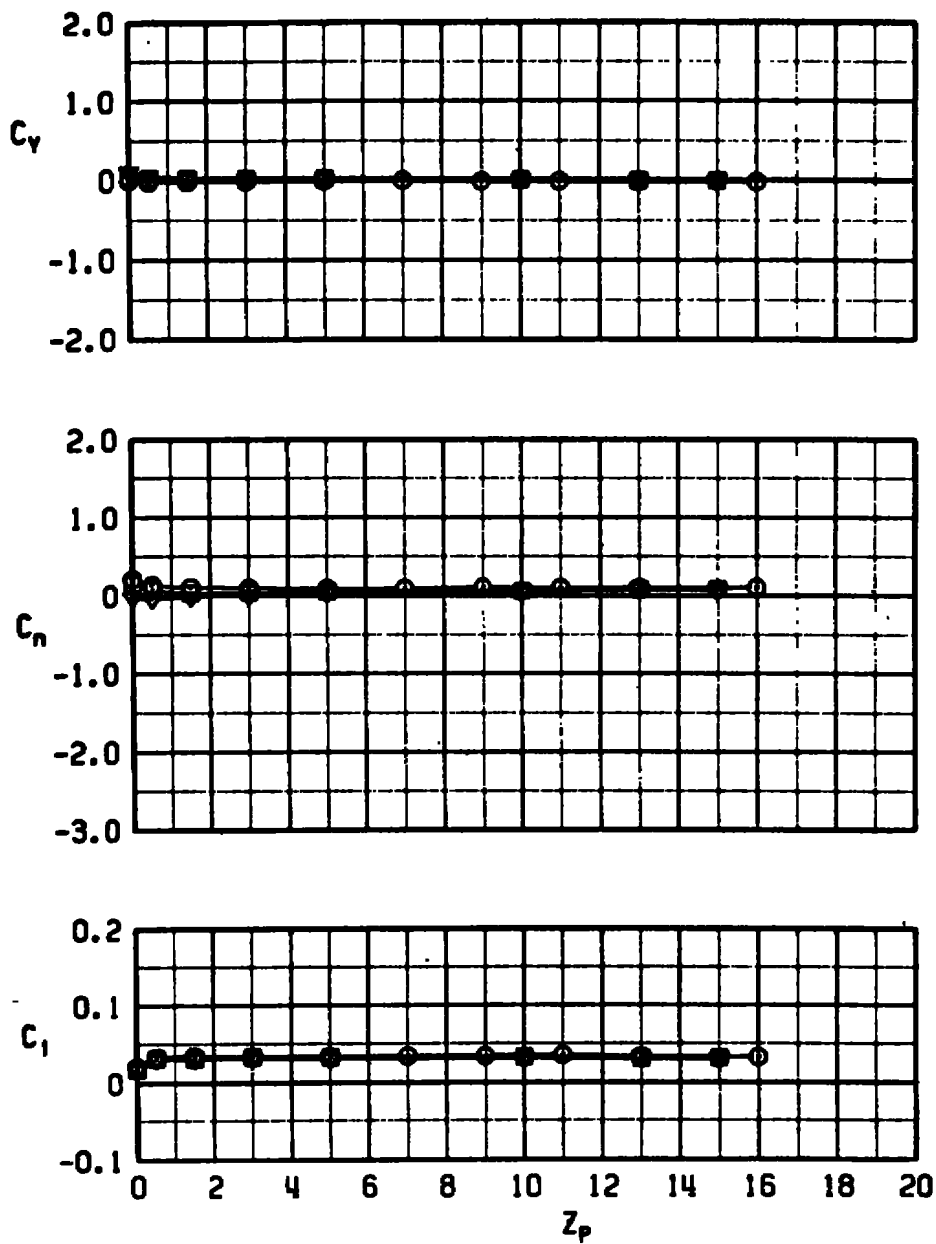
SYM	$M_\infty$	$\alpha_p$	CONFIG	$L/L$
○	0.60	4	1	0
□	0.60	4	1	4
▼	0.60	4	1	15



a.  $\alpha_p = 4$

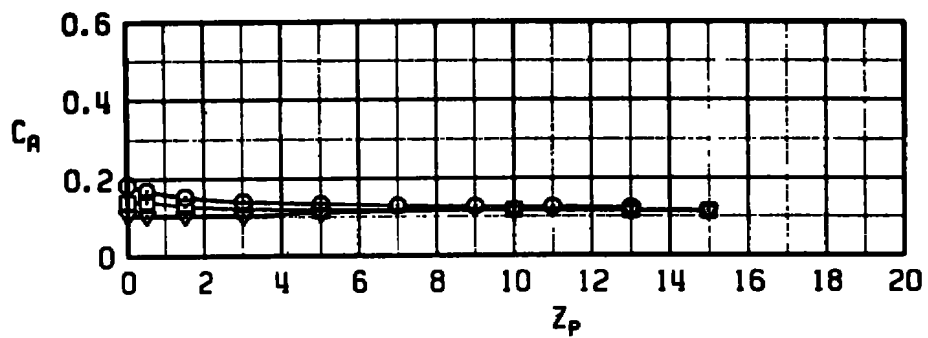
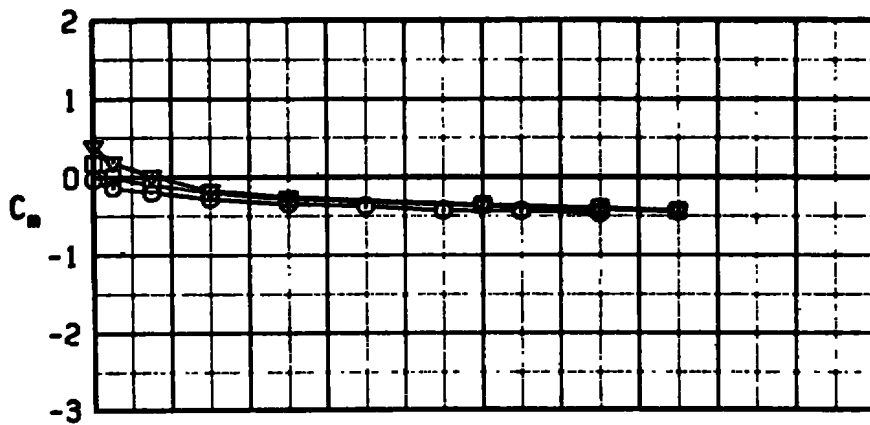
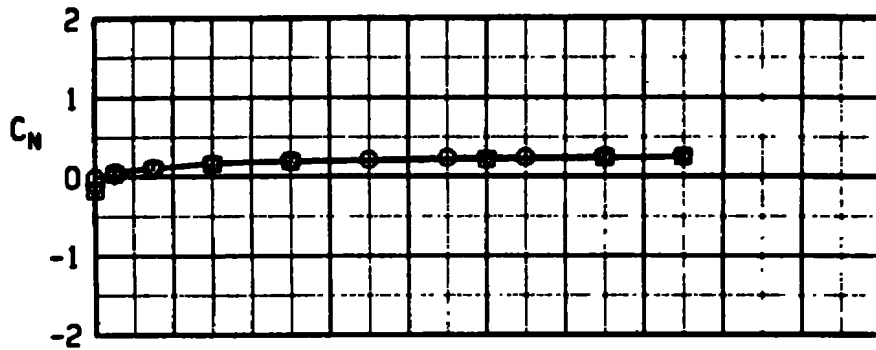
Figure 11. Aerodynamic coefficients obtained in the F-16 parent flow field.

SYM	$M_\infty$	$\alpha_p$	CONFIG	$z_{pL}$
○	0.60	4	1	0
□	0.60	4	1	4
▼	0.60	4	1	15



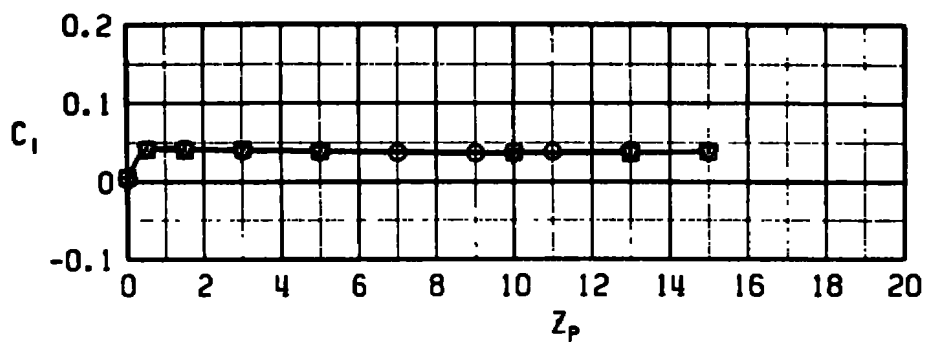
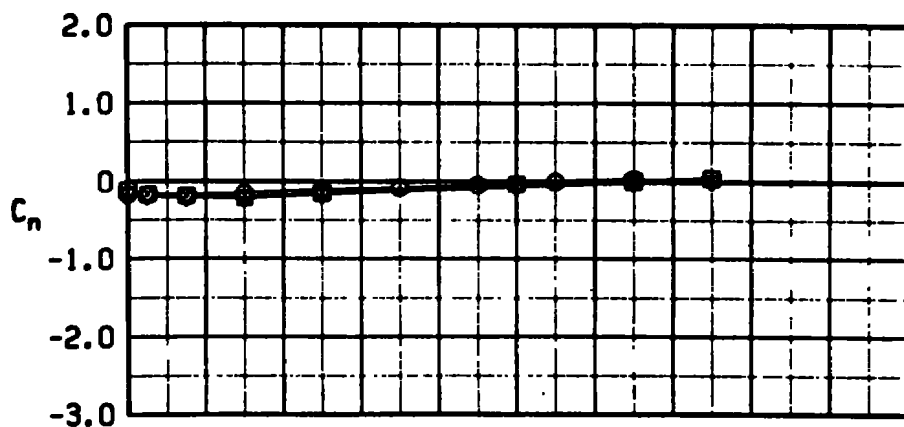
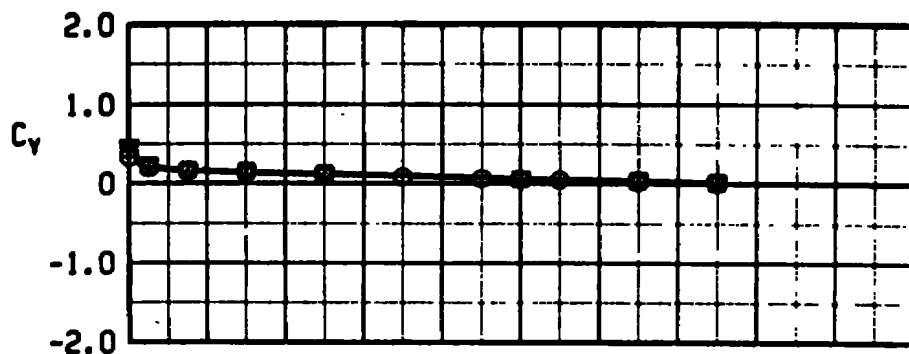
a. Concluded  
Figure 11. Continued.

SYM	$M_\infty$	$a_p$	CONFIG	$L/E$
○	0.6	8	1	0
□	0.6	8	1	4
▽	0.6	8	1	15



b.  $a_p = 8$   
Figure 11. Continued.

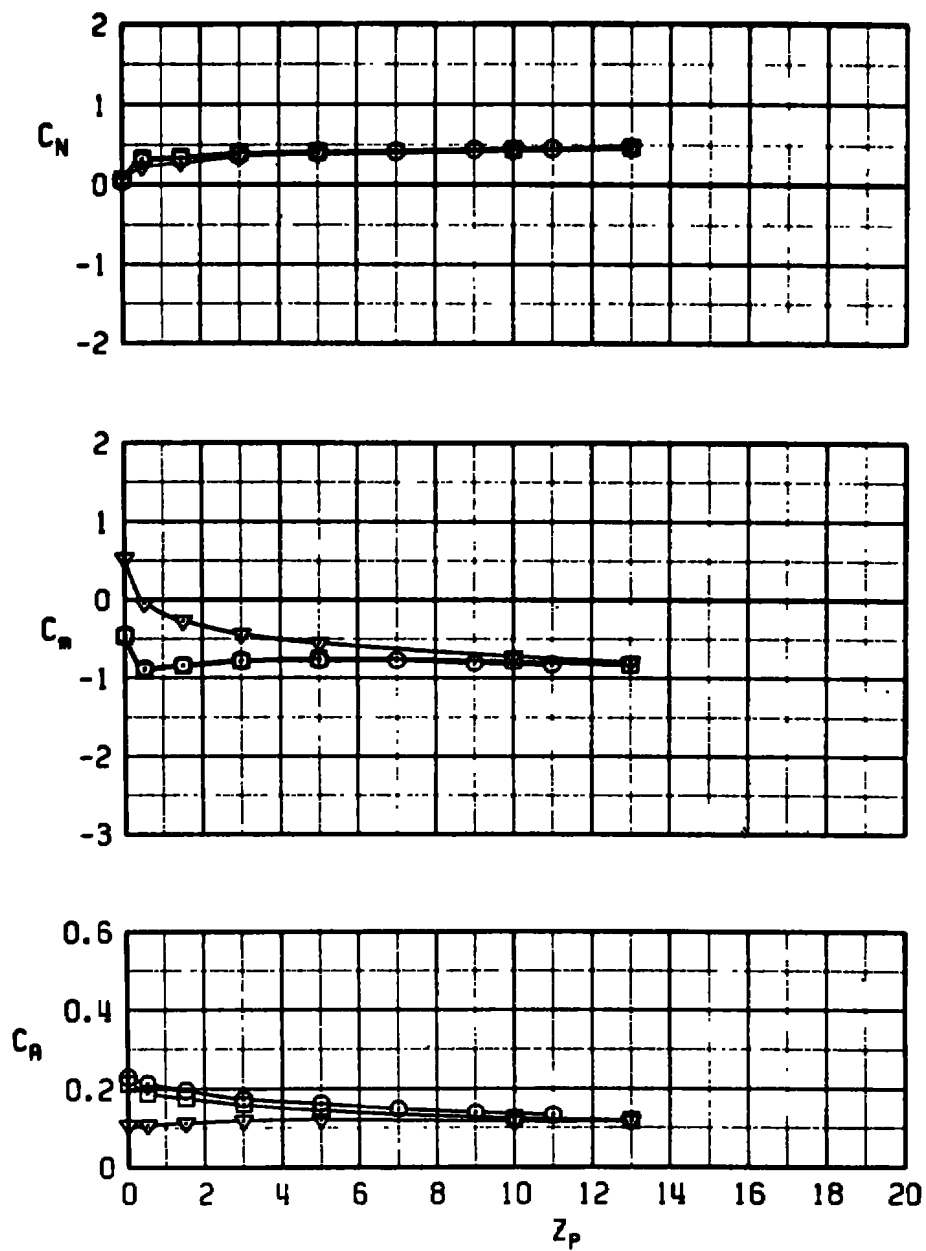
SYM	$M_\infty$	$\alpha_p$	CONFIG	$h_L$
○	0.6	8	1	0
□	0.6	8	1	4
▽	0.6	8	1	15



b. Concluded  
Figure 11. Continued.

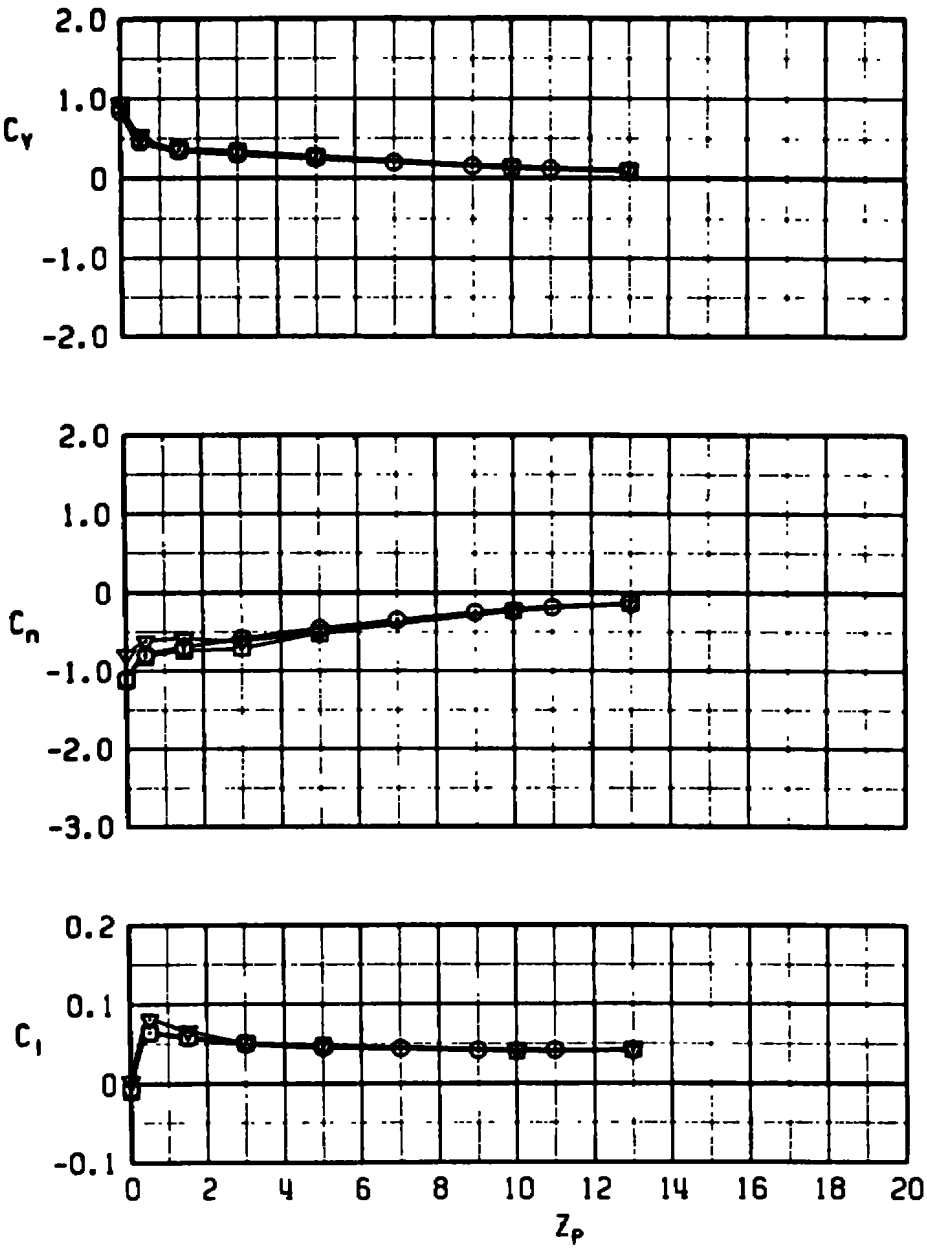


SYM	$M_\infty$	$a_p$	CONFIG	$\delta_{LE}$
○	0.6	12	1	0
□	0.6	12	1	4
▽	0.6	12	1	15



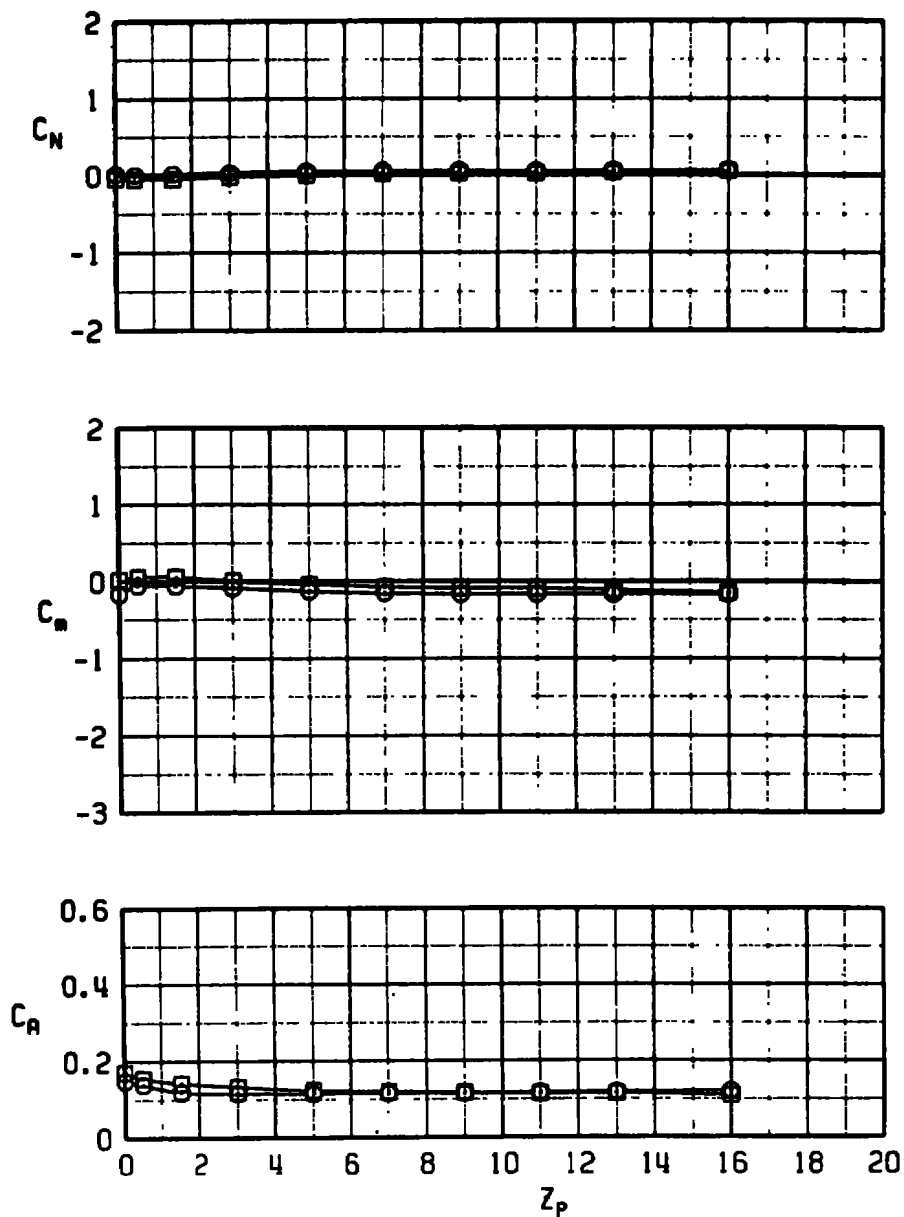
c.  $a_p = 12$   
Figure 11. Continued.

SYM	M <sub>∞</sub>	α <sub>p</sub>	CONFIG	h <sub>LE</sub>
○	0.6	12	1	0
□	0.6	12	1	4
▽	0.6	12	1	15



c. Concluded  
Figure 11. Concluded.

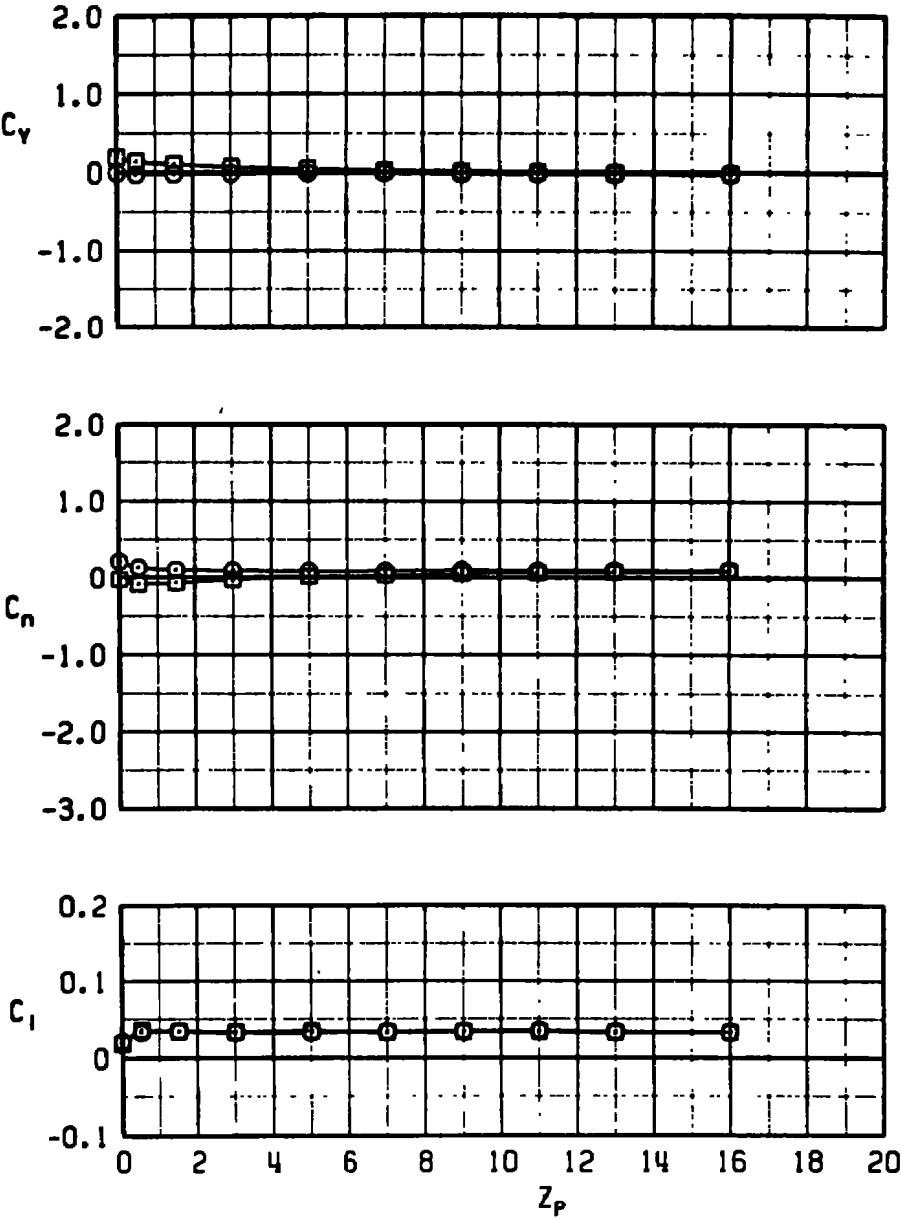
SYM	$M_\infty$	$\alpha_p$	CONFIG	$h_{LE}$
⊙	0.60	4	1	0
⊠	0.60	4	2	0



a.  $\alpha_p = 4$

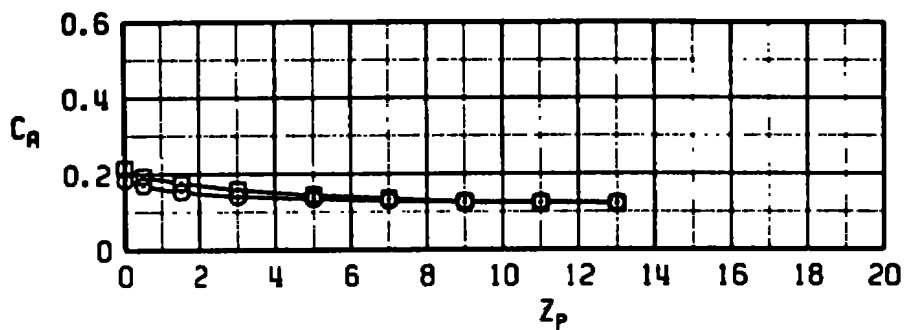
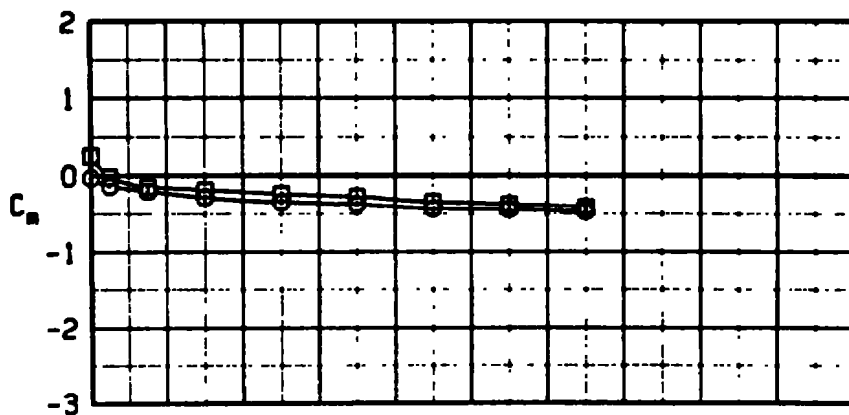
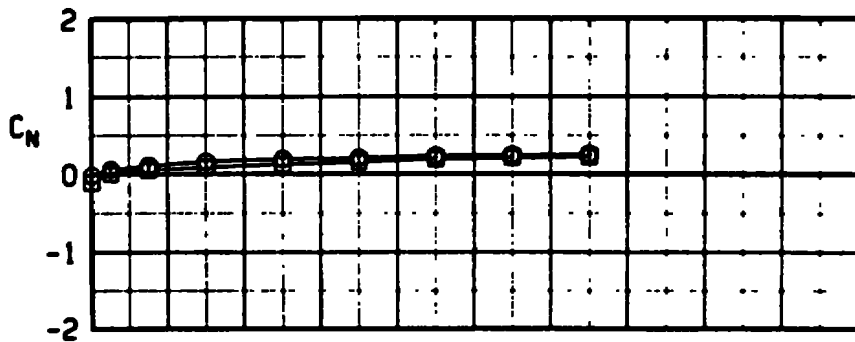
Figure 12. Effects of the removal of the 370-gal fuel tank on the aerodynamic coefficients at  $M_\infty = 0.6$ .

SYM	$M_\infty$	$\alpha_p$	CONFIG	$h_{LE}$
○	0.60	4	1	0
□	0.60	4	2	0



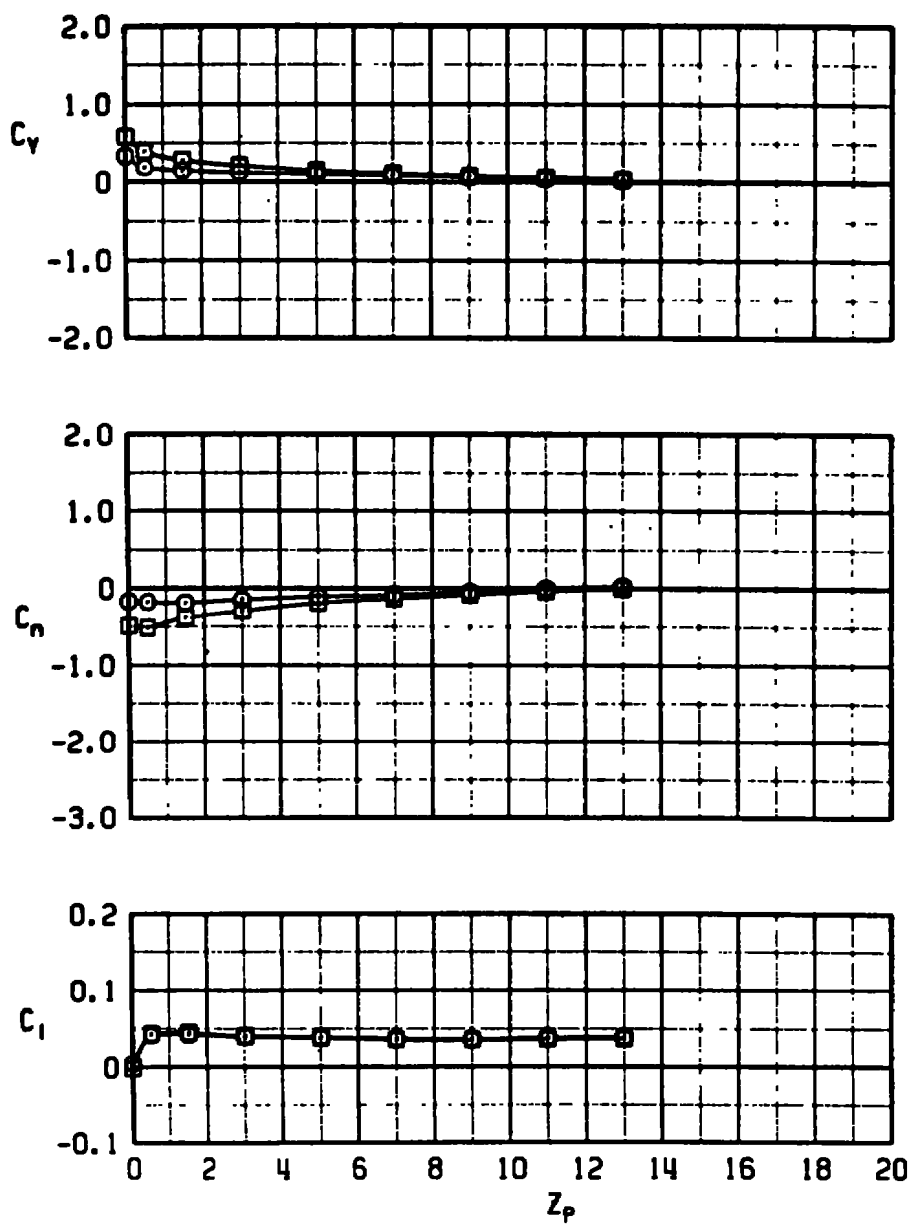
a. Concluded  
Figure 12. Continued.

SYM	$M_\infty$	$\alpha_p$	CONFIG	$b_{LE}$
○	0.60	8	1	0
□	0.60	8	2	0



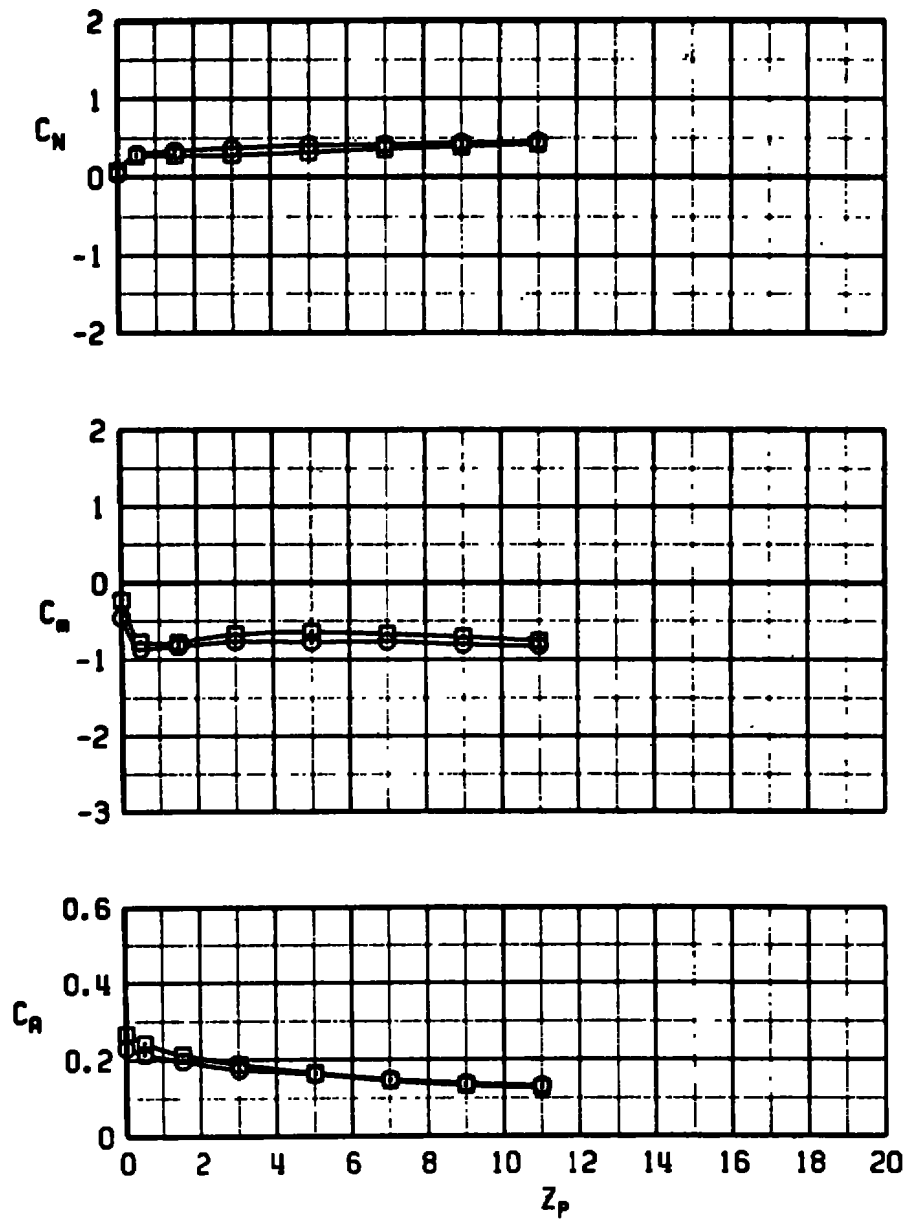
b.  $\alpha_p = 8$   
Figure 12. Continued.

SYM	$M_\infty$	$\alpha_p$	CONFIG	$h_{LE}$
○	0.60	8	1	0
□	0.60	8	2	0



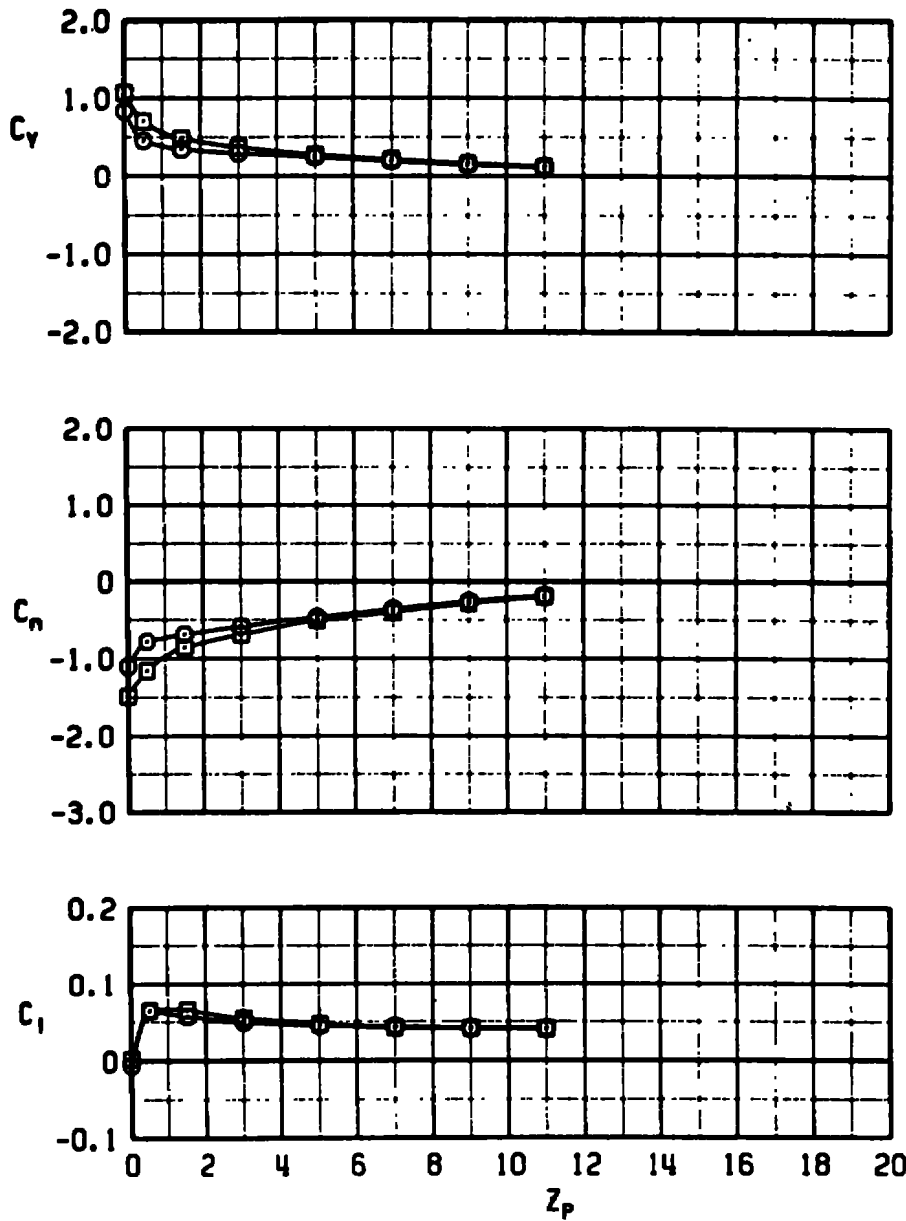
b. Concluded  
Figure 12. Continued.

SYM	$M_\infty$	$a_p$	CONFIG	$h_L$
○	0.60	12	1	0
□	0.60	12	2	0



c.  $a_p = 12$   
Figure 12. Continued.

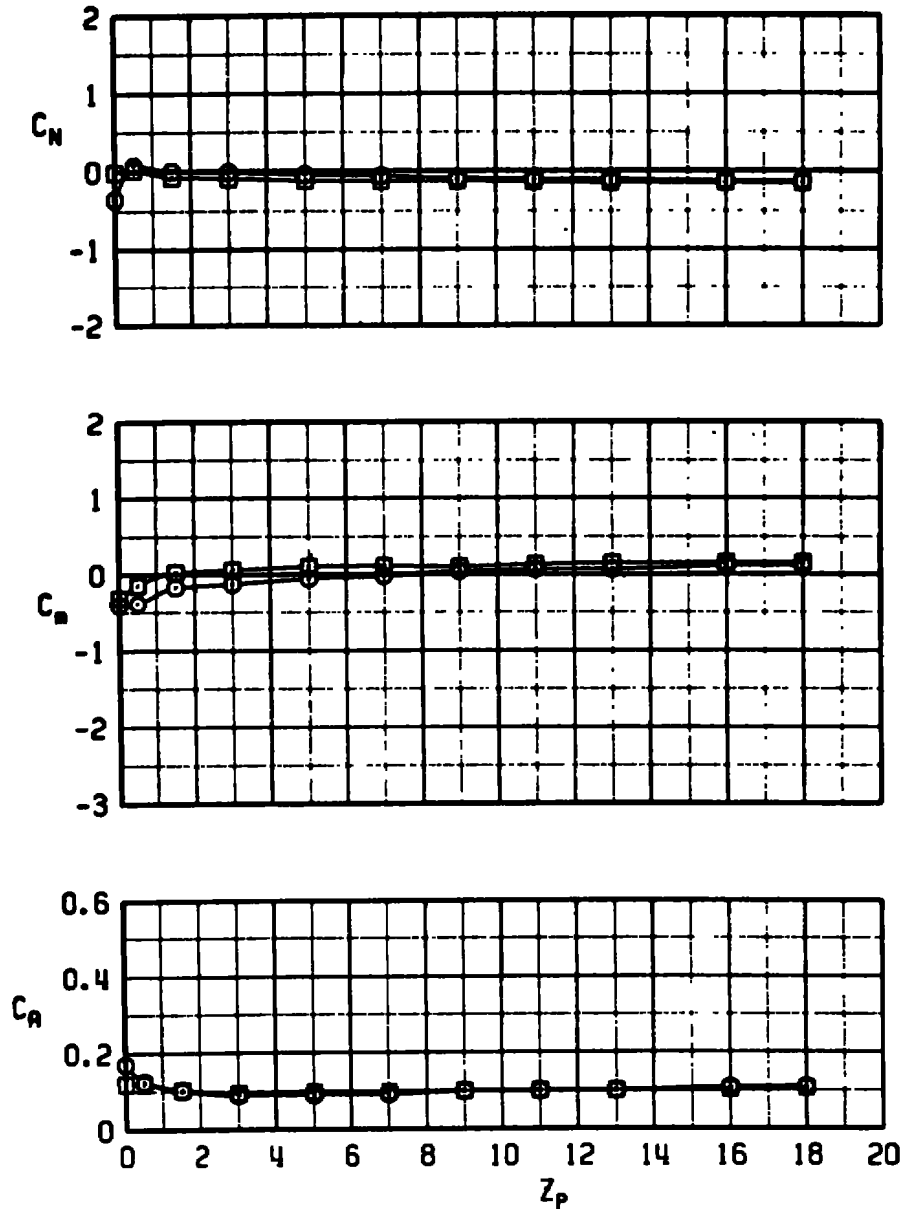
SYM	$M_\infty$	$\alpha_p$	CONFIG	$\lambda_{LE}$
⊖	0.60	12	1	0
⊠	0.60	12	2	0



c. Concluded  
Figure 12. Concluded.



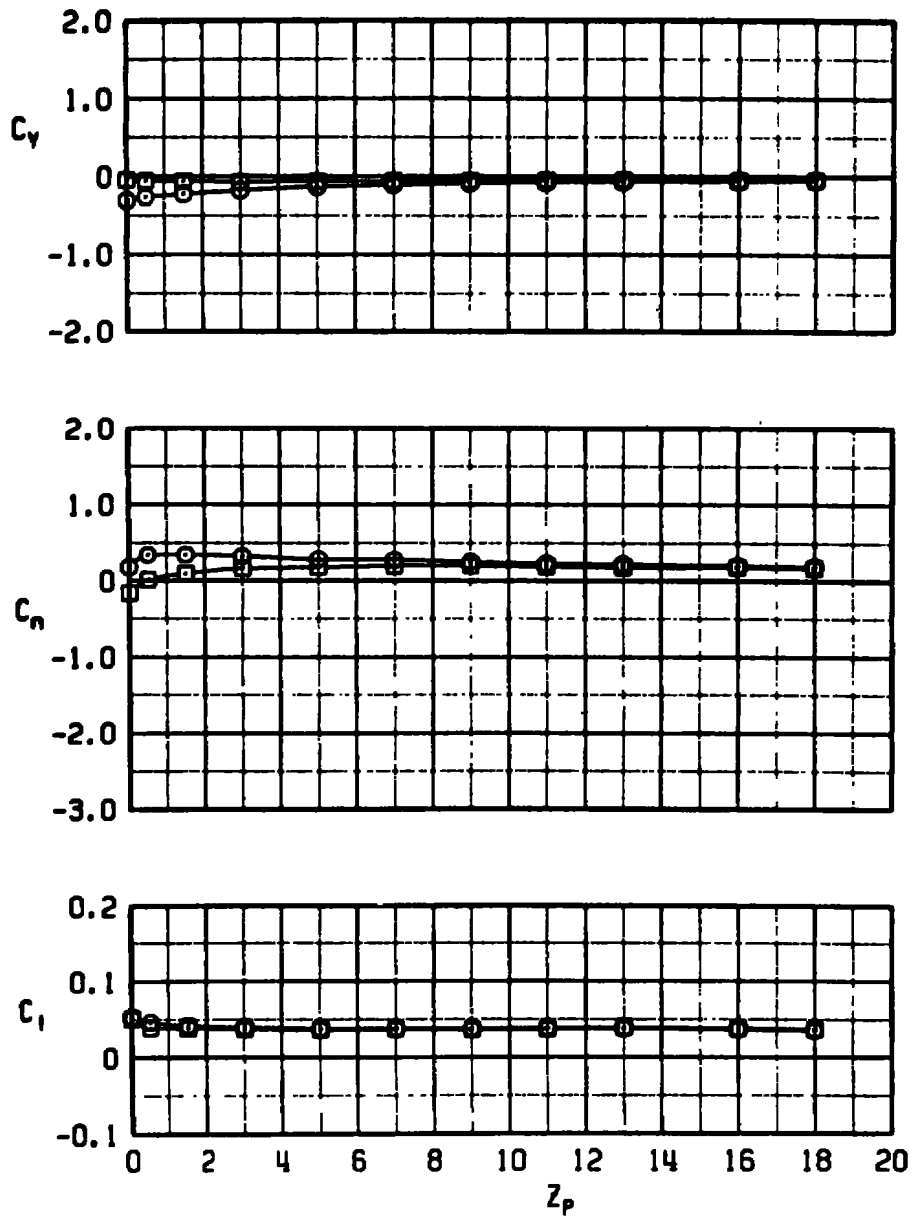
SYM	$M_\infty$	$\alpha_p$	CONFIG	$\delta_{LE}$
○	0.80	0	1	0
□	0.80	0	2	0



a.  $\alpha_p = 0$

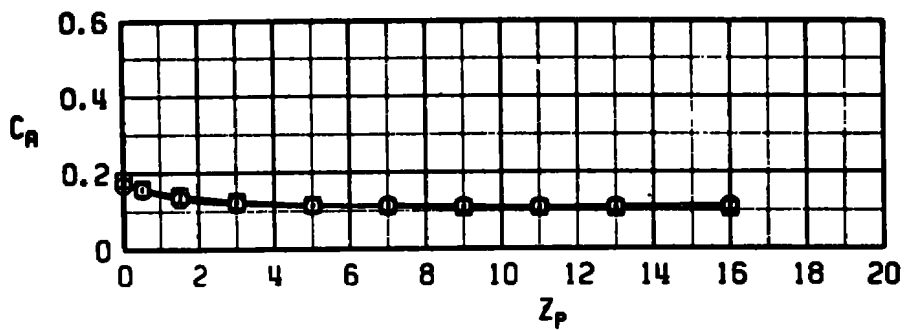
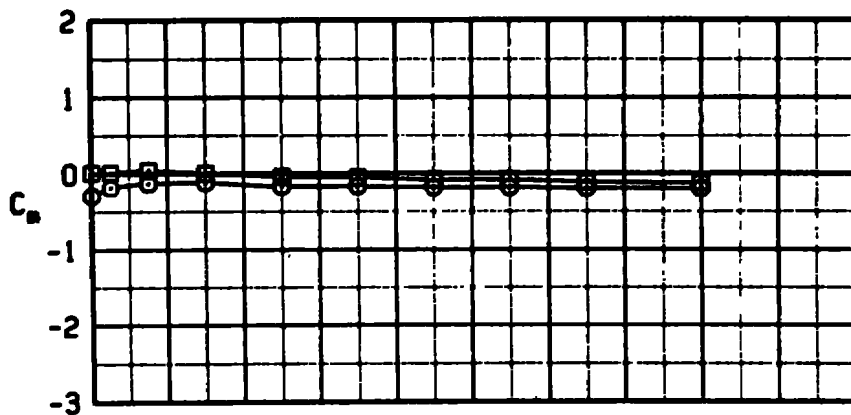
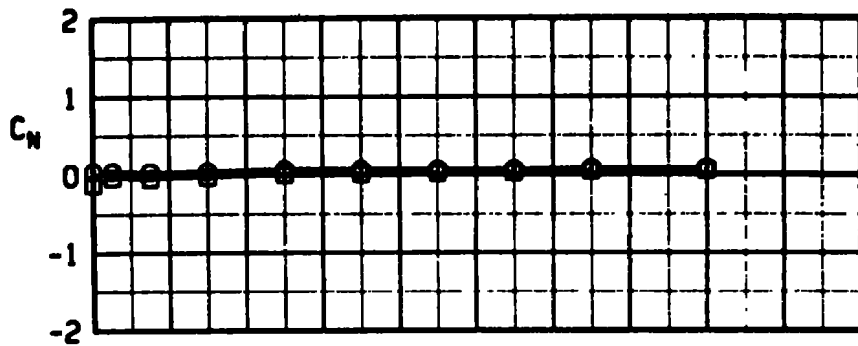
Figure 13. Effects of the removal of the 370-gal fuel tank on the aerodynamic coefficients at  $M_\infty = 0.8$ .

SYM	$M_\infty$	$\alpha_p$	CONFIG	$\beta_{LE}$
○	0.80	0	1	0
□	0.60	0	2	0



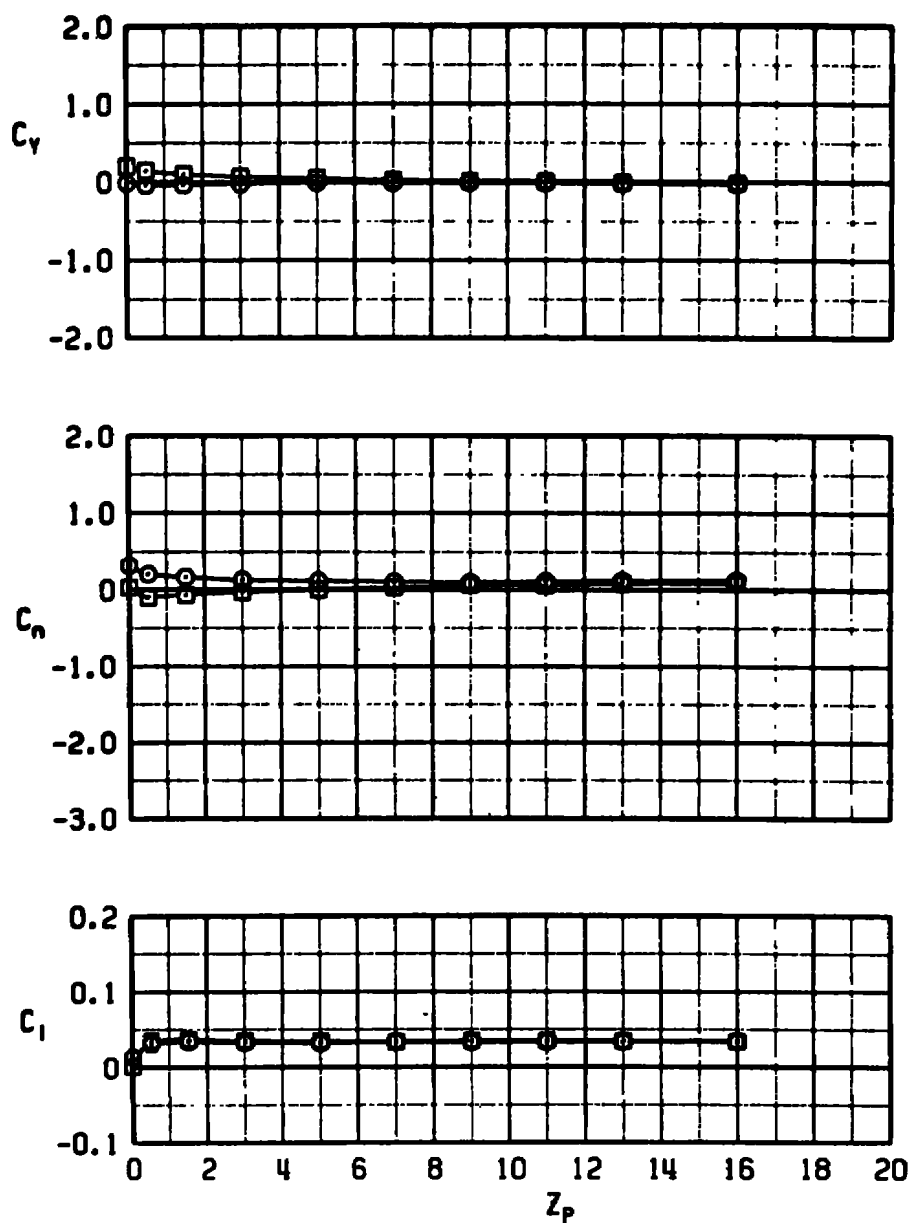
a. Concluded  
Figure 13. Continued.

SYM	$M_\infty$	$a_p$	CONFIG	$\alpha_{\text{ref}}$
○	0.80	4	1	0
□	0.80	4	2	0



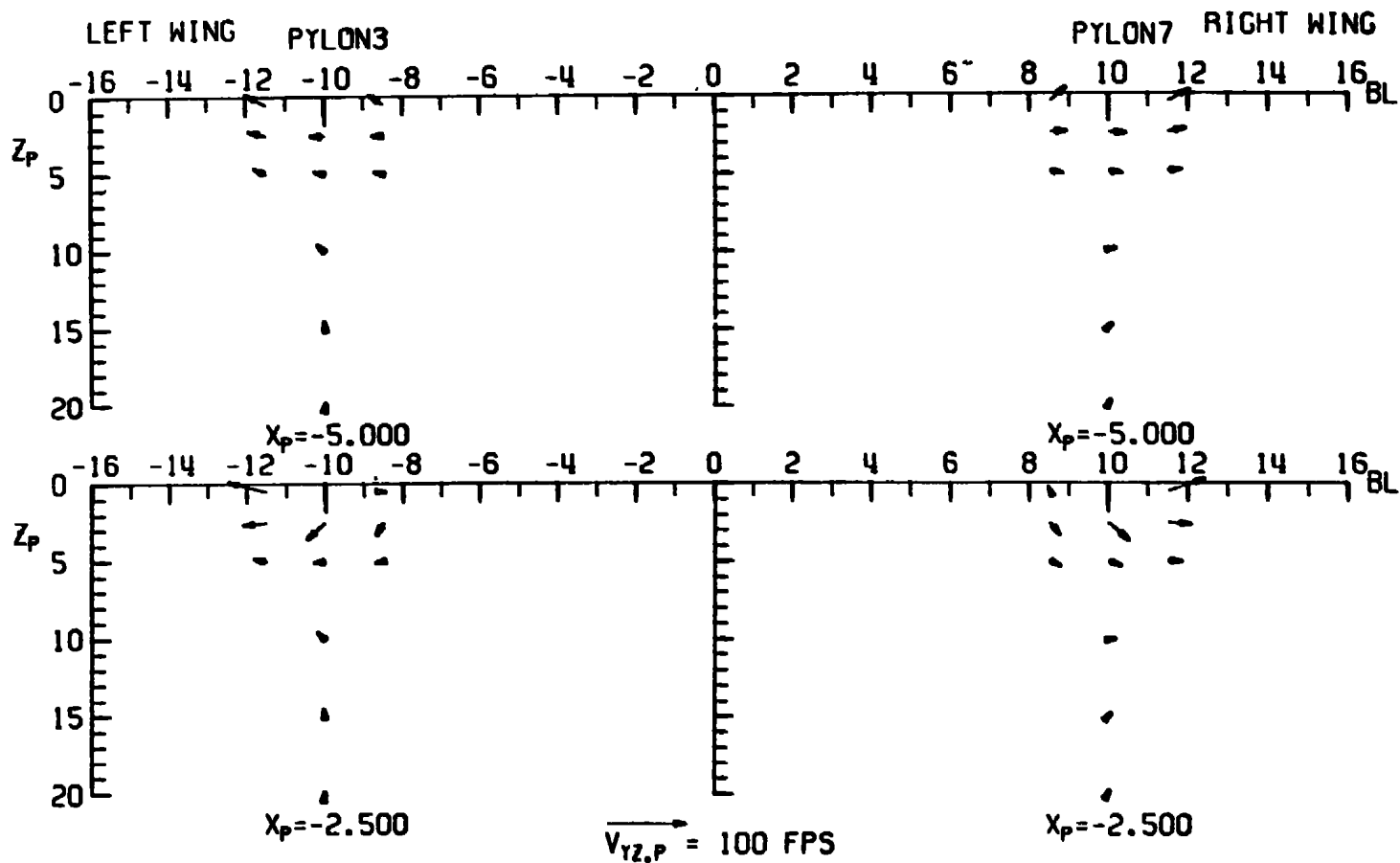
b.  $a_p = 4$   
Figure 13. Continued.

SYM	$M_\infty$	$\alpha_p$	CONFIG	$\delta_{LE}$
○	0.80	4	1	0
□	0.80	4	2	0



b. Concluded  
Figure 13. Concluded.

CONFIG: 3     $M_\infty$ : 0.60     $\alpha_p$ : 4     $\delta_{LE}$ : 0

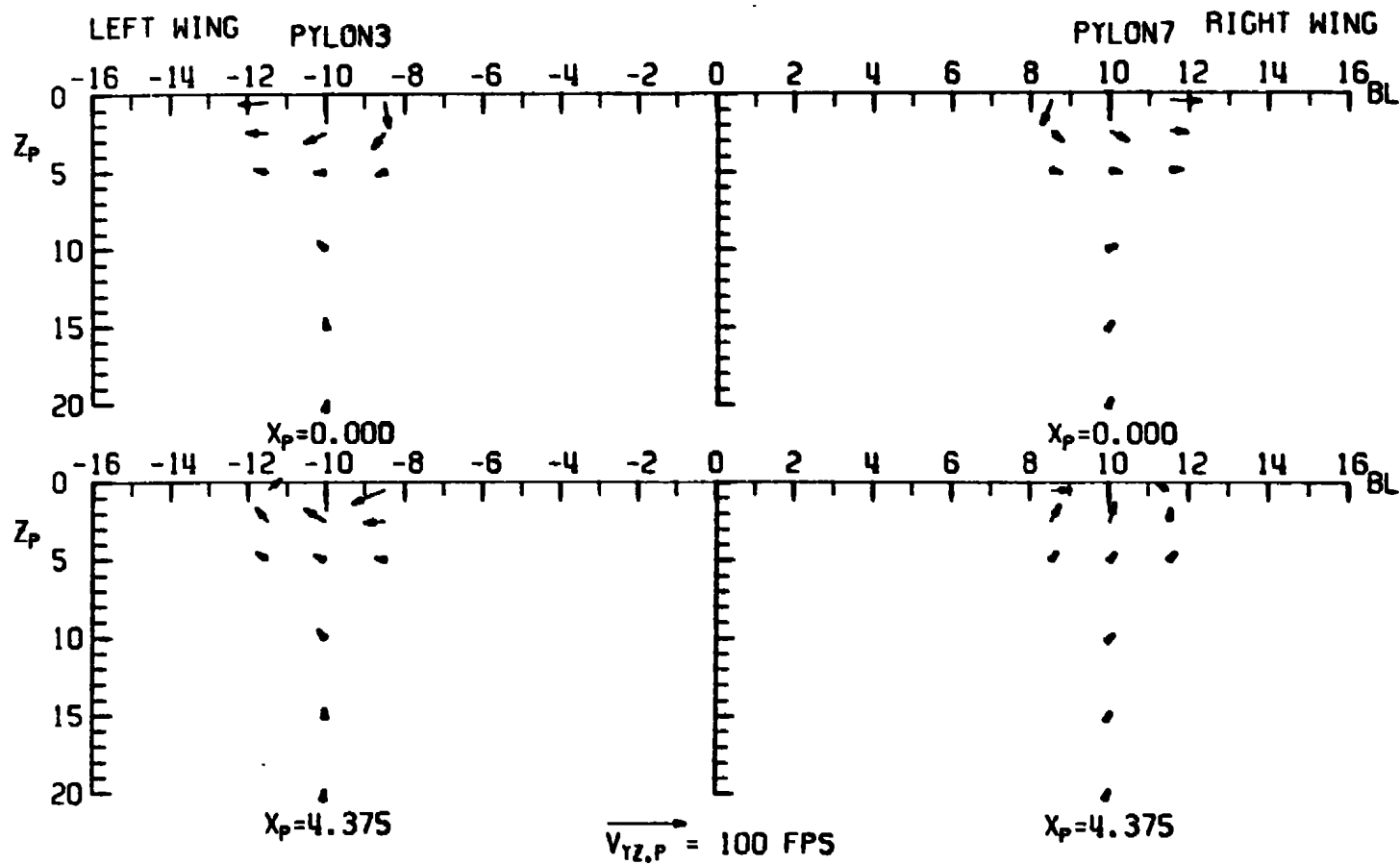


a.  $\alpha_p = 4$ ;  $X_p = -5.0$  and  $-2.5$

Figure 14. Flow-field measurements about the midwing weapons pylon with the MK-84 LDGP installed, configuration 3,  $M_\infty = 0.6$ ,  $\delta_{LE} = 0$ .

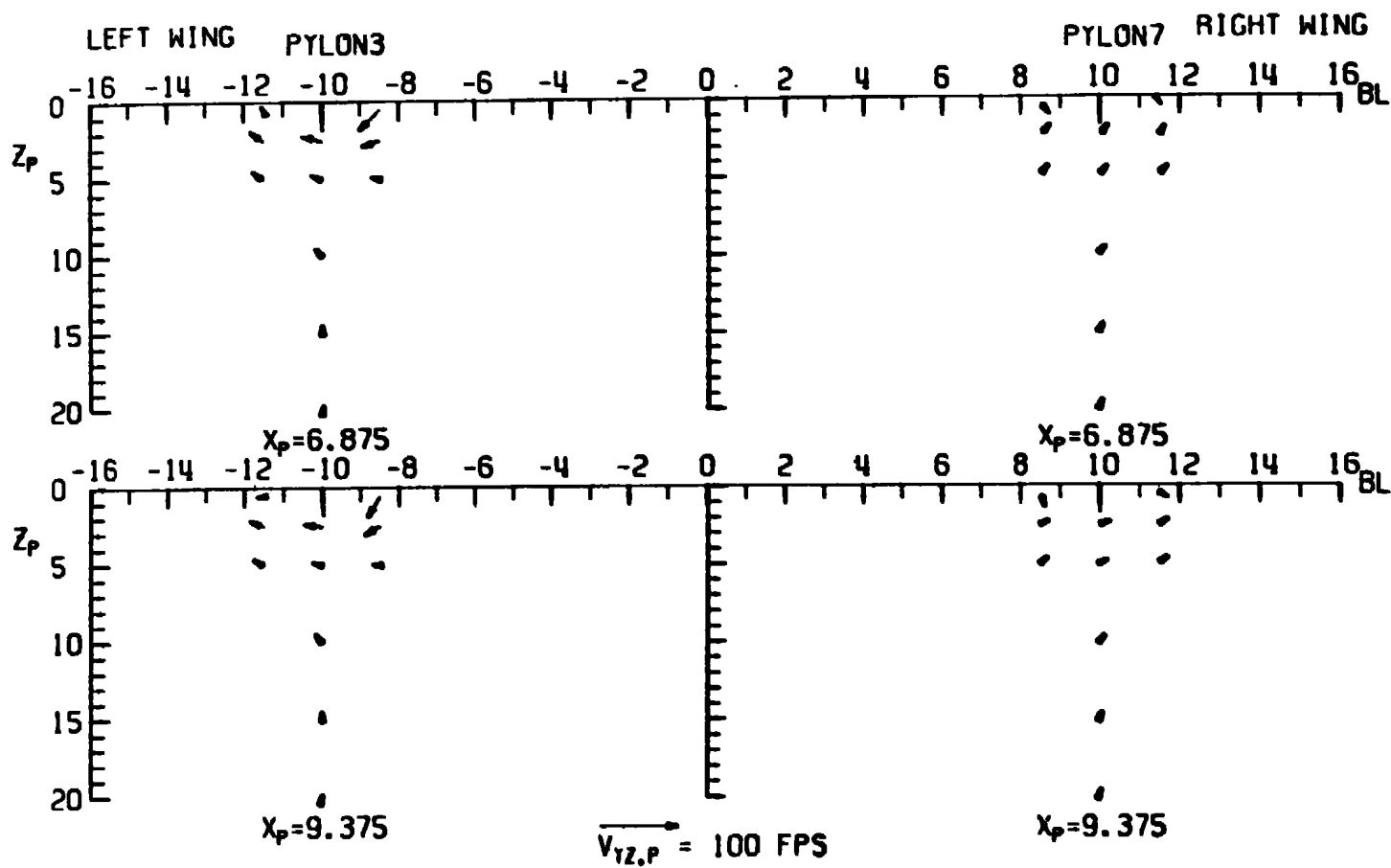
CONFIG: 3     $M_\infty$ : 0.60     $\alpha_p$ : 4     $\delta_{LE}$ : 0

AEBC-TR-76-44

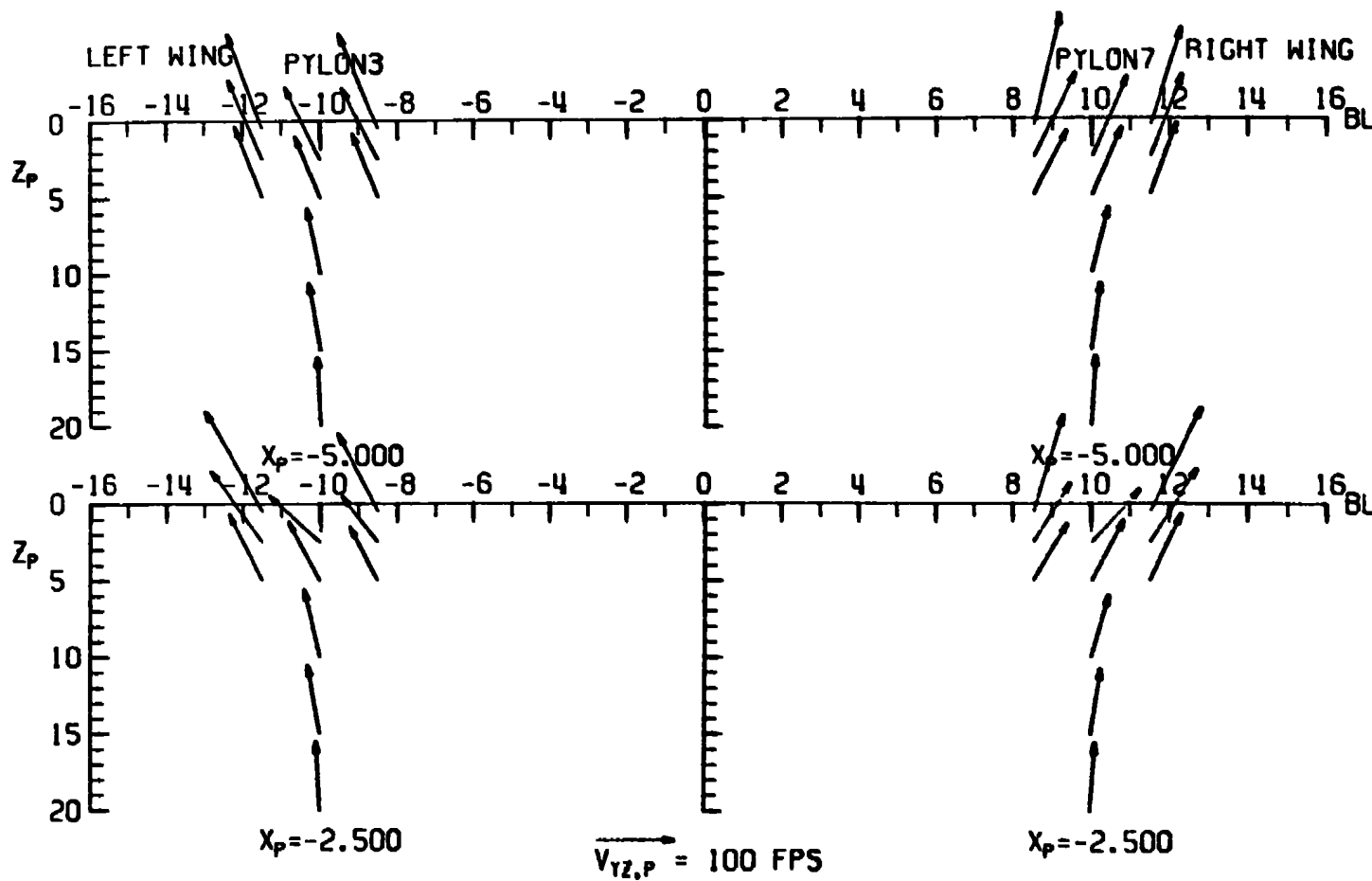


b.  $\alpha_p = 4$ ;  $X_p = 0$  and  $4.375$   
Figure 14. Continued.

CONFIG: 3     $M_\infty$ : 0.60     $\alpha_p$ : 4     $\delta_{LE}$ : 0



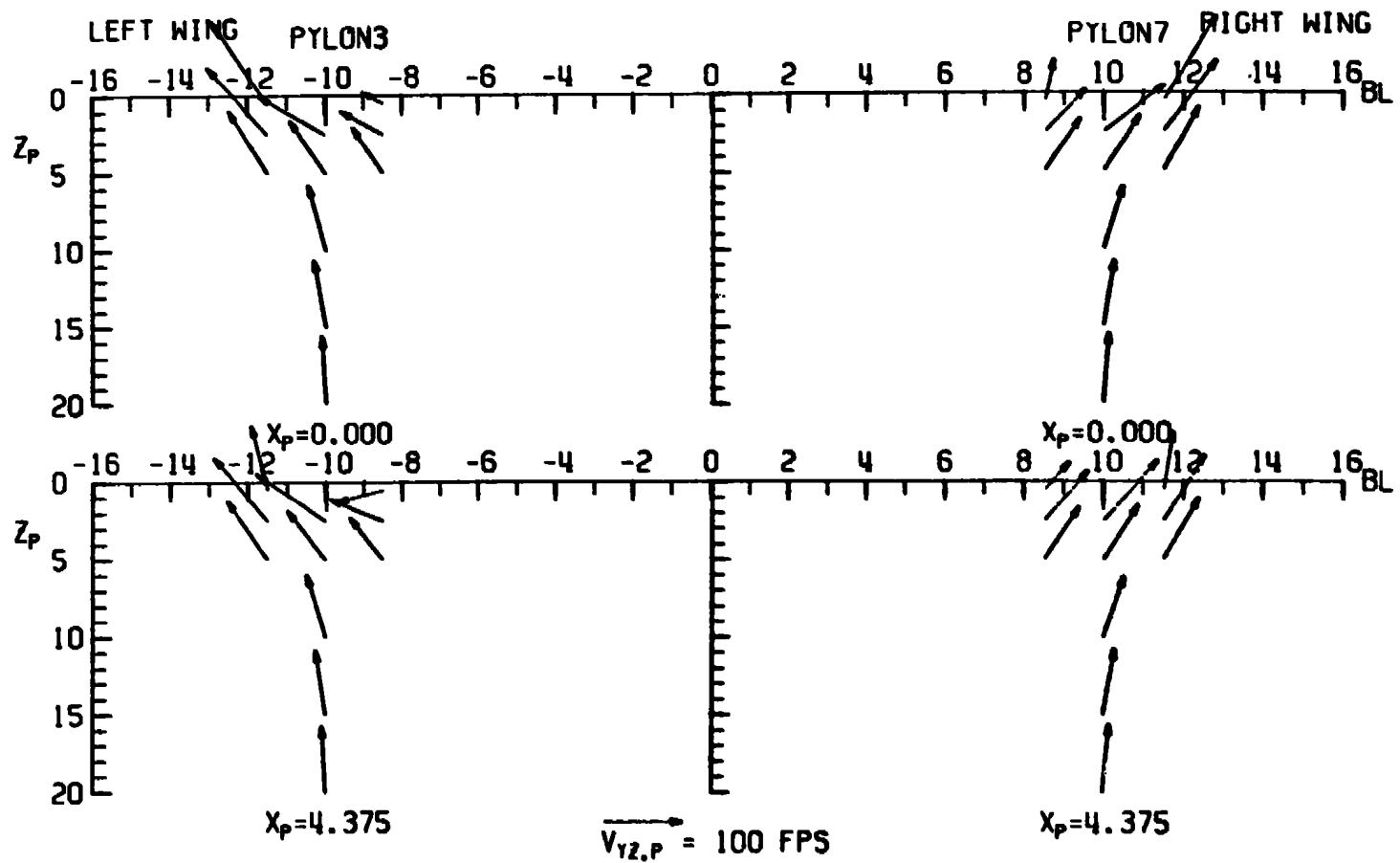
c.  $\alpha_p = 4$ ;  $X_p = 6.875$  and  $9.375$   
Figure 14. Continued.

CONFIG: 3     $M_\infty$ : 0.60     $\alpha_p$ : 12     $\delta_{LE}$ : 0

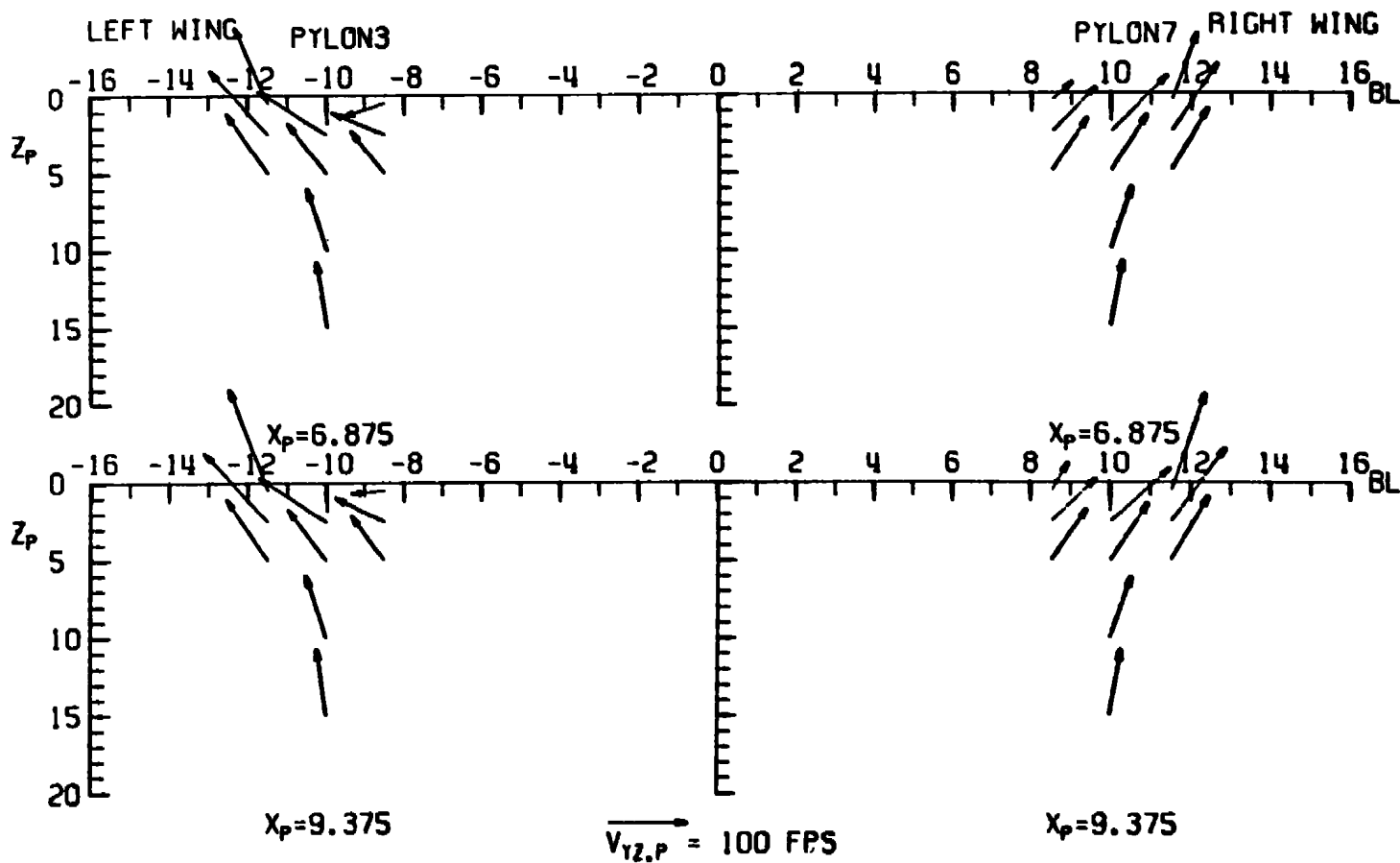
d.  $\alpha_p = 12$ ;  $X_p = -5.0$  and  $-2.5$   
Figure 14: Continued,



CONFIG: 3     $M_\infty$ : 0.60     $\alpha_p$ : 12     $\delta_{LE}$ : 0

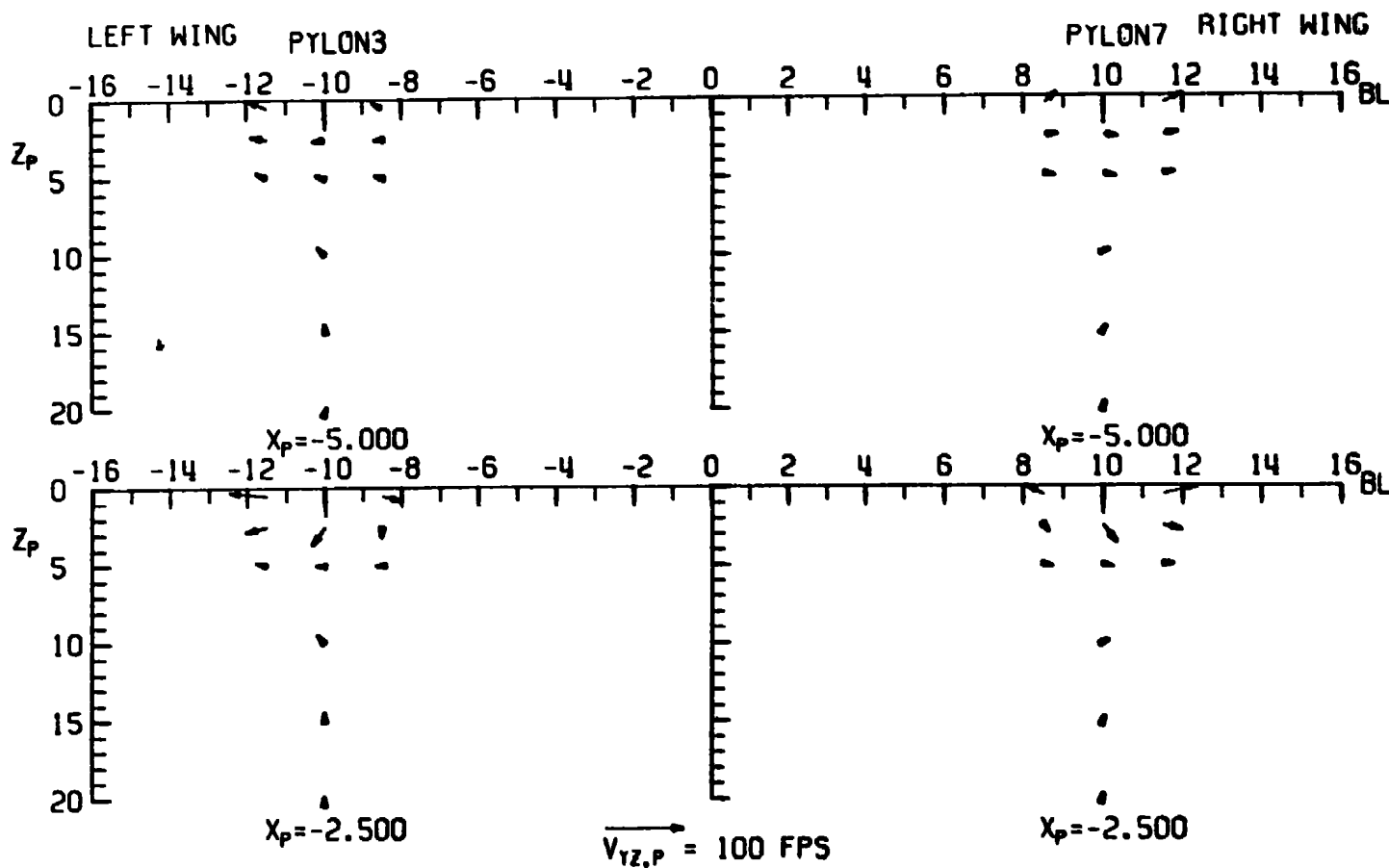


e.  $\alpha_p = 12$ ;  $X_p = 0$  and  $4.375$   
Figure 14. Continued.

CONFIG: 3     $M_\infty$ : 0.60     $\alpha_p$ : 12     $\delta_{LE}$ : 0

f.  $\alpha_p = 12$ ;  $X_p = 6.875$  and  $9.375$   
Figure 14. Concluded.

CONFIG: 3     $M_\infty$ : 0.60     $\alpha_p$ : 4     $\delta_{LE}$ : 15



a.  $\alpha_p = 4$ ;  $X_p = -5.0$  and  $-2.5$

Figure 15. Flow-field measurements about the midwing weapons pylon with the MK-84 LDGP installed, configuration 3,  $M_\infty = 0.6$ ,  $\delta_{LE} = 15$ .

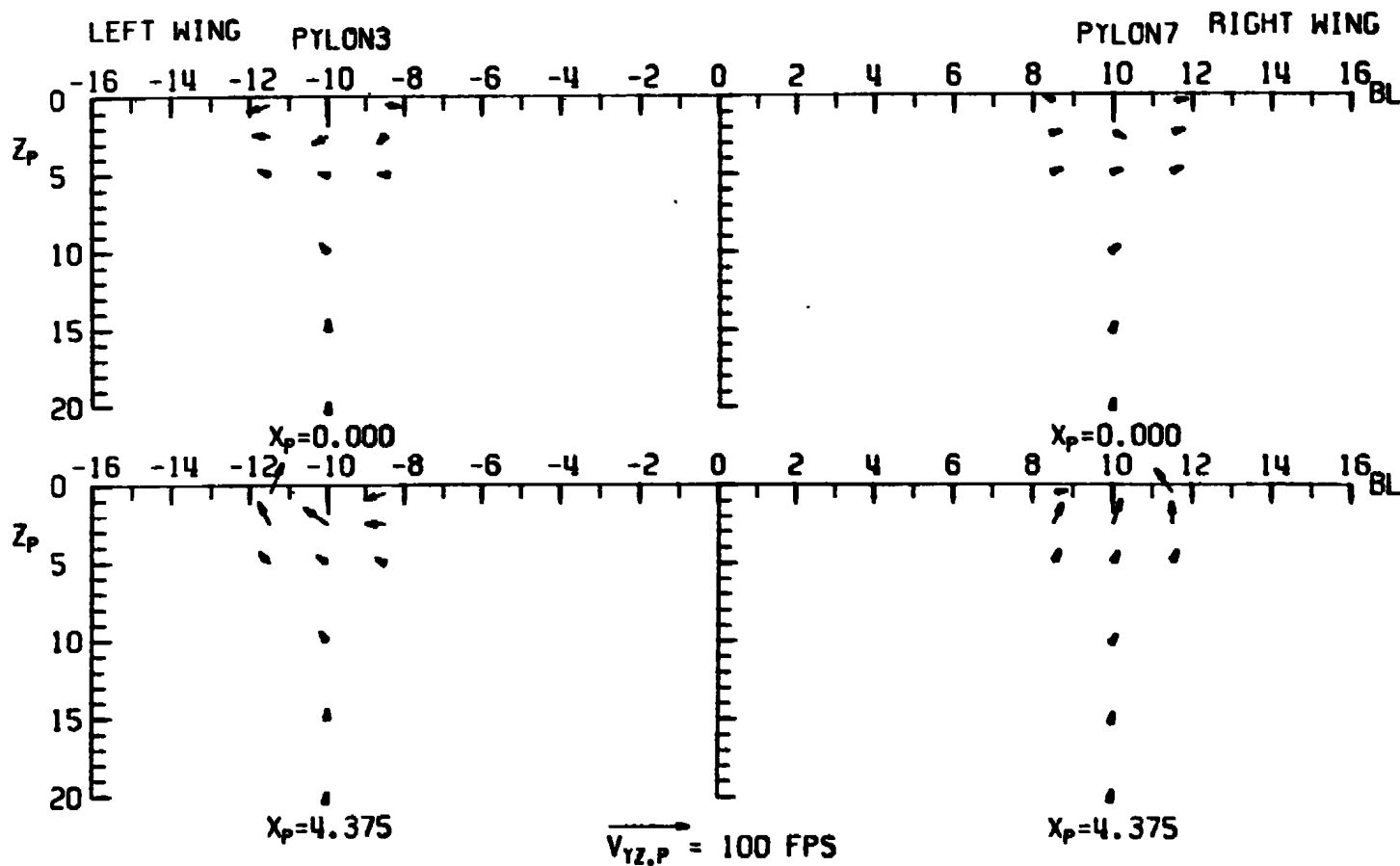
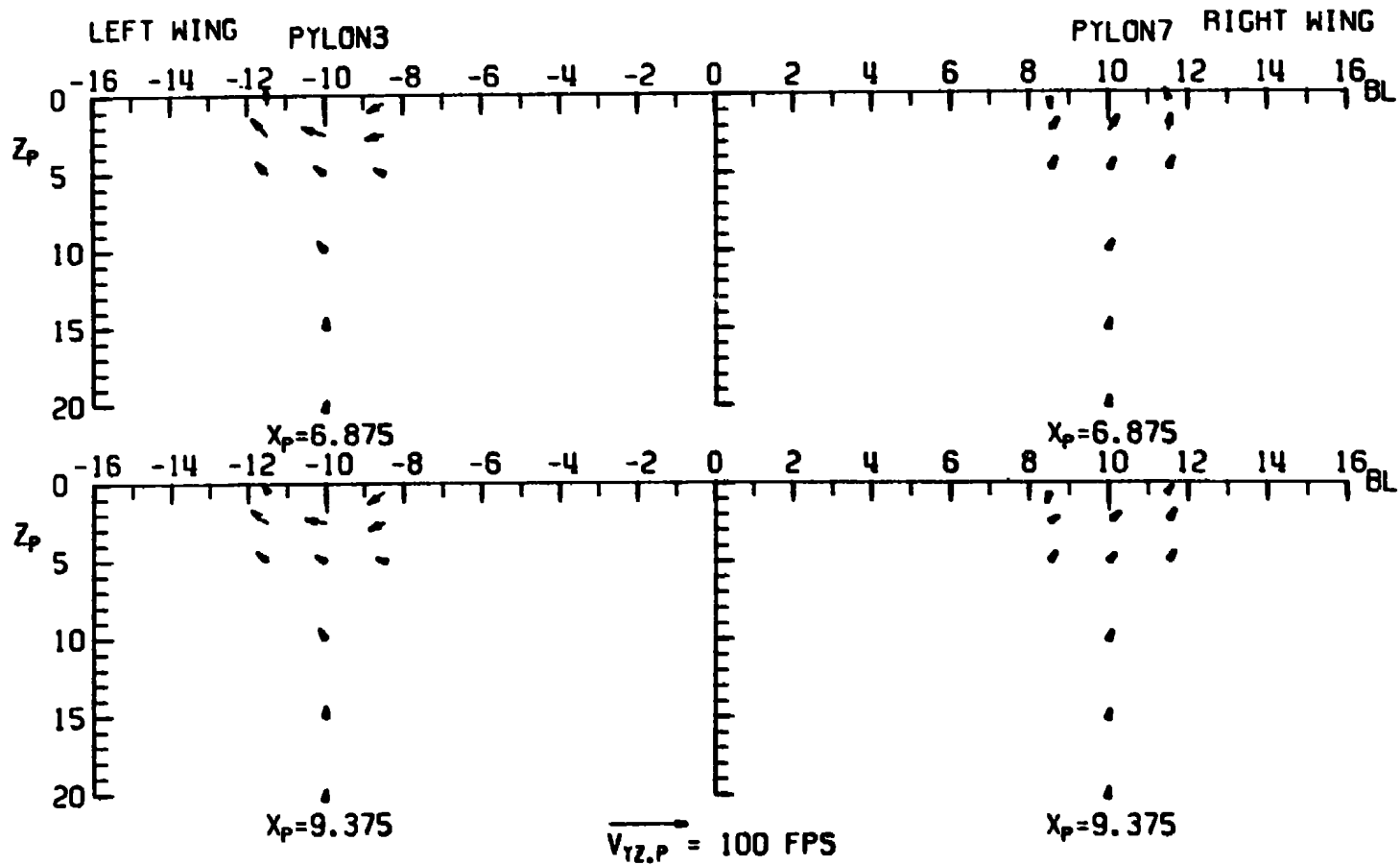
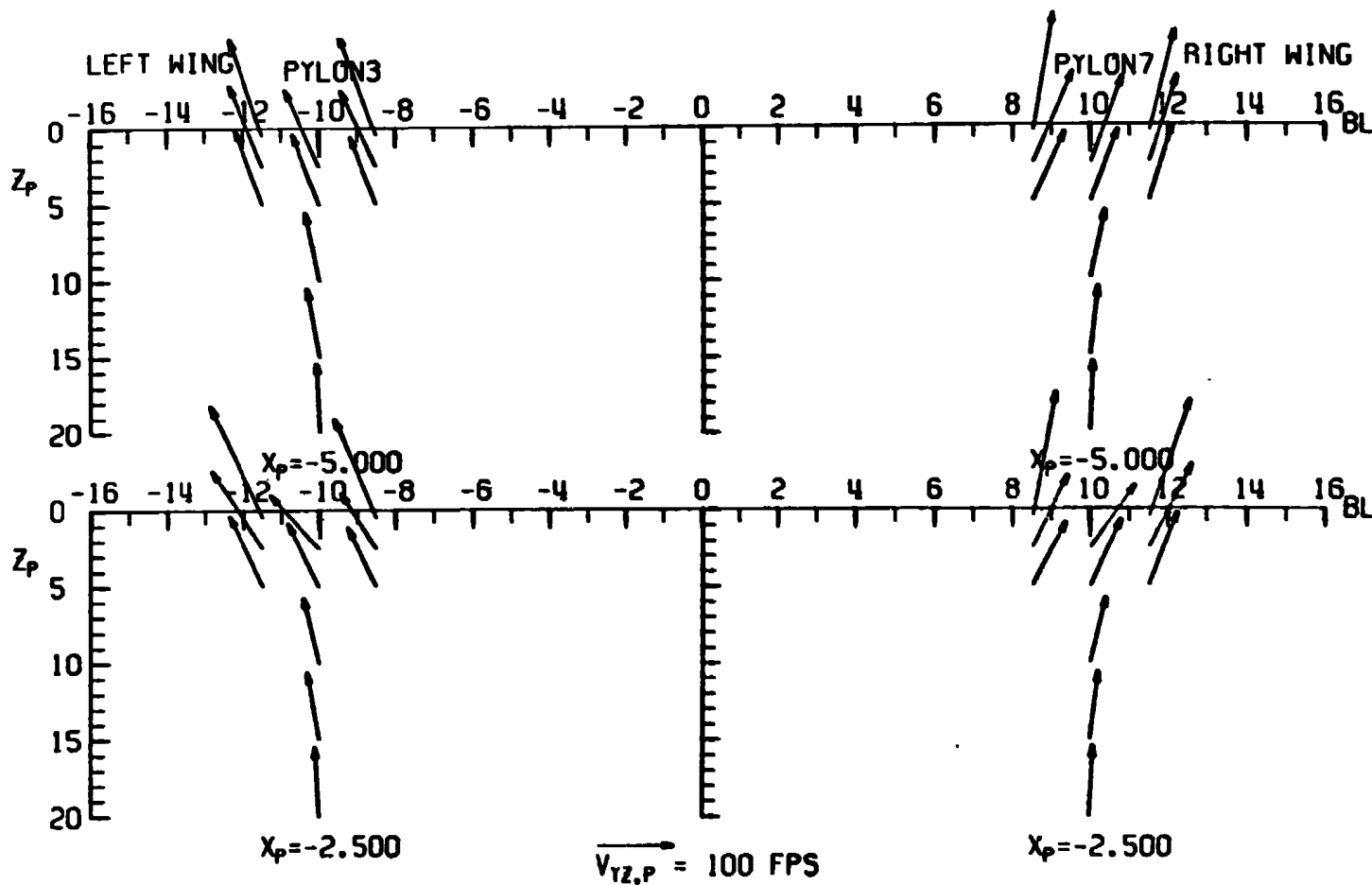
CONFIG: 3     $M_\infty$ : 0.60     $\alpha_p$ : 4     $\delta_{LE}$ : 15b.  $\alpha_p = 4$ ;  $X_p = 0$  and  $4.375$ 

Figure 15. Continued.

CONFIG: 3     $M_\infty$ : 0.60     $\alpha_p$ : 4     $\delta_{LE}$ : 15

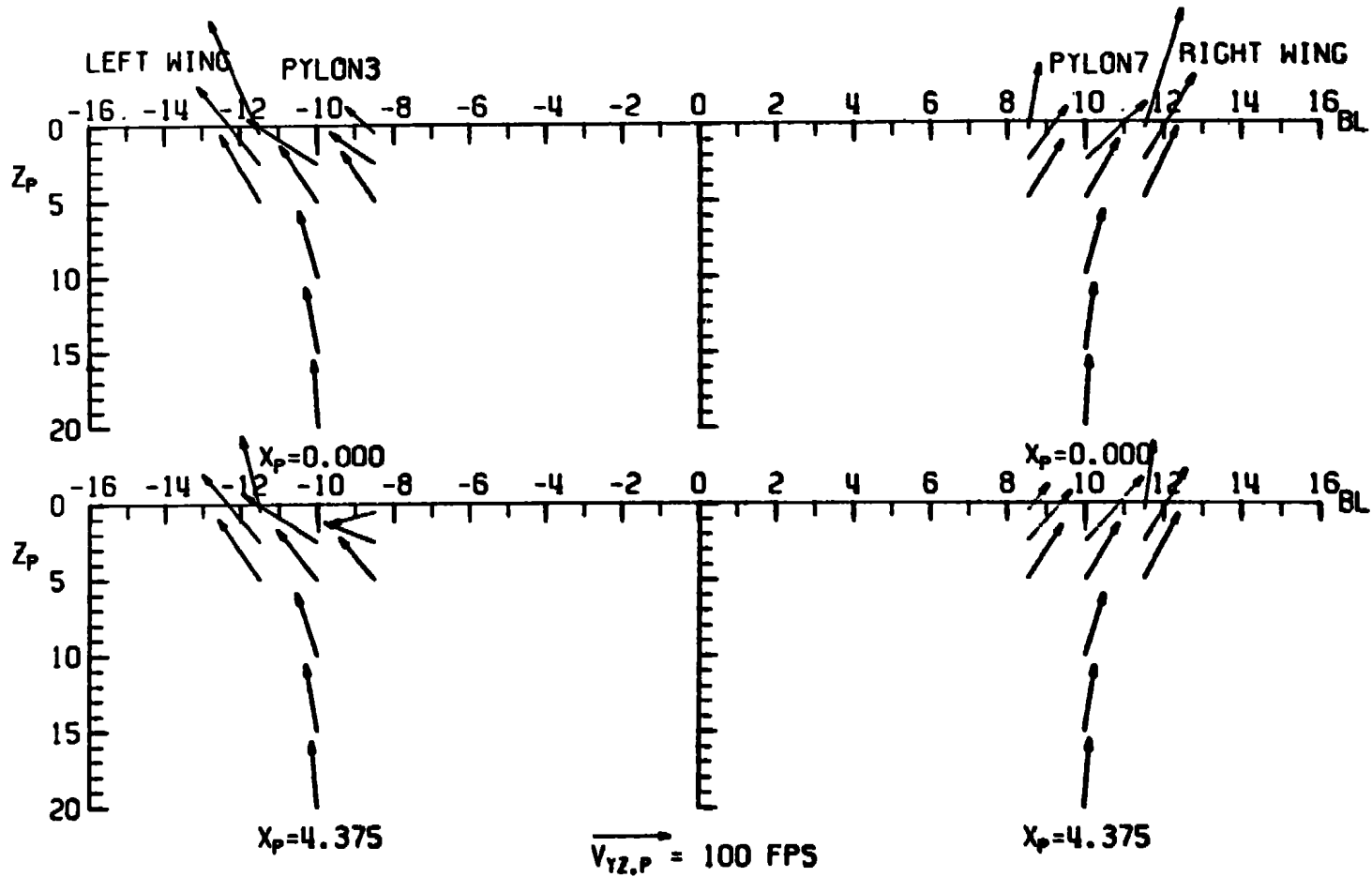


c.  $\alpha_p = 4$ ;  $x_p = 6.875$  and  $9.375$   
Figure 15. Continued.

CONFIG: 3     $M_\infty$ : 0.60     $\alpha_p$ : 12     $\delta_{LE}$ : 15

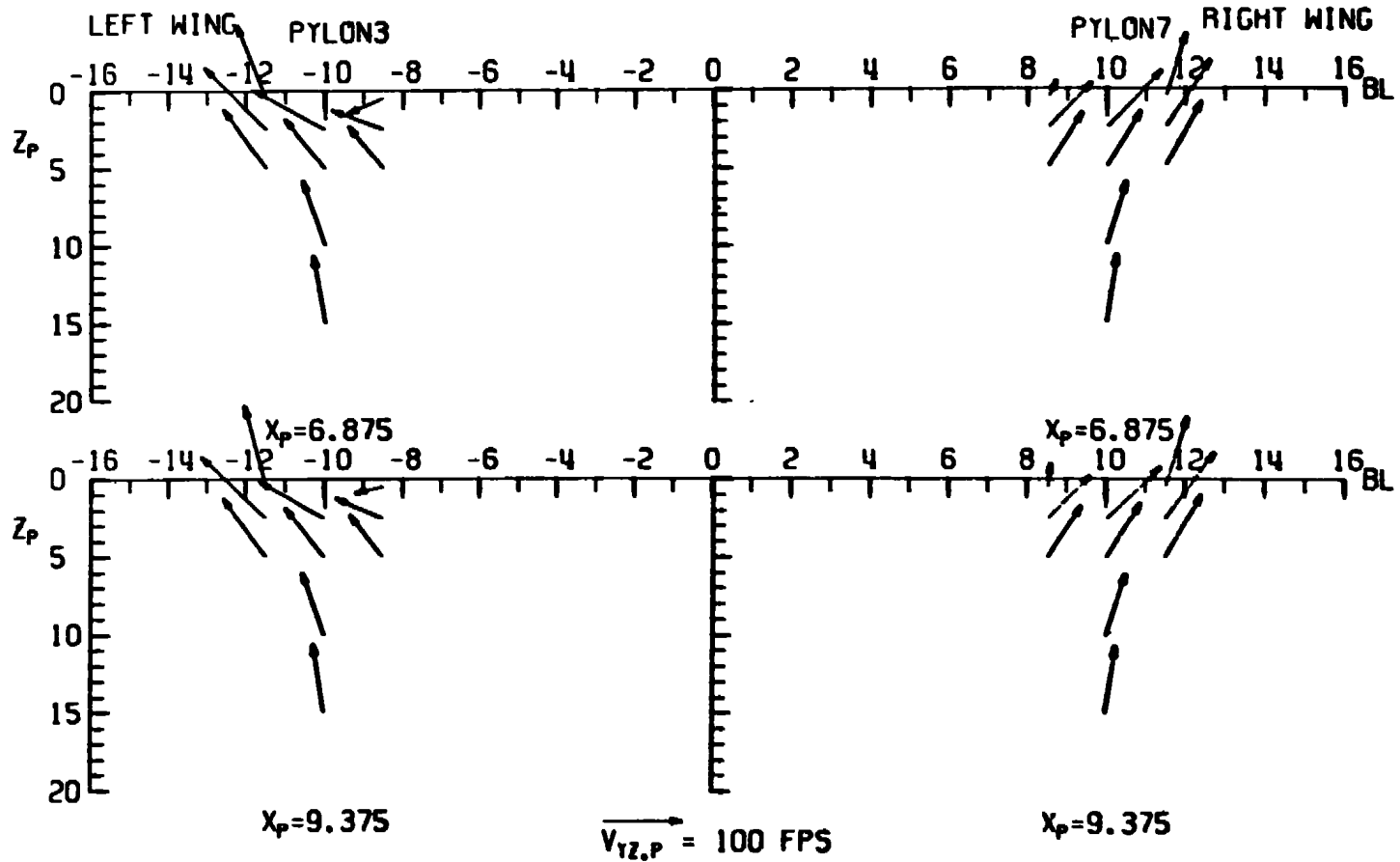
d.  $\alpha_p = 12$ ;  $X_p = -5.0$  and  $-2.5$   
Figure 15. Continued.

CONFIG: 3  $M_\infty$ : 0.60  $\alpha_p$ : 12  $\delta_{LE}$ : 15



e.  $\alpha_p = 12$ ;  $X_p = 0$  and  $4.375$   
Figure 16. Continued.

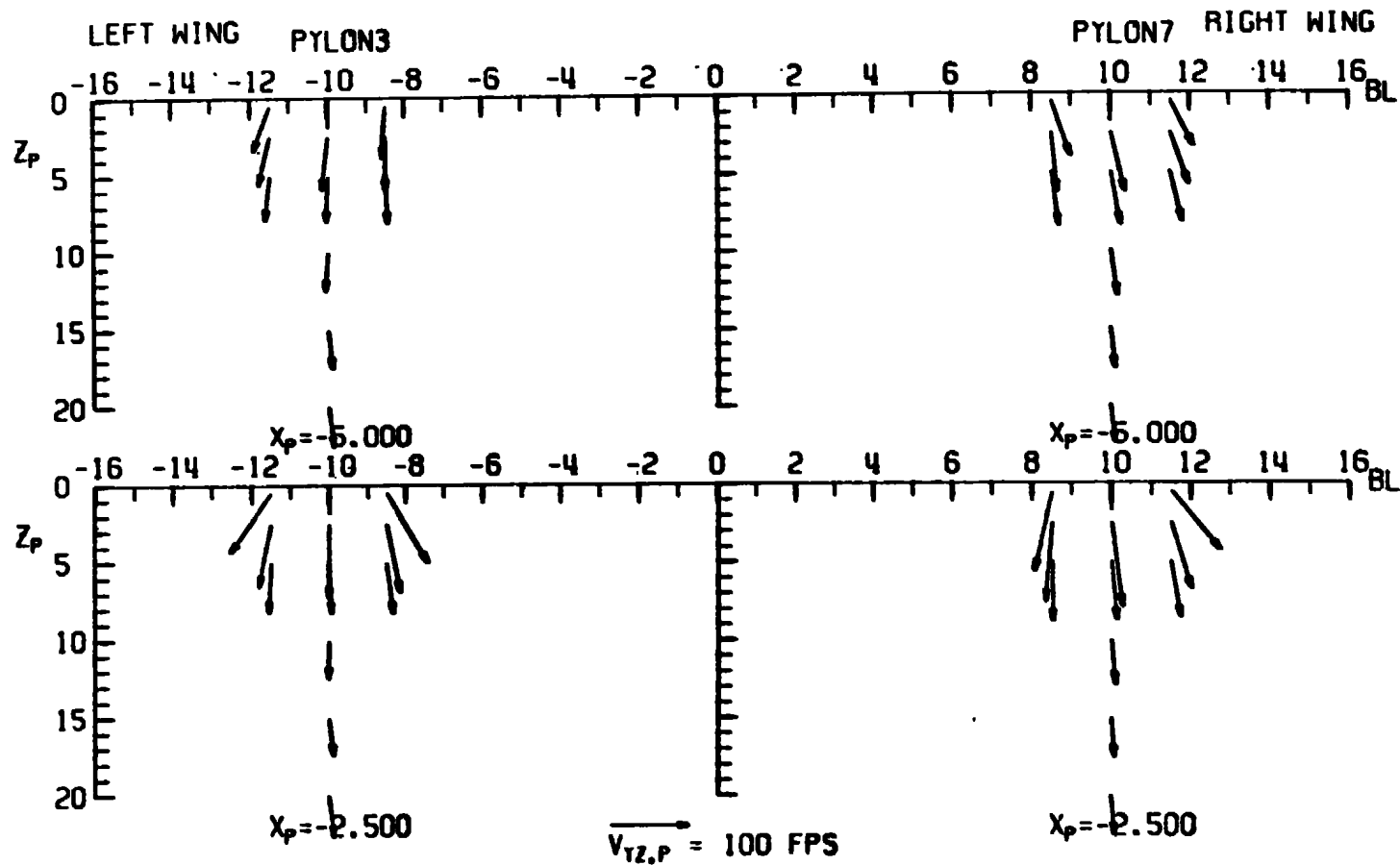
CONFIG: 3  $M_\infty$ : 0.60  $\alpha_p$ : 12  $\delta_{LE}$ : 15



f.  $\alpha_p = 12$ ;  $X_p = 6.875$  and  $9.375$   
Figure 15. Concluded.



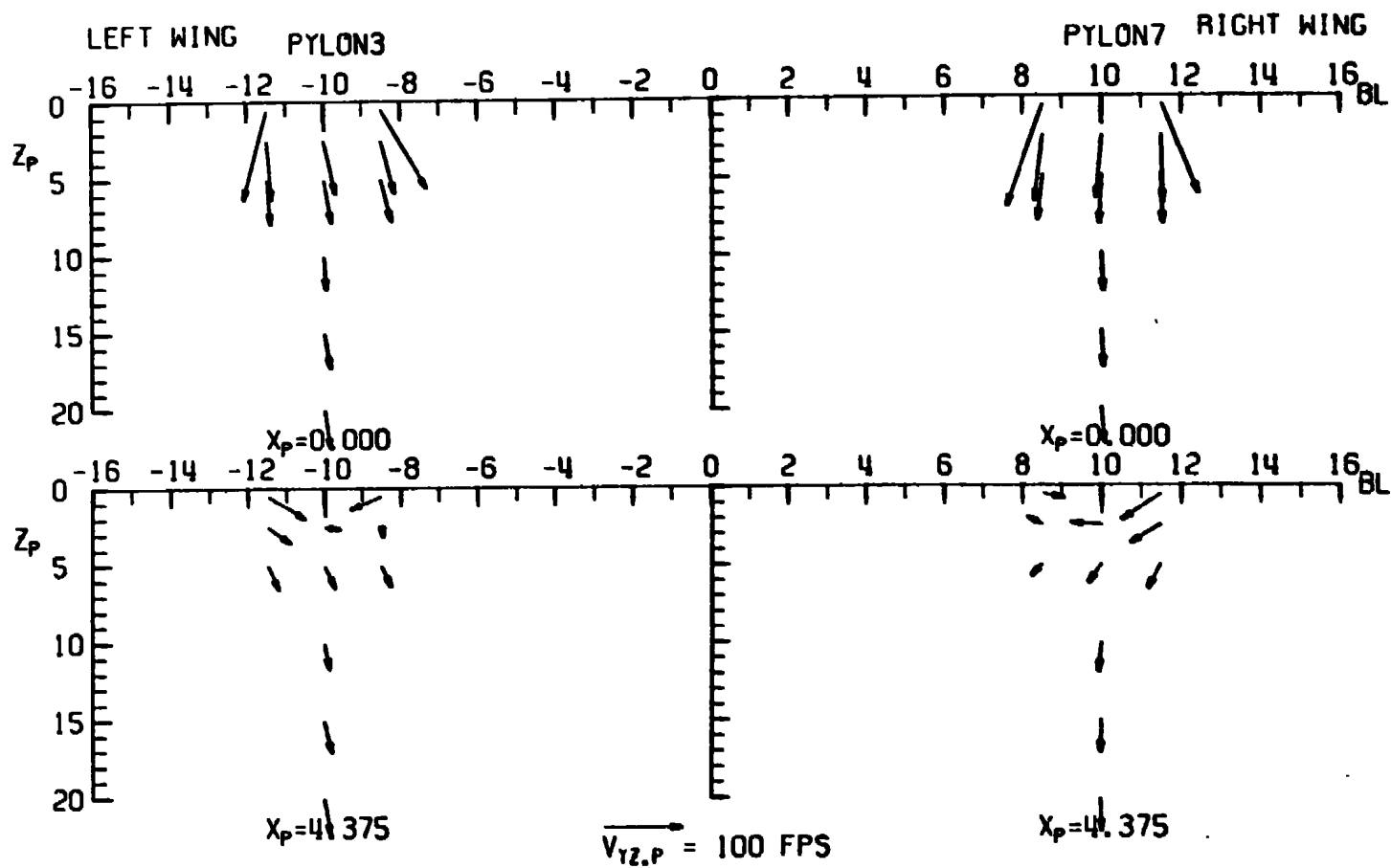
CONFIG: 3  $M_\infty: 0.80$   $\alpha_p: 0$   $\delta_{LE}: 0$



a.  $\alpha_p = 0$ ;  $X_p = -5.0$  and  $-2.5$

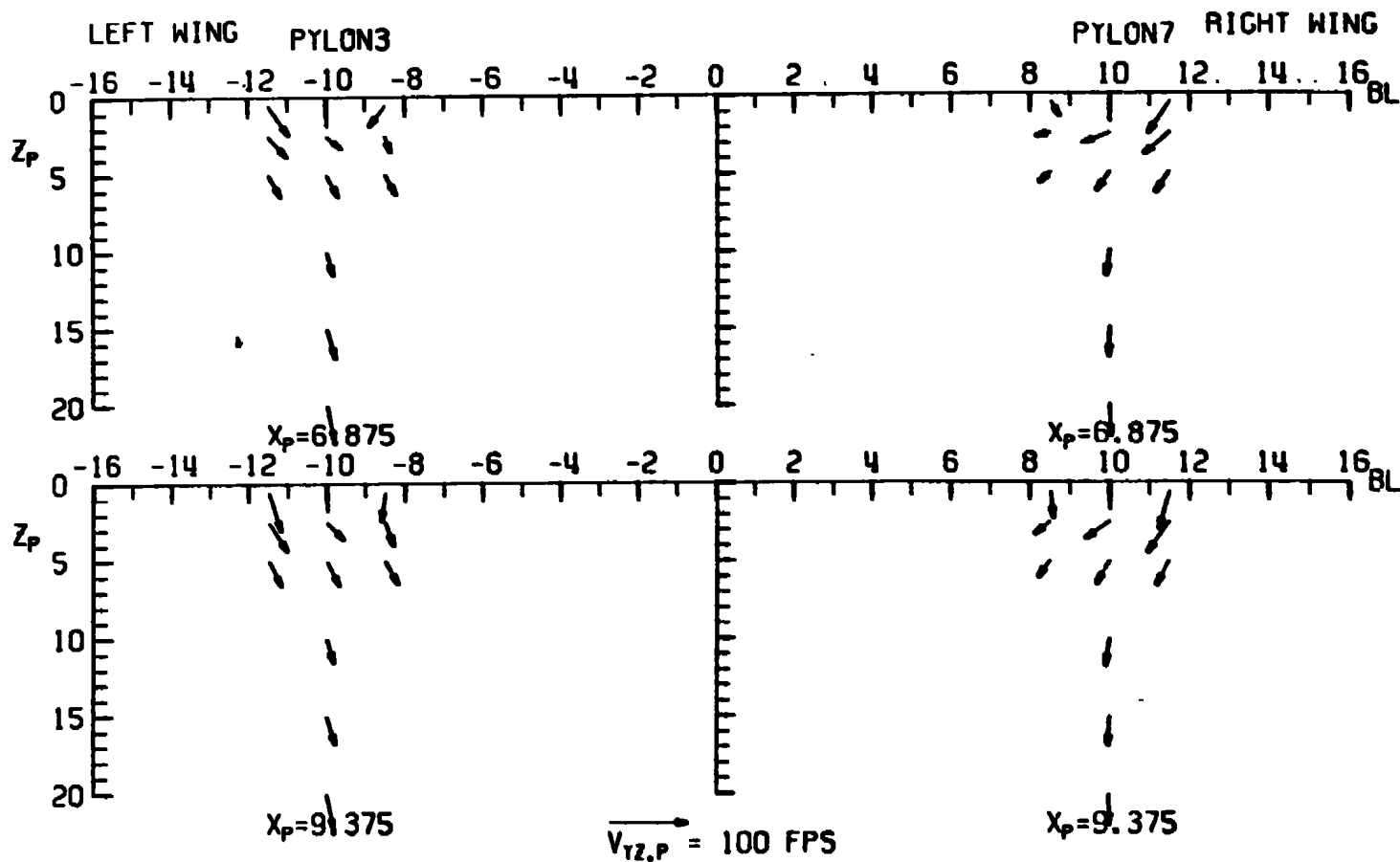
Figure 16. Flow-field measurements about the midwing weapons pylon with the MK-84 LDGP installed, configuration 3,  $M_\infty = 0.8$ ,  $\delta_{LE} = 0$ .

CONFIG: 3     $M_\infty$ : 0.80     $\alpha_p$ : 0     $\delta_{LE}$ : 0



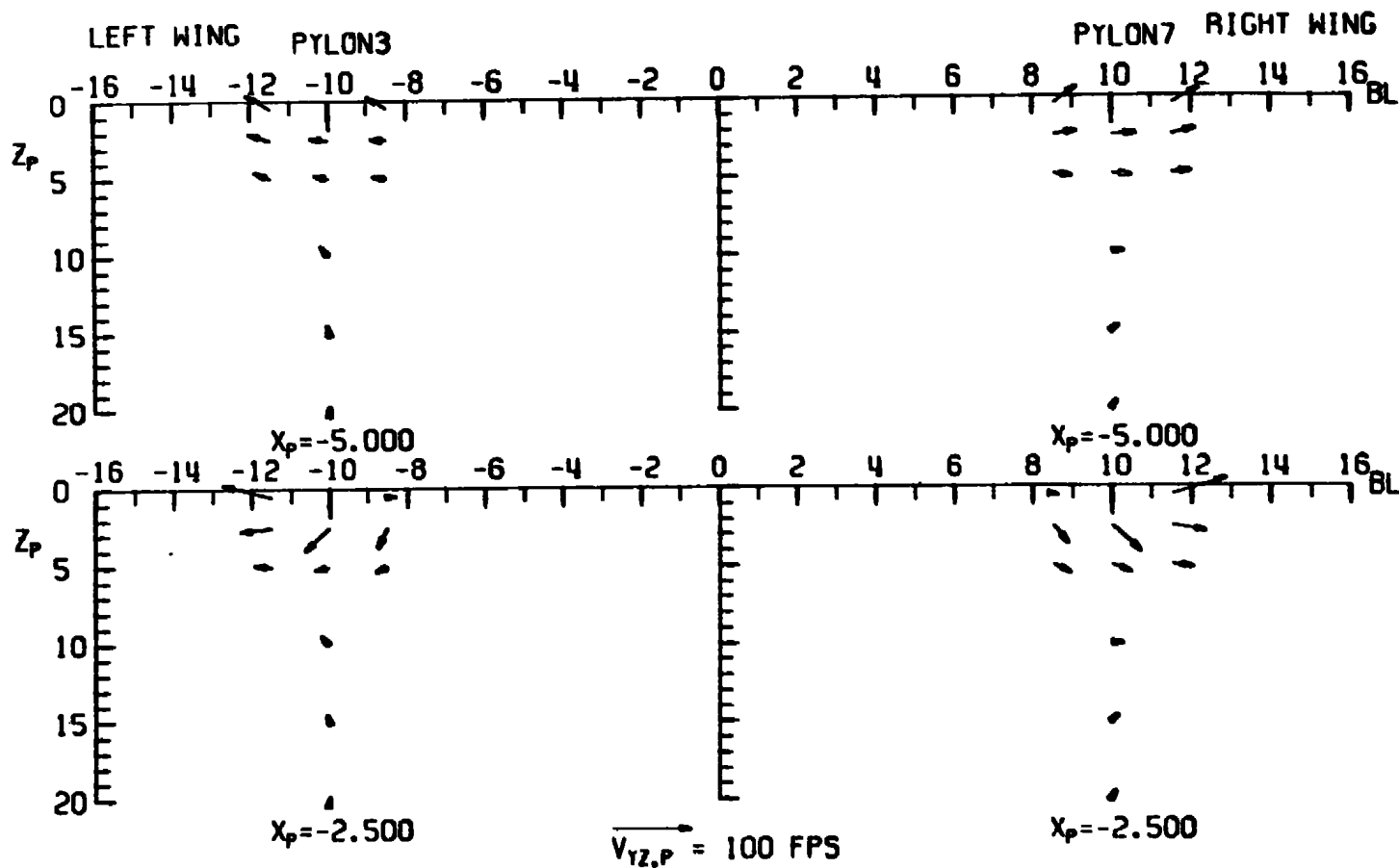
b.  $\alpha_p = 0$ ;  $X_p = 0$  and 4.375  
Figure 16. Continued.

CONFIG: 3     $M_\infty$ : 0.80     $\alpha_p$ : 0     $\delta_{LE}$ : 0



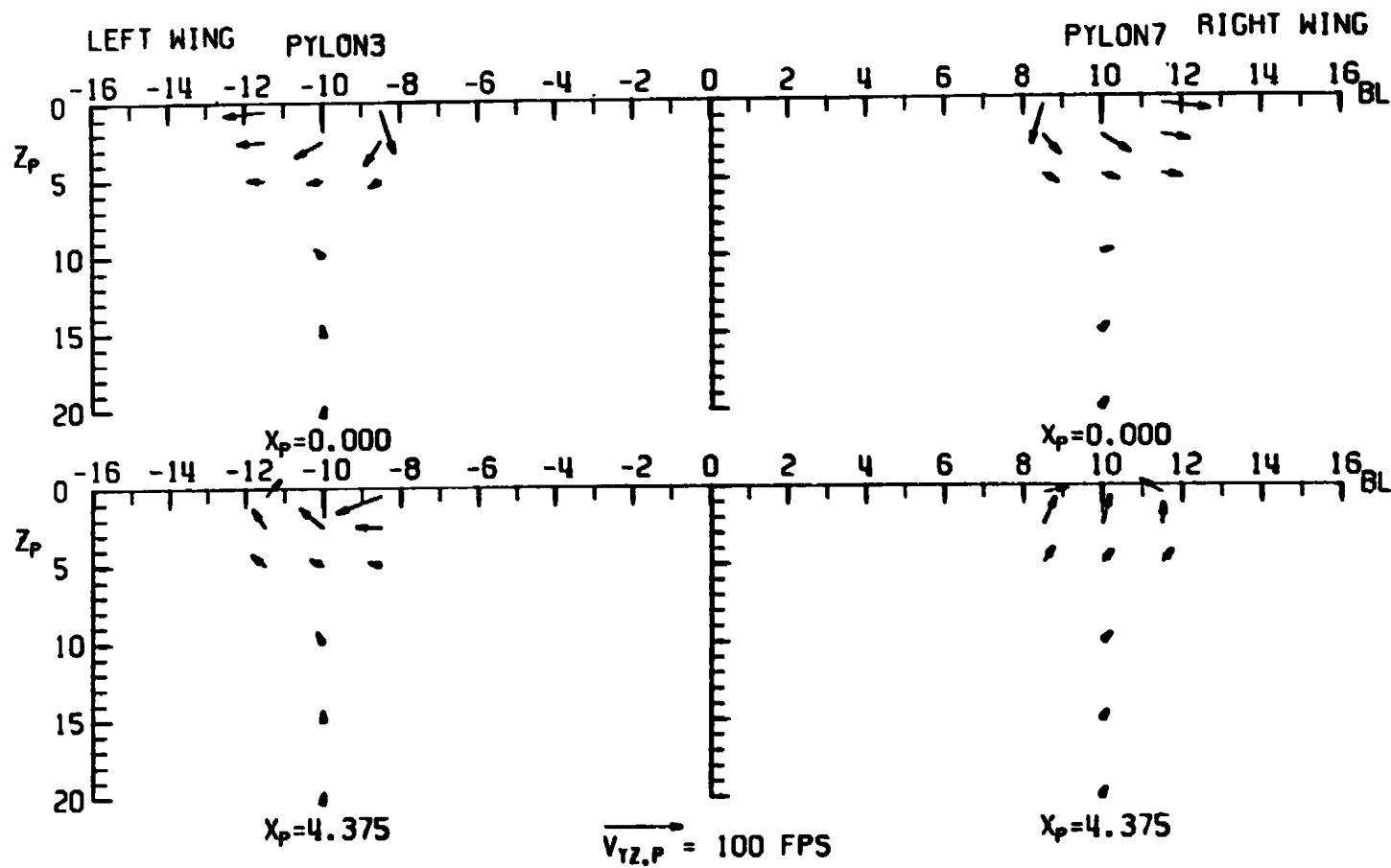
c.  $\alpha_p = 0$ ;  $X_p = 6.875$  and  $9.375$   
Figure 16. Continued.

CONFIG: 3  $M_\infty$ : 0.80  $\alpha_p$ : 4  $\delta_{LE}$ : 0

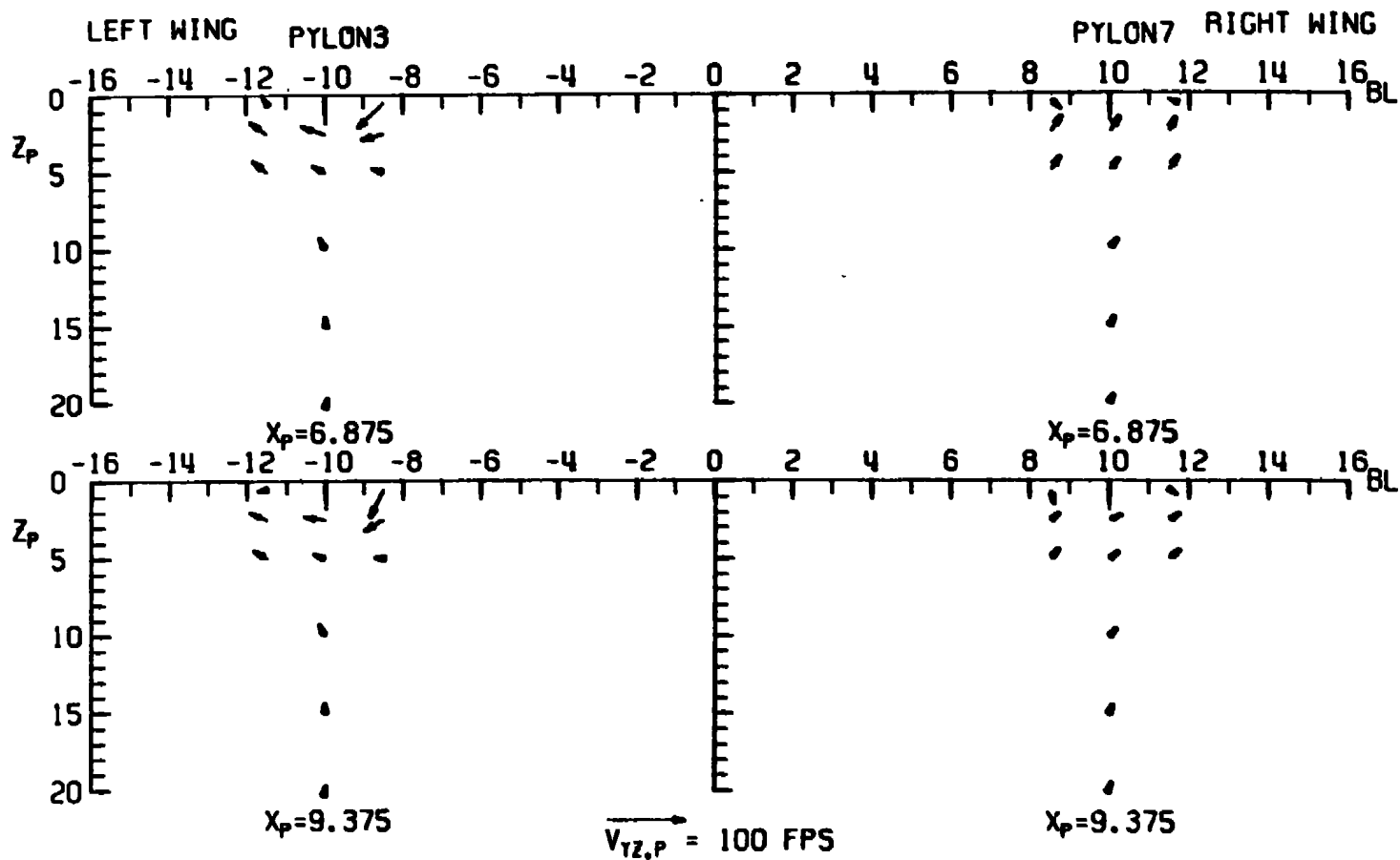


d.  $\alpha_p = 4$ ;  $X_p = -5.0$  and  $-2.5$   
Figure 16. Continued.

CONFIG: 3     $M_\infty$ : 0.80     $\alpha_p$ : 4     $\delta_{LE}$ : 0

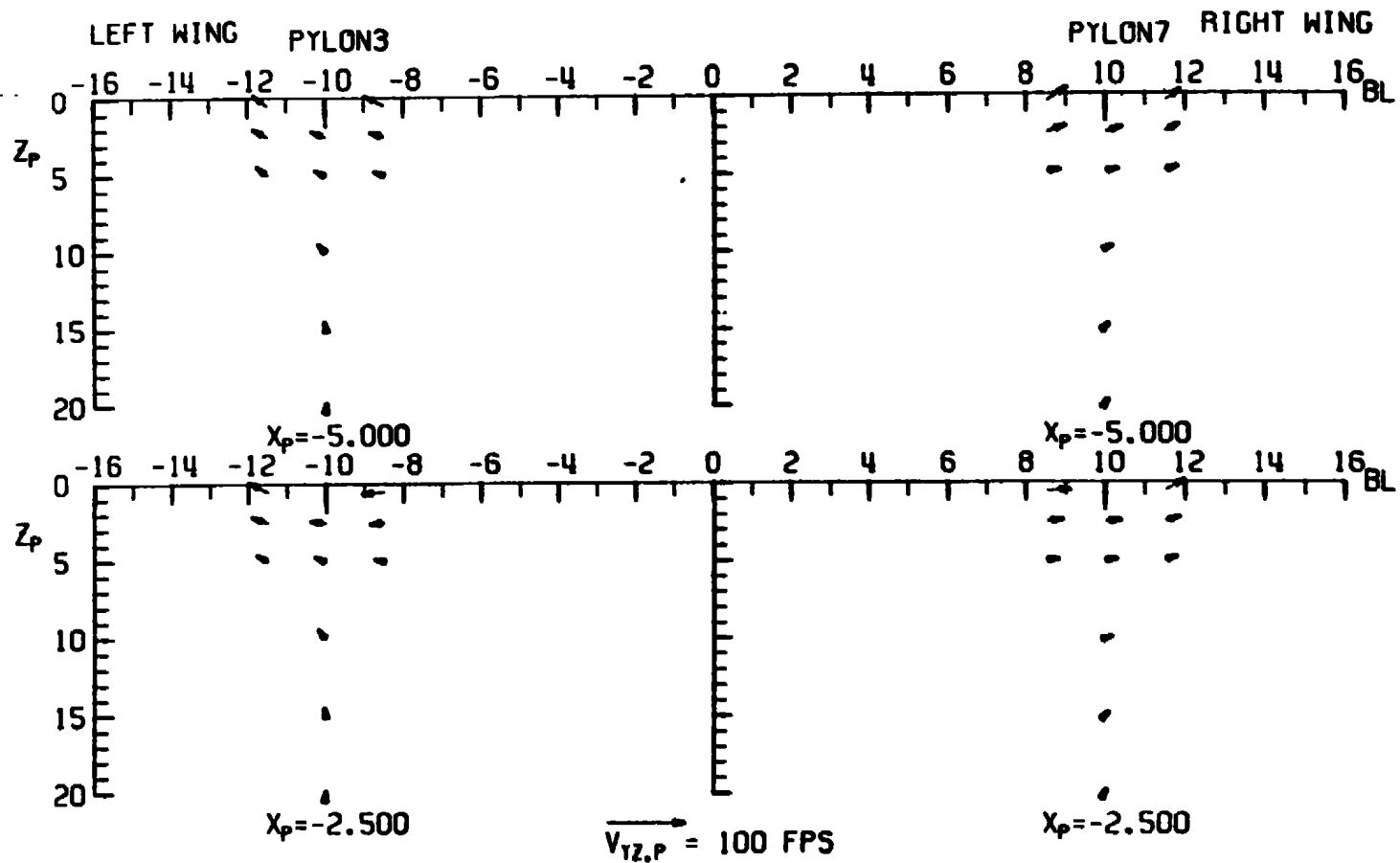


e.  $\alpha_p = 4$ ;  $X_p = 0$  and  $4.375$   
Figure 16. Continued.

CONFIG: 3     $M_\infty$ : 0.80     $\alpha_p$ : 4     $\delta_{LE}$ : 0

f.  $\alpha_p = 4$ ;  $X_p = 6.875$  and  $9.375$   
Figure 16. Concluded.

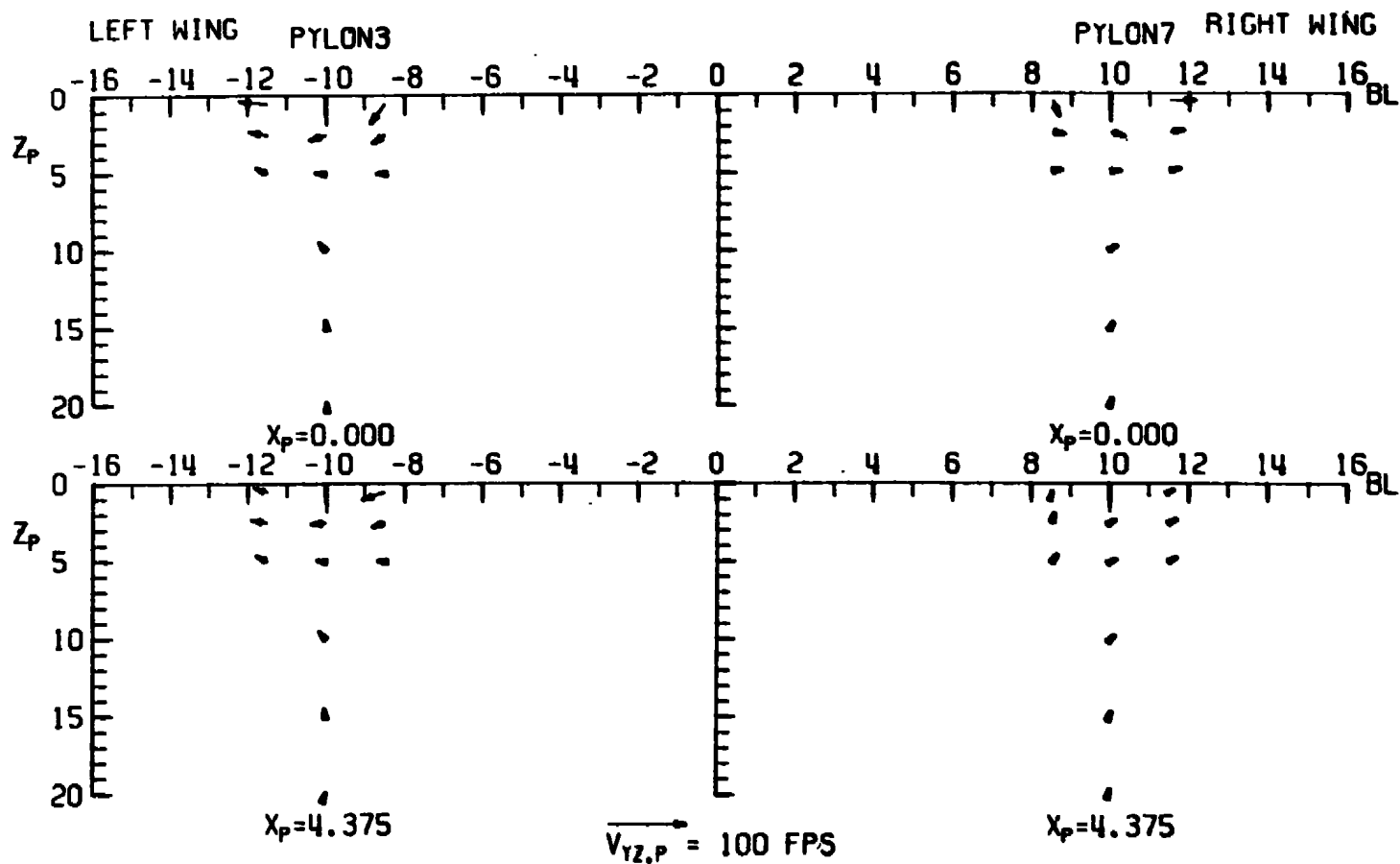
CONFIG: 4     $M_\infty = 0.60$      $\alpha_p = 4$      $\delta_{LE} = 0$



a.  $\alpha_p = 4$ ;  $X_p = -5.0$  and  $-2.5$

Figure 17. Flow-field measurements about the midwing weapons pylon without the MK-84 LDGP installed, configuration 4,  $M_\infty = 0.6$ ,  $\delta_{LE} = 0$ .

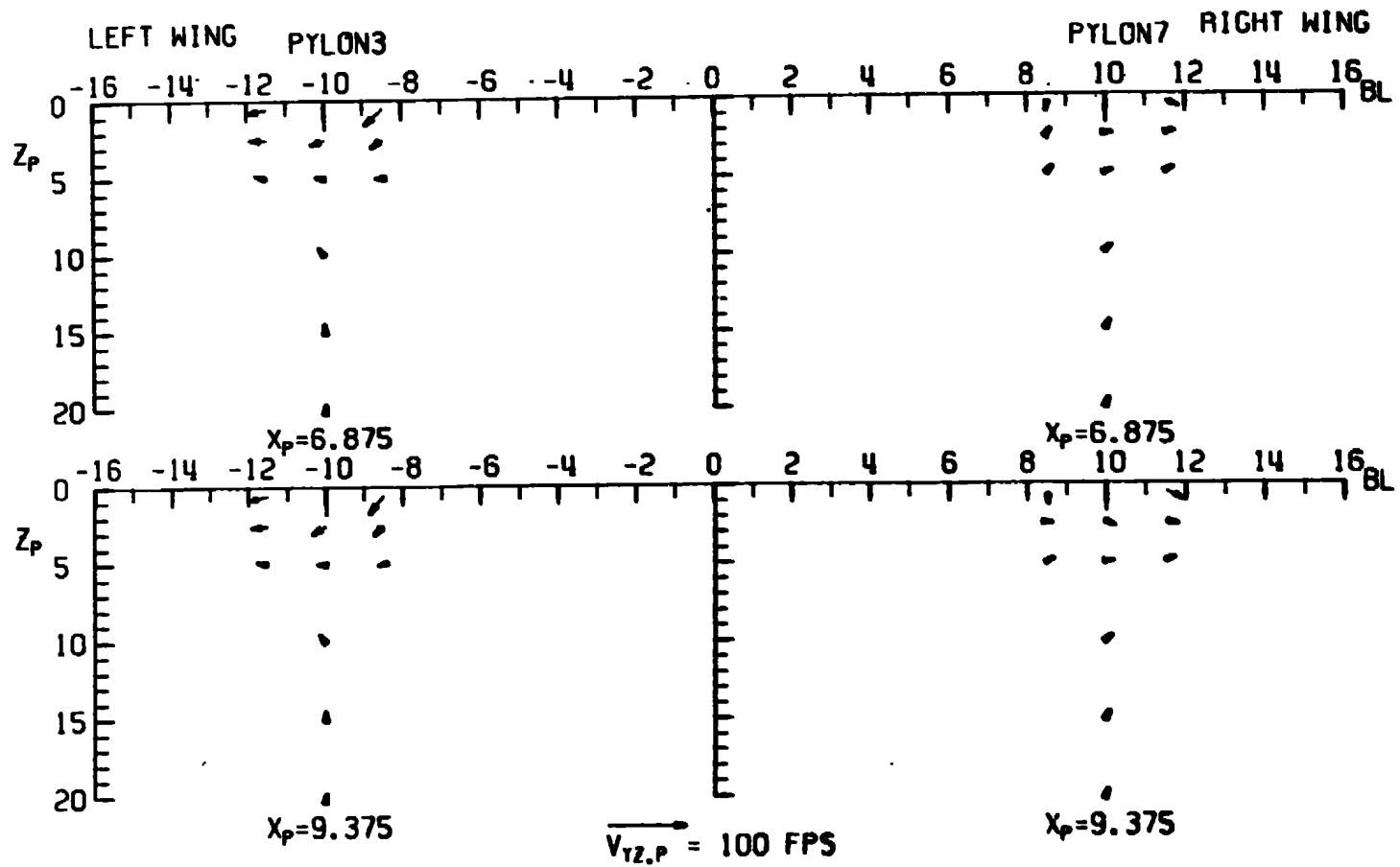
CONFIG: 4     $M_\infty$ : 0.60     $\alpha_p$ : 4     $\delta_{LE}$ : 0



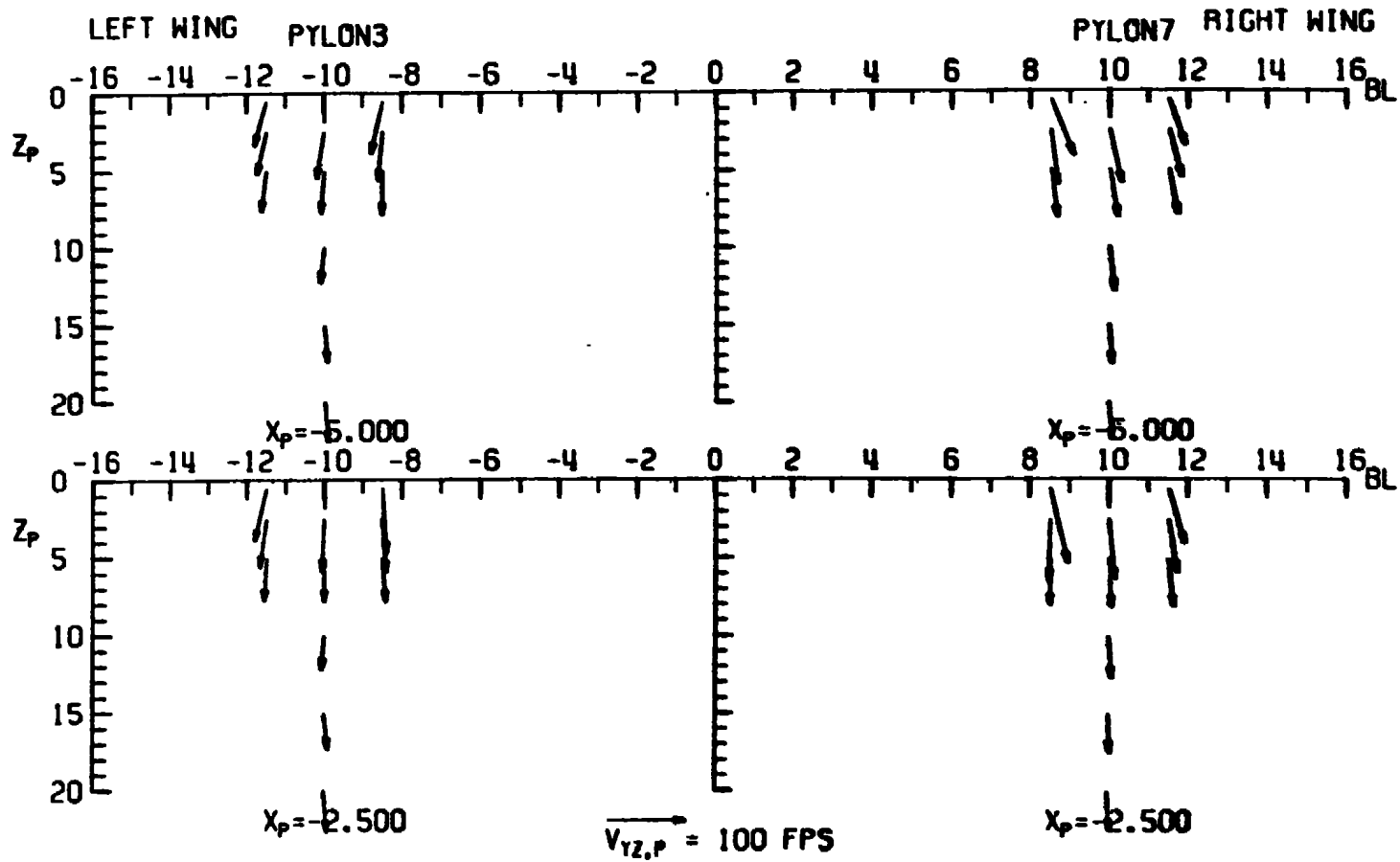
b.  $\alpha_p = 4$ ;  $X_p = 0$  and  $4.375$   
Figure 17. Continued.



CONFIG: 4     $M_\infty$ : 0.60     $\alpha_p$ : 4     $\delta_{LE}$ : 0



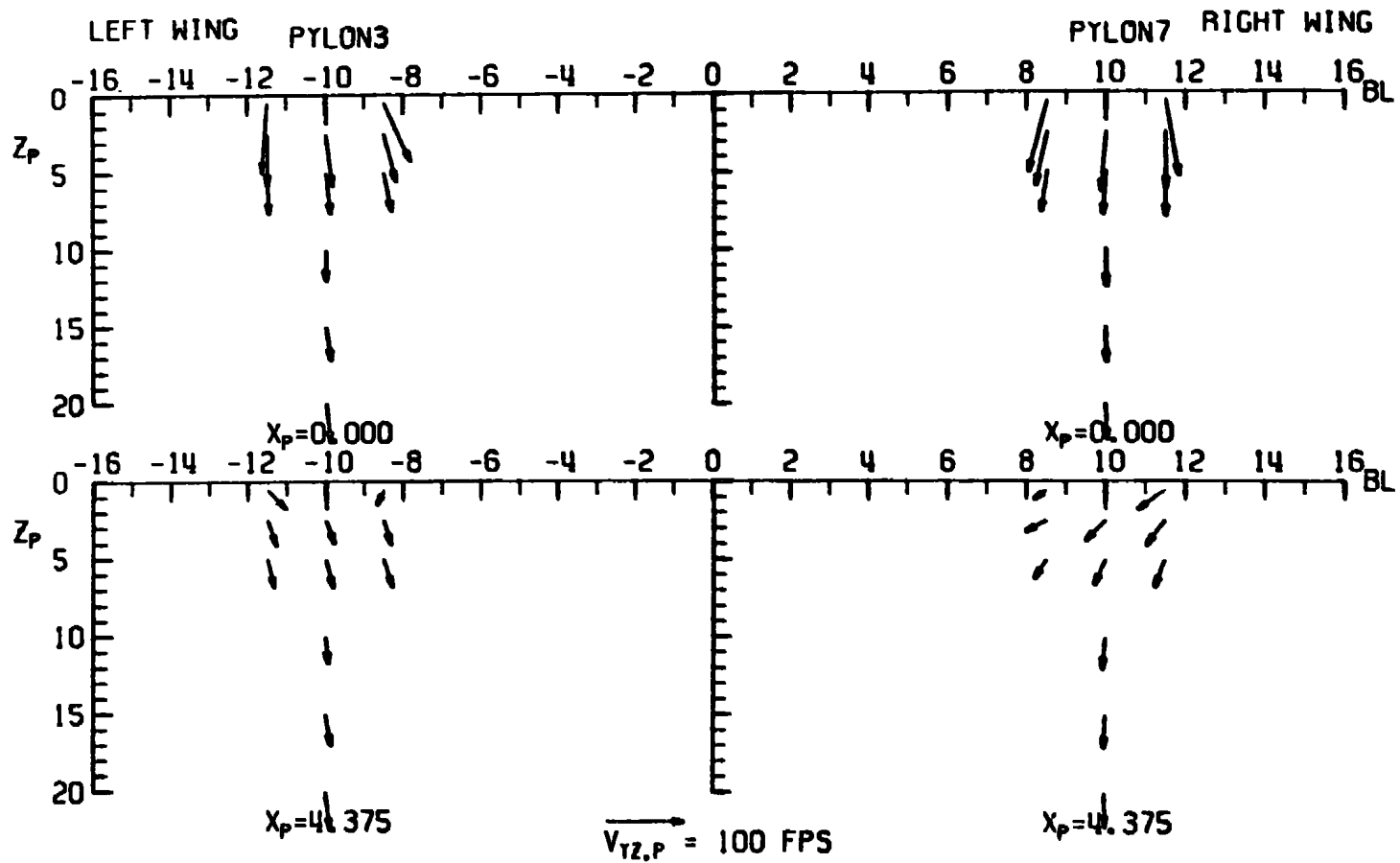
c.  $\alpha_p = 4$ ;  $X_p = 6.875$  and  $9.375$   
Figure 17. Concluded.



a.  $\alpha_p = 0$ ;  $x_p = -5.0$  and  $-2.5$

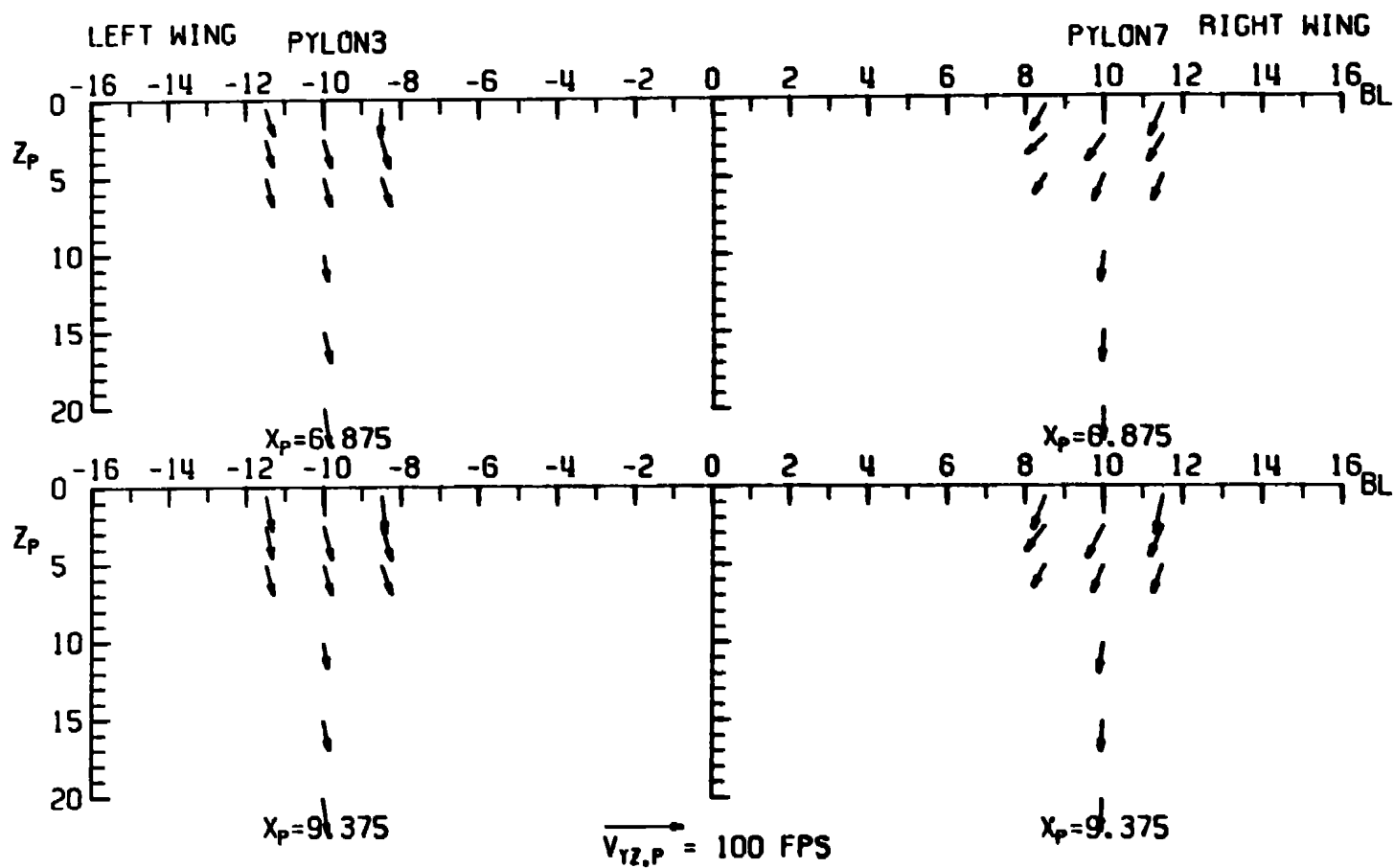
Figure 18. Flow-field measurements about the midwing weapons pylon without the MK-84 LDGP installed, configuration 4,  $M_\infty = 0.8$ ,  $\delta_{LE} = 0$ .

CONFIG: 4     $M_\infty$ : 0.80     $\alpha_p$ : 0     $\delta_{LE}$ : 0



b.  $\alpha_p = 0$ ;  $X_p = 0$  and  $4.375$   
Figure 18. Continued.

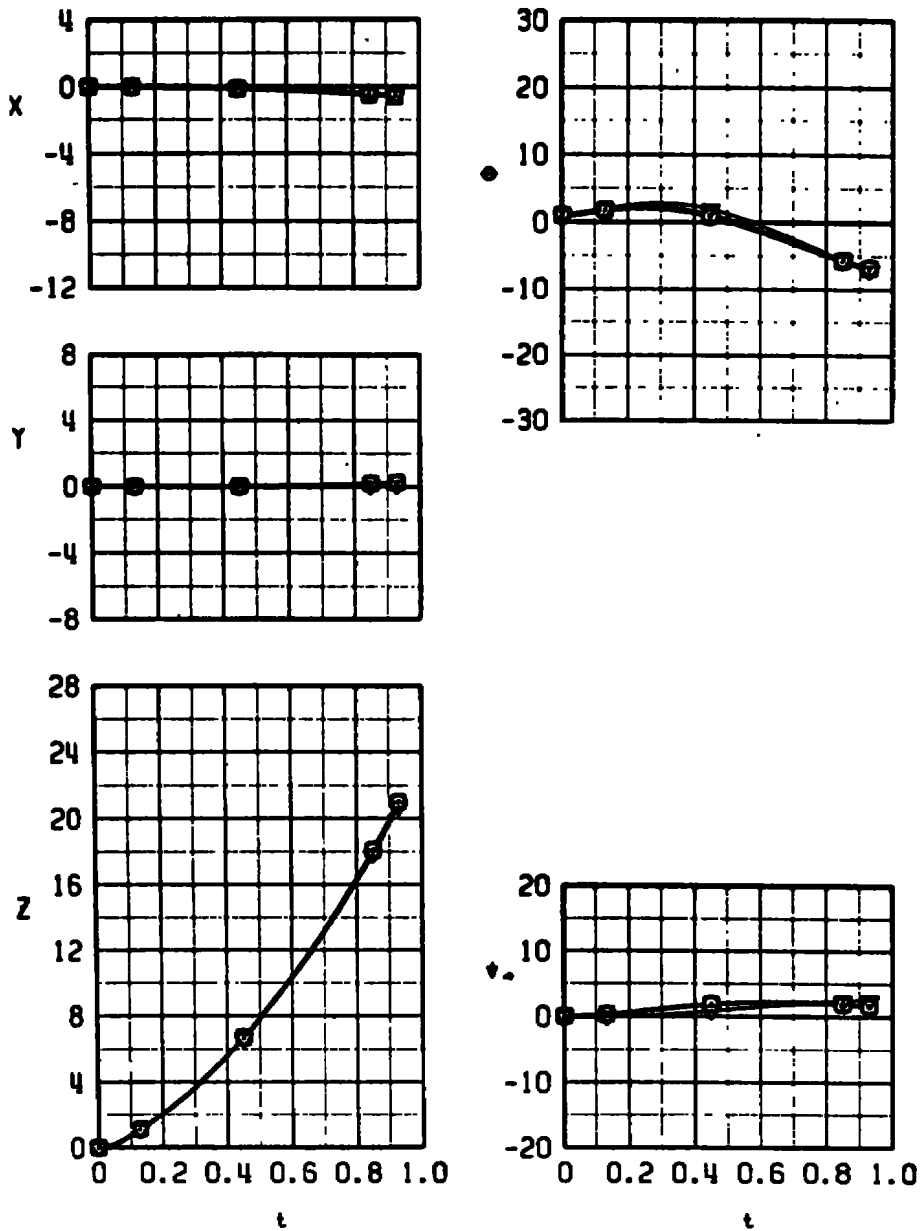
CONFIG: 4     $M_\infty$ : 0.80     $\alpha_p$ : 0     $\delta_{LE}$ : 0



c.  $\alpha_p = 0$ ;  $X_p = 6.875$  and  $9.375$

Figure 18. Concluded.

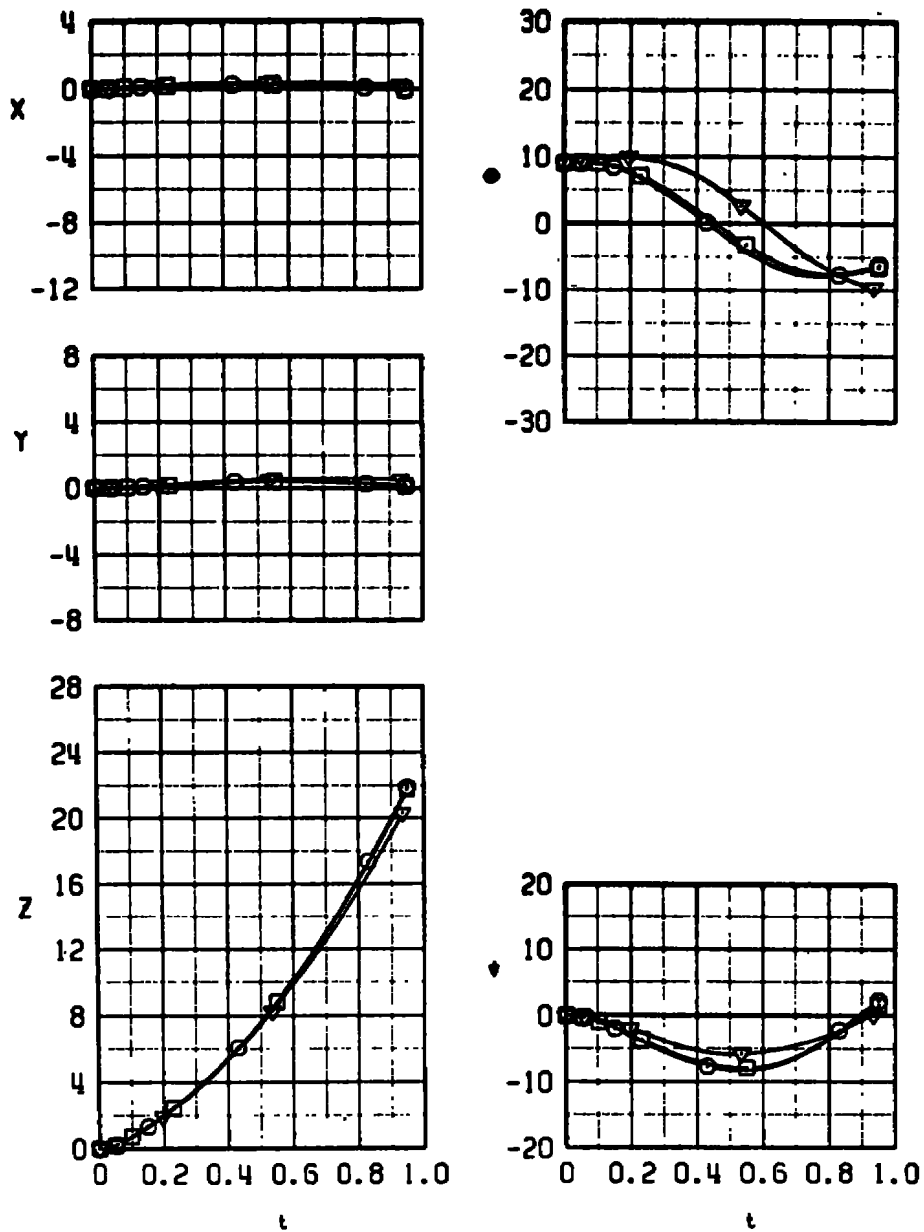
SYM	$M_\infty$	$\alpha_p$	CONFIG	$L_{LE}$
○	0.60	4	1	0
□	0.60	4	1	4
▽	0.60	4	1	15



a.  $\alpha_p = 4$

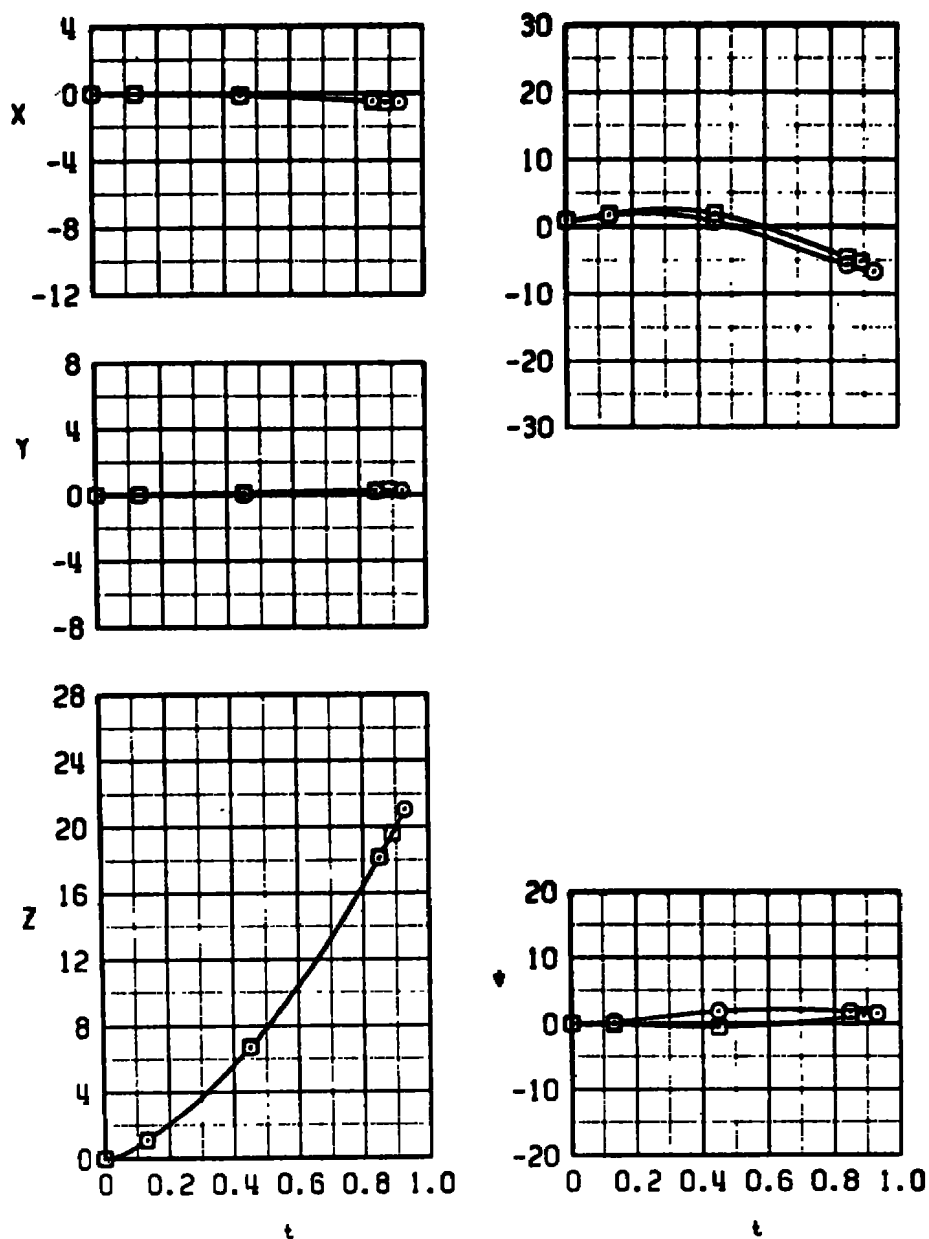
Figure 19. Effects of wing leading-edge flap deflections on trajectories of the MK-84 LDGP, configuration 1.

SYM	$M_\infty$	$a_p$	CONFIG	$\lambda_x$
○	0.60	12	1	0
□	0.60	12	1	4
▽	0.60	12	1	15



b.  $a_p = 12$   
Figure 19. Concluded.

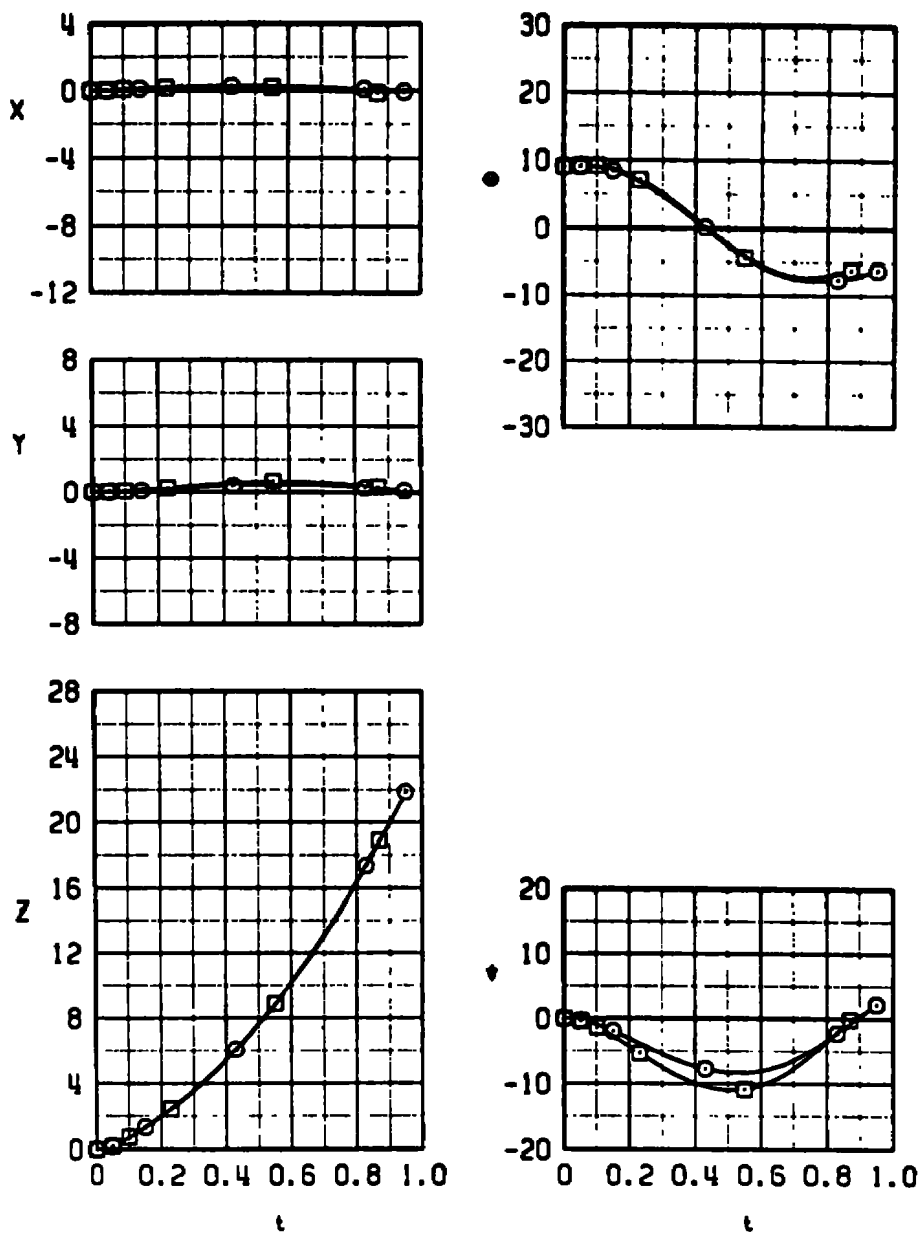
SYM	$M_\infty$	$\alpha_p$	CONFIG	$\delta_{LE}$
○	0.60	4	1	0
□	0.60	4	2	0



a.  $M_\infty = 0.6$ ,  $\alpha_p = 4$

Figure 20. Comparison of trajectories of the MK-84 LDGP with and without the 370-gal inboard fuel tank,  $\delta_{LE} = 0$ , configurations 1 and 2.

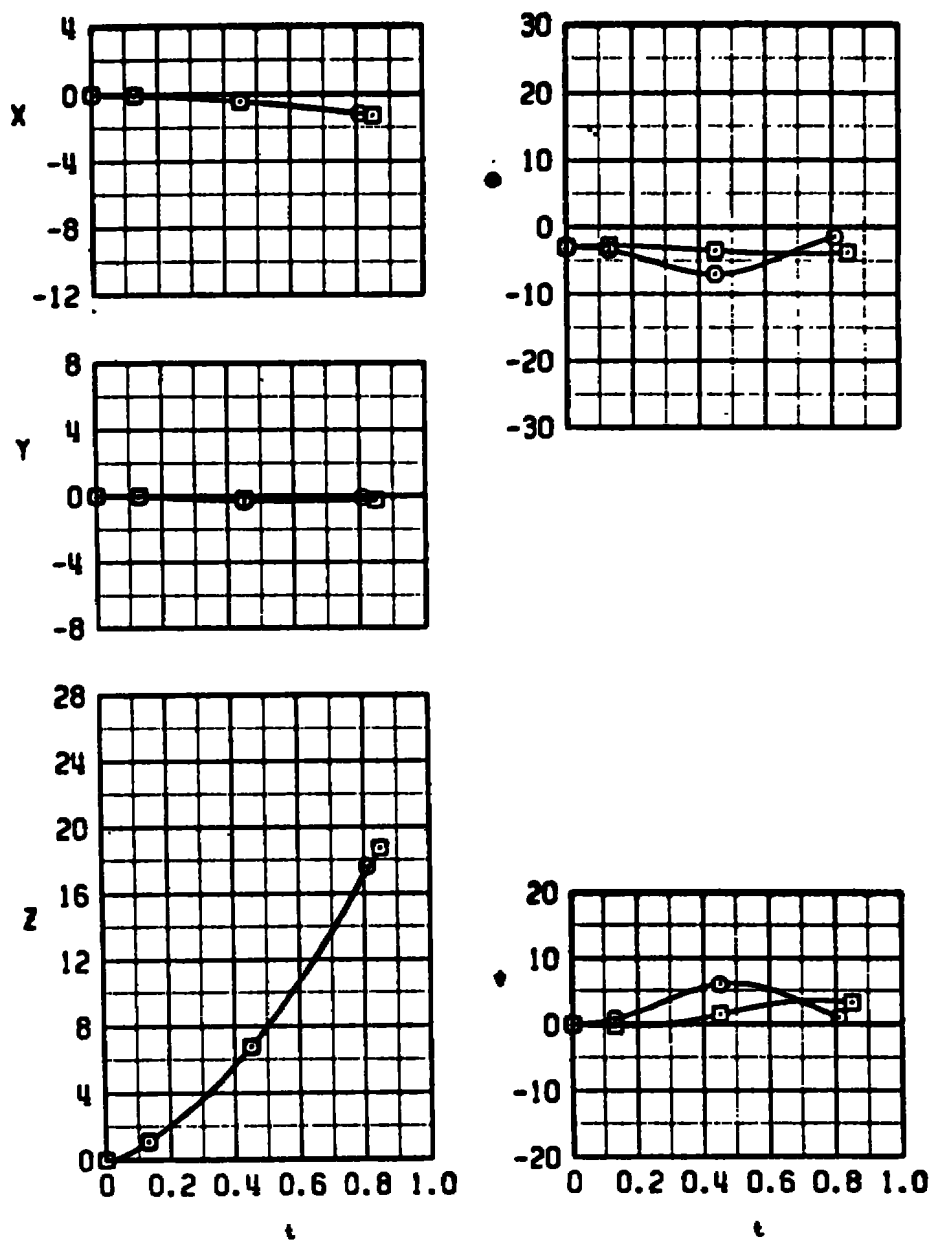
SYM	$M_\infty$	$a_p$	CONFIG	$t_{LE}$
○	0.60	12	1	0
□	0.60	12	2	0



b.  $M_\infty = 0.6$ ,  $a_p = 12$   
Figure 20. Continued.

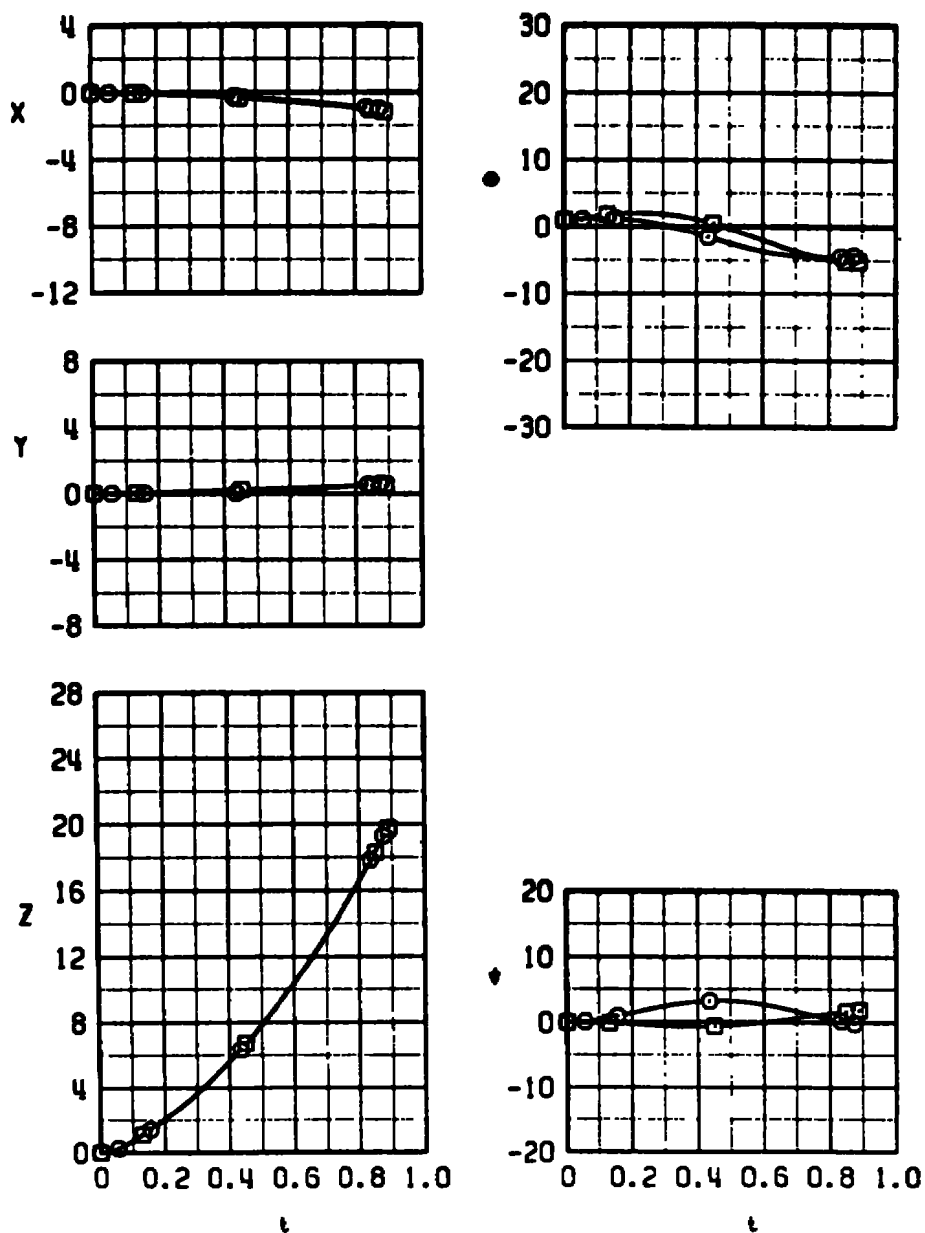


SYM	$M_\infty$	$\alpha_p$	CONFIG	$A_{LE}$
○	0.80	0	1	0
□	0.80	0	2	0



c.  $M_\infty = 0.8$ ,  $\alpha_p = 0$   
Figure 20. Continued.

SYM	$M_\infty$	$a_p$	CONFIG	$t_L$
○	0.80	4	1	0
□	0.80	4	2	0



d.  $M_\infty = 0.8$ ,  $a_p = 4$   
Figure 20. Concluded.

Table 1. Run Compendium

Phase	Configuration	$M_\infty$	$\alpha_p$	$\delta_{LE}$	Pylon
Trajectory ↓	1 ↓	0.6	4, 8, 12	0	7
		0.6	4, 8, 12	4	
		0.6	4, 8, 12	15	
	2 ↓	0.8	0, 2, 4	0	
		0.6	4, 8, 12	0	
		0.6	4, 8, 12	4	
		0.6	4, 8, 12	15	
		0.8	0, 2, 4	0	↓
Aerodynamic Loads ↓	1 ↓	0.4	8, 12, 16	0	7
		0.4	8, 12, 16	4	
		0.4	8, 12, 16	15	
		0.6	0, 2, 4, 8, 12	0	
		0.6	4, 8, 12	4	
		0.6	4, 8, 12	15	
		0.8	0, 2, 4	0	
		0.85	0, 2, 4, 8, 12	↓	
		0.9	0, 2, 4, 8, 12		
		0.95	0, 2, 4	↓	
		0.4	8, 12, 16	↓	
		0.4	8, 12, 16	4	
		0.4	8, 12, 16	15	
		0.6	0, 2, 4, 8, 12	0	
	Free Stream ↓	0.6	4, 8, 12	4	
		0.6	4, 8, 12	15	
		0.8	0, 2, 4	0	
		0.85	0, 2, 4, 8, 12	↓	
		0.9	0, 2, 4, 8, 12	↓	
		0.95	0, 2, 4	↓	
		0.4	NA	NA	NA
		0.6	↓	↓	↓
		0.8	↓	↓	↓
		0.85	↓	↓	↓
		0.9	↓	↓	↓
		0.95	↓	↓	↓
Flow Field ↓	3 ↓	0.6	4, 8, 12	0	7
		0.6	4, 8, 12	15	7
		0.8	0, 2, 4	0	7
		0.6	4, 8, 12	0	3
		0.6	4, 8, 12	15	3
	4 ↓	0.8	0, 2, 4	0	3
		0.6	4, 8, 12	0	7
		0.6	4, 8, 12	15	7
		0.8	0, 2, 4	0	7
		0.6	4, 8, 12	0	3
		0.6	4, 8, 12	15	3
		0.8	0, 2, 4	0	3
		0.6	4, 8, 12	0	3
		0.6	4, 8, 12	15	3
		0.8	0, 2, 4	0	3

Table 2. Survey Points

Phase	X <sub>P</sub>	Y <sub>P</sub>	Z <sub>P</sub>
Flow Field <sup>1</sup>	-5, -2.5, 0, 4.375, 6.875, 9.375 -5, -2.5, 0, 4.375, 6.875, 9.375	0 ±1.5	2.5, 5, 10, 15, 20 0.5, 2.5, 5
Aerodynamic Loads <sup>2</sup>	0	0	0, 0.5, 1.5, 3, 5, 7, 9, 11 13, 16, 18

<sup>1</sup>Referenced to the forward 30-in. suspension point.

<sup>2</sup>Referenced to the store cg with the store in the carriage position.

All dimensions in full-scale feet

**Table 3. Uncertainties  
Tunnel Conditions**

$M_\infty$	$\Delta M_\infty$	$\Delta p_t$ psf	$\Delta p_\infty$ psf	$\Delta q_\infty$ psf
0.4	$\pm 0.002$	$\pm 4.3$	$\pm 4.5$	$\pm 2.2$
0.6	$\pm 0.002$	$\pm 4.3$	$\pm 3.9$	$\pm 1.9$
0.8	$\pm 0.002$	$\pm 4.3$	$\pm 2.9$	$\pm 1.5$
0.85	$\pm 0.003$	$\pm 3.7$	$\pm 3.3$	$\pm 1.9$
0.9	$\pm 0.003$	$\pm 3.7$	$\pm 3.2$	$\pm 1.9$
0.95	$\pm 0.003$	$\pm 3.7$	$\pm 3.1$	$\pm 1.8$

**Aerodynamic Loads**

$M_\infty$	$\Delta C_N$	$\Delta C_m$	$\Delta C_A$	$\Delta C_l$	$\Delta C_Y$	$\Delta C_n$
0.4	$\pm 0.009$	$\pm 0.026$	$\pm 0.015$	$\pm 0.007$	$\pm 0.010$	$\pm 0.025$
0.6	$\pm 0.006$	$\pm 0.018$	$\pm 0.011$	$\pm 0.005$	$\pm 0.007$	$\pm 0.018$
0.8	$\pm 0.005$	$\pm 0.017$	$\pm 0.011$	$\pm 0.005$	$\pm 0.006$	$\pm 0.017$
0.85	$\pm 0.005$	$\pm 0.016$	$\pm 0.010$	$\pm 0.004$	$\pm 0.006$	$\pm 0.016$
0.9	$\pm 0.005$	$\pm 0.015$	$\pm 0.009$	$\pm 0.004$	$\pm 0.006$	$\pm 0.015$
0.95	$\pm 0.005$	$\pm 0.014$	$\pm 0.009$	$\pm 0.004$	$\pm 0.005$	$\pm 0.014$

**Trajectory Data**

$M_\infty$	t	$\Delta X$	$\Delta Y$	$\Delta Z$	$\Delta \theta$	$\Delta \psi$
0.6	0.4	$\pm 0.011$	$\pm 0.006$	$\pm 0.005$	$\pm 0.18$	$\pm 0.14$
0.8	0.4	$\pm 0.019$	$\pm 0.010$	$\pm 0.009$	$\pm 0.30$	$\pm 0.23$

**Flow-Field Data**

$M_\infty$	$\Delta V_{YZ}$
0.6	$\pm 5$
0.8	$\pm 5$

## NOMENCLATURE

BL	Aircraft buttock line from plane of symmetry, in., model scale
b	Store reference dimension, 1.5 ft, full scale
$C_A$	Store measured axial-force coefficient, axial force/ $q_\infty S$
$C_\ell$	Store rolling-moment coefficient, rolling moment/ $q_\infty S b$
$C_{\ell p}$	Store roll-damping derivative, $dC_m/d(pb/2V_\infty)$ , -0.10 per radian
$C_m$	Store pitching-moment coefficient, referenced to the store cg, pitching moment/ $q_\infty S b$
$C_{m q}$	Store pitch-damping derivative, $dC_m/d(qb/2V_\infty)$ , -120 per radian
$C_N$	Store normal-force coefficient, normal force/ $q_\infty S$
$C_n$	Store yawing-moment coefficient, referenced to the store cg, yawing moment/ $q_\infty S b$
$C_{n r}$	Store yaw-damping derivative, $dC_n/d(rb/2V_\infty)$ , -120 per radian
$C_Y$	Store side-force coefficient, side force/ $q_\infty S$
FS	Aircraft fuselage station, in., model scale
$F_{Z_1}$	Forward ejector force, 4,275 lb
$F_{Z_2}$	Aft ejector force, 3,775 lb
$I_{xx}$	Full-scale moment of inertia about the store $X_B$ axis, 24.8 slug-ft <sup>2</sup>
$I_{yy}$	Full-scale moment of inertia about the store $Y_B$ axis, 360 slug-ft <sup>2</sup>
$I_{zz}$	Full-scale moment of inertia about the store $Z_B$ axis, 360 slug-ft <sup>2</sup>
$M_\infty$	Free-stream Mach number
$\bar{m}$	Full-scale store mass, 61.2 slugs
$p_t$	Free-stream total pressure, psfa
$p_\infty$	Free-stream static pressure, psfa

$q_{\infty}$	Free-stream dynamic pressure, psf
$S$	Store reference area, 1.767 ft <sup>2</sup> , full scale
$t$	Real trajectory time from initiation of trajectory, sec
$V_L$	Local velocity vector, ft/sec (see Fig. 9)
$V_X$	Component of local velocity along probe $X_P$ axis, ft/sec (see Fig. 9)
$V_{XY}$	Component of local velocity in probe $X_P$ - $Y_P$ plane, ft/sec (see Fig. 9)
$V_{XZ}$	Component of local velocity in probe $X_P$ - $Z_P$ plane, ft/sec (see Fig. 9)
$V_Y$	Component of local velocity along probe $Y_P$ axis, ft/sec (see Fig. 9)
$V_Z$	Component of local velocity along probe $Z_P$ axis, ft/sec (see Fig. 9)
$V_{\infty}$	Free-stream velocity, ft/sec
$WL$	Aircraft waterline from reference horizontal plane, in., model scale
$X$	Separation distance of the store cg parallel to the flight-axis system $X_F$ direction, ft, full scale measured from the prelaunch position
$X_{cg}$	Full-scale cg location, 5.0 ft from nose of store
$X_{L1}$	Forward ejector location relative to the store cg, positive forward of store cg, 0.6667 ft, full scale
$X_{L2}$	Aft ejector piston location relative to the store cg, positive forward of store cg, -1.000 ft, full scale
$Y$	Separation distance of the store cg parallel to the flight-axis system $Y_F$ direction, ft, full scale measured from the prelaunch position
$Z$	Separation distance of the store cg parallel to the flight-axis system $Z_F$ direction, ft, full scale measured from the prelaunch position
$Z_E$	Ejector stroke, 0.34 ft, full scale
$\alpha_p$	Parent-aircraft model angle of attack relative to the free-stream velocity vector, deg

$\alpha_s$	Store model angle of attack relative to the free-stream velocity vector, deg
$\theta$	Angle between the store longitudinal axis and its projection in the $X_F$ - $Y_F$ plane, positive when store nose is raised as seen by pilot, deg
$\psi$	Angle between the projection of the store longitudinal axis in the $X_F$ - $Y_F$ plane and the $X_F$ axis, positive when the store nose is to the right as seen by the pilot, deg

## FLIGHT-AXIS SYSTEM COORDINATES

### Directions

$X_F$	Parallel to the free-stream wind vector, positive direction is forward as seen by the pilot
$Y_F$	Perpendicular to the $X_F$ and $Z_F$ directions, positive direction is to the right as seen by the pilot
$Z_F$	In the aircraft plane of symmetry, perpendicular to the free-stream wind vector, positive direction is downward

The flight-axis system origin is coincident with the aircraft cg and remains fixed with respect to the parent aircraft during store separation. The  $X_F$ ,  $Y_F$ , and  $Z_F$  coordinate axes do not rotate with respect to the initial flight direction and attitude.

## STORE BODY-AXIS SYSTEM COORDINATES

### Directions

$X_B$	Parallel to the store longitudinal axis, positive direction is upstream in the prelaunch position
$Y_B$	Perpendicular to the store longitudinal axis, and parallel to the flight-axis system $X_F$ - $Y_F$ plane when the store is at zero roll angle, positive direction is to the right looking upstream when the store is at zero yaw and roll angles
$Z_B$	Perpendicular to both the $X_B$ and $Y_B$ axes, positive direction is downward as seen by the pilot when the store is at zero pitch and roll angles.

The store body-axis system origin is coincident with the store cg and moves with the store during separation from the parent aircraft. The  $X_B$ ,  $Y_B$ , and  $Z_B$  coordinate axes rotate with the store in pitch, yaw, and roll so that mass moments of inertia about the three axes are not time-varying quantities.



## PYLON-AXIS SYSTEM COORDINATES

### Directions

- $X_P$  Parallel to the store (or probe) longitudinal axis in the prelaunch carriage position, positive direction is forward as seen by the pilot
- $Y_P$  Perpendicular to the  $X_P$  axis and parallel to the flight-axis system  $X_F$ - $Y_F$  plane, positive direction is to the right as seen by the pilot
- $Z_P$  Perpendicular to both the  $X_P$  and  $Y_P$  axes, positive direction is downward

For the aerodynamic loads test phase, the pylon-axis system origin is coincident with the store cg in the prelaunch carriage position. For the flow-field test phase, the pylon-axis system origin (see Fig. 9) is defined as the forward 30-in. suspension point of the midwing weapons pylon.

The axes are rotated with respect to the flight-axis system by the prelaunch yaw and pitch angles of the store or probe. Both the origin and the direction of the coordinate axes remain fixed with respect to the flight-axis system throughout the trajectory or survey.